APL/JHU
TG 1315A
OCTOBER 1977
Copy No. 9

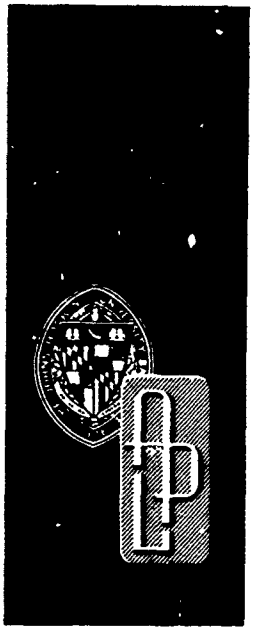

Technical Memorandum

OCEAN MAGNETICS I. FUNDAMENTAL SURVEY AND ESTIMATES OF INDUCTION PHENOMENA

J. F. BIRD

H. W. KO

THE JOHNS HOPKINS UNIVERSITY ■ APPLIED PHYSICS LABORATORY

PLEASE FOLD BACK IF NOT NEEDED FOR BIBLIOGRAPHIC PURPOSES

REPORT DOCUMENTATION PAGE

1 REPORT NUMBER	2 GOVT ACCESSION NO	3. RECIPIENT'S CATALOG NUMBER
APL/JHU TG 1315A		

4 TITLE (*and Subtitle*)	5 TYPE OF REPORT & PERIOD COVERED
OCEAN MAGNETICS: I. FUNDAMENTAL SURVEY AND ESTIMATES OF INDUCTION PHENOMENA	Technical Memorandum
	6 PERFORMING ORG. REPORT NUMBER APL/JHU TG 1315A
7 AUTHOR(s) J. F. Bird and H. W. Ko	8 CONTRACT OR GRANT NUMBER(s) N00017-72-C-4401
9 PERFORMING ORGANIZATION NAME & ADDRESS The Johns Hopkins University Applied Physics Laboratory Johns Hopkins Road Laurel, MD 20810	10 PROGRAM ELEMENT, PROJECT, TASK AREA & WORK UNIT NUMBERS X8
11 CONTROLLING OFFICE NAME & ADDRESS Naval Plant Representative Office Johns Hopkins Road Laurel, MD 20810	12. REPORT DATE October 1977 13. NUMBER OF PAGES 100
14 MONITORING AGENCY NAME & ADDRESS Naval Plant Representative Office Johns Hopkins Road Laurel, MD 20810	15 SECURITY CLASS. (*of this report*) Unclassified 15a DECLASSIFICATION/DOWNGRADING SCHEDULE --
16 DISTRIBUTION STATEMENT (*of this Report*) Approved for public release; distribution unlimited.	
17 DISTRIBUTION STATEMENT (*of the abstract entered in Block 20 if different from Report*) --	
18 SUPPLEMENTARY NOTES --	

19 KEY WORDS (*Continue on reverse side if necessary and identify by block number*)

Boat wakes	Internal waves	Magnetized body	Sea currents
Electromagnetic induction	Magnetic field	Magnetohydrodynamics	Seawater motions
Geomagnetism	Magnetic pseudowaves	Ocean	Sonomagnetism
Hydromagnetism	Magnetic Reynolds number	Ocean waves	Submerged bodies

(over)

20 ABSTRACT (*Continue on reverse side if necessary and identify by block number*)

Hydromagnetic phenomena are induced in the ocean environment by motions of the electrically conducting seawater across ambient fields. The present report is intended to survey and estimate possible effects from a fundamental theoretic standpoint. The ocean motions considered include both those of natural origin and those associated with moving ocean vehicles. The ambient magnetic field is that due to the earth, plus that due to the vehicle if it is magnetizable. These various motions and fields produce a broad multitude of ocean magnetic (OM) phenomena. The manifold of OM effects is surveyed theoretically, and from basic physical principles we derive simple numerical estimators for the effects. The potentially more significant include several pure-induction types (nonpropagating) and several pseudowave types (OM induction effects propagated by mechanical waves). Detailed analyses of these OM phenomena will be presented in subsequent reports.

DD FORM 1 JAN 73 1473

APL/JHU
TG 1315A
OCTOBER 1977

Technical Memorandum

OCEAN MAGNETICS I. FUNDAMENTAL SURVEY AND ESTIMATES OF INDUCTION PHENOMENA

J. F. BIRD

H. W. KO

THE JOHNS HOPKINS UNIVERSITY ■ APPLIED PHYSICS LABORATORY
Johns Hopkins Road ○ Laurel, Maryland ○ 20810
Operating under Contract N00017-72-C-4401 with the Department of the Navy

19. Key words (cont'd)

Surface waves
Tides
Underwater sound

THE JOHNS HOPKINS UNIVERSITY
APPLIED PHYSICS LABORATORY
LAUREL MARYLAND

ABSTRACT

Hydromagnetic phenomena are induced in the ocean environment by motions of the electrically conducting seawater across ambient magnetic fields. This report surveys and estimates possible effects from a fundamental theoretic standpoint. The ocean motions considered include those of natural origin and those associated with moving ocean vehicles. The ambient magnetic field is that due to the earth, plus that due to the vehicle if it is magnetizable. These various motions and fields produce a broad multitude of ocean magnetic (OM) phenomena. The manifold of OM effects is surveyed theoretically, and from basic physical principles we derive simple numerical estimators for the effects. The potentially more significant include several pure-induction types (nonpropagating) and several pseudowave types (OM induction effects propagated by mechanical waves). Detailed analyses of these OM phenomena will be presented in subsequent reports.

CONTENTS

LIST OF ILLUSTRATIONS

1. INTRODUCTION

Seawater has moderate electrical conductivity so that ocean motions across ambient magnetic fields induce electrical currents and associated magnetic fields, electric fields, and charges. Such hydromagnetic (HM) effects have long been known, are firmly based in electromagnetic (EM) theory, and are readily measurable (e.g., Refs. 1 through 4). Nonetheless, because the oceanic electrical conductivity is relatively small, the effects are far weaker than ordinary laboratory HM or MHD (magnetohydrodynamic) phenomena. To emphasize this, we use the term "ocean magnetics" (OM) for the phenomena to be considered here. These OM phenomena are distinguished from the oceanic induction often considered in geomagnetism (cf. Ref. 5) that arises from time variation of the earth's field rather than from seawater movements.

The OM phenomena treated up to now have been those arising from the interaction of natural motions of the ocean with the geomagnetic field. For example, Weaver (Ref. 6) has discussed wind waves and ocean swell, Beal and Weaver (Ref. 7) internal waves, and

---

Ref. 1. K. C. Maclure, R. A. Hafer, and J. T. Weaver, "Magnetic variations produced by ocean swell," Nature, Vol. 204, 1964, p. 1290.

Ref. 2. Ye. M. Groskaya, R. G. Skrynnikov, and G. V. Sokolov, "Magnetic field variations induced by the motion of sea waves in shallow water," Geomagn. Aeron., Vol. 12, 1972, p. 131 (translation).

Ref. 3. N. A. Cochrane and S. P. Srivastava, "Tidal influence on electric and magnetic fields recorded at coastal sites in Nova Scotia, Canada," J. Atmos. Terr. Phys., Vol. 36, 1974, p. 49.

Ref. 4. M. Klein, P. Louvet, and P. Morat, "Measurement of electromagnetic effects generated by swell," Physics of the Earth and Planetary Interiors, Vol. 10, 1975, p. 49.

Ref. 5. E. C. Bullard and R. L. Parker, "Electromagnetic induction in the ocean," Chapt. 18, Vol. 4, The Sea, Wiley-Interscience, New York, NY, 1970.

Ref. 6. J. T. Weaver, "Magnetic variations associated with ocean waves and swell," J. Geophys. Res., Vol. 70, 1965, p. 1921.

Ref. 7. H. T. Beal and J. T. Weaver, "Calculations of magnetic variations induced by internal ocean waves," J. Geophys. Res., Vol. 75, 1970, p. 6846.

recently Podney (Ref. 8) has generalized these analyses, while Larsen (Ref. 9) has analyzed tidal wave effects. A recent review and bibliography of natural-motion OM studies will be found under "hydromagnetic noises" in Akindonov et al. (Ref. 10).

Further OM phenomena arise when a moving body is introduced into the ocean environment. On the one hand, the ocean motions induced by the vehicle interact with the geomagnetic field to produce OM fields, currents, and charges. On the other hand, when the vehicle is significantly magnetized, as the ferromagnetic construction of ships and boats generally permits via the geomagnetic field, the interaction of the body magnetic field with ocean motions can produce further OM effects.

We plan in this report to survey, summarize, and estimate the broad spectrum of OM effects that can arise from the interactions of either natural or body-induced ocean motions with either geomagnetic or body-magnetization fields. Our approach, through theoretical fundamentals, recommends itself because the basic physical principles of the problem are well established and mathematically formulated. We begin by reviewing the basic governing equations (Sec. 2) from which the general character of OM phenomena and a summary catalog of effects are outlined (Sec. 3). Theoretical methods of analysis are then presented (Sec. 4 and Appendix A) by means of which we deduce simple numerical estimates for the various OM fields induced by natural and body-related sea motions (Secs. 5 and 6).

In keeping with the survey purpose of this report, the estimates of Sec. 5 and 6 are designed for ready comprehension at the expense of full precision, in order to give a feeling for the various phenomena. Where available, precise analyses will be cited. Finally, a summary epilogue of the survey is given in Sec. 7, along with a glossary guide to the detailed estimates, giving the major symbols used.

Ref. 8. W. Podney, "Electromagnetic fields generated by ocean waves," J. Geophys. Res., Vol. 80, 1975, p. 2977.

Ref. 9. J. C. Larsen, "The electromagnetic field of long and intermediate water waves," J. Marine Res., Vol. 29, 1971, p. 28.

Ref. 10. V. V. Akindonov, V. I. Naryshkin, and A. M. Ryazantsev, "Electromagnetic waves in sea water (Review)," Radioteknika i Elektronika, Vol. 21, No. 1, English translation in Radioeng. Electron. Phys., Vol. 21, No. 1, May 1976.

2. FUNDAMENTALS

The EM field generated by the ocean motions is governed by Maxwell's equations. The ocean flowfield conversely is subject to EM body forces through Navier-Stokes' equations. The combined Maxwell-Navier-Stokes fields at sufficiently slow rates of variation (see Eqs. 3 and 4, below) comprise the diverse phenomena of MHD of both cosmic and laboratory interest (e.g., Roberts in Ref. 11). The case of the ocean falls between these two extremes, with neither conductivity nor flow-scale nor ambient magnetism particularly large, so that the flow-induced Maxwell field is small and the EM force on the flowfield is extremely weak. Thus we have to deal with a degenerate variant of MHD, which we call ocean magnetics to emphasize its special characteristics.

2.1 THE MAGNETIC FIELD IN THE OCEAN

The primary relations for OM will be the Maxwell equations,

$$\text{curl } \underset{\sim}{E} + \frac{\partial \underset{\sim}{B}}{\partial t} = 0, \qquad \text{div } \underset{\sim}{B} = 0 \quad , \tag{1a,1b}$$

$$\text{curl } \underset{\sim}{H} - \frac{\partial \underset{\sim}{D}}{\partial t} = \underset{\sim}{j}, \qquad \text{div } \underset{\sim}{D} = \rho_e \quad , \tag{1c,1d}$$

where ρ_e is charge density, $\underset{\sim}{j}$ the current density, and $\underset{\sim}{E}$, $\underset{\sim}{B}$, $\underset{\sim}{D}$, $\underset{\sim}{H}$ the EM field. Equations 1 are invariant with reference frame, but, for a stationary observer of the moving ocean, its constitutive relations among $\underset{\sim}{B}$, $\underset{\sim}{H}$, $\underset{\sim}{D}$, $\underset{\sim}{E}$, and $\underset{\sim}{j}$ must be transformed from those of seawater at rest. Assuming the relations to be linear and isotropic with dielectric constant ε, permeability μ, and conductivity σ, and denoting the ocean flowfield as $\underset{\sim}{u}$, one finds (Ref. 12, Part IV)

$$\underset{\sim}{j} = \sigma(\underset{\sim}{E} + \underset{\sim}{u} \times \underset{\sim}{B}) + \rho_e \underset{\sim}{u} \quad , \tag{2a}$$

Ref. 11. P. H. Roberts, An Introduction to Magnetohydrodynamics, American Elsevier, New York, NY, 1967.

Ref. 12. A. Sommerfeld, Electrodynamics, Academic Press, New York, NY, 1952.

$$\underset{\sim}{D} = \varepsilon \underset{\sim}{E} + (\varepsilon\mu - \varepsilon_0\mu_0)\underset{\sim}{u} \times \underset{\sim}{H} \quad , \tag{2b}$$

$$\underset{\sim}{B} = \mu \underset{\sim}{H} - (\varepsilon\mu - \varepsilon_0\mu_0)\underset{\sim}{u} \times \underset{\sim}{E} \quad , \tag{2c}$$

where ε_0, μ_0 are vacuum constants ($\mu_0 = 4\pi \cdot 10^{-7}$, $\varepsilon_0\mu_0 = 1/c^2$) and where terms $O(u^2/c^2)$ are neglected since we deal with nonrelativistic flowfields,

$$u << c \quad . \tag{3}$$

In addition, we restrict consideration for the Maxwell field to length and time scales, L and T, such that

$$\frac{L}{T} << c \quad , \tag{4}$$

the usual MHD limit that bars EM waves. Then, Eq. 1a gives $E/B \sim L/T << c$ so that Eq. 2c becomes $\underset{\sim}{B} = \mu \underset{\sim}{H}$ to $O(uL/c^2T)$. Comparing $\partial D/\partial t$ and $\rho_e \underset{\sim}{u}$ to curl $\underset{\sim}{H}$, we have in Eqs. 1c and 2a that curl $\underset{\sim}{H} = \underset{\sim}{j}$ to $O(L^2/c^2T^2)$ and $\underset{\sim}{j} = \sigma(\underset{\sim}{E} + \mu \underset{\sim}{u} \times \underset{\sim}{H})$ to $O(uL/c^2T)$. In other words, we can neglect "flow magnetization," displacement current, and convection current in Eqs. 1 and 2, and they remain valid up to second order in the smallness assumptions of Eqs. 3 and 4. None of the surviving terms is of first-order smallness; e.g., the "flow polarization" in Eq. 2b as well as the induction current in Eq. 2a are each of relative order $u/(L/T)$.

A governing set of equations that determines each OM field variable individually as a functional of the flowfield $\underset{\sim}{u}$ emerges from Eqs. 1 and 2 on the assumptions of Eqs. 3 and 4. We consider $\underset{\sim}{H}$ as the primary field variable and eliminate $\underset{\sim}{B}$, $\underset{\sim}{E}$, and $\underset{\sim}{j}$ between Eqs. 1a, 1c, 2a, and 2c to obtain the basic HM equation

$$\frac{\partial \underset{\sim}{H}}{\partial t} = \frac{1}{\mu\sigma} \Delta \underset{\sim}{H} + \text{curl } (\underset{\sim}{u} \times \underset{\sim}{H}) \quad , \tag{5a}$$

taking the ocean μ and σ to be constant. In addition to Eq. 5a, $\underset{\sim}{H}$ is subject to the subsidiary condition from Eqs. 1b and 2c,

$$\text{div } \underset{\sim}{H} = 0 \quad , \tag{5b}$$

and to the boundary conditions that follow from Maxwell's Eqs. 1b and 1c (Ref. 12),

$$\hat{\underset{\sim}{n}} \times \underset{\sim}{H} \quad \text{and} \quad \hat{\underset{\sim}{n}} \cdot (\underset{\sim}{H} + \underset{\sim}{M}) \quad \text{continuous} \quad , \qquad (6a,6b)$$

where $\hat{\underset{\sim}{n}}$ is boundary normal, $\underset{\sim}{M}$ denotes magnetization of adjoining media (e.g., steel hull), and surface currents are assumed negligible. Finally, the remaining OM variables can be written in terms of $\underset{\sim}{H}$ and $\underset{\sim}{u}$ through Eqs. 1 through 4:

$$\underset{\sim}{B} = \mu \underset{\sim}{H} \quad , \qquad (7a)$$

$$\underset{\sim}{j} = \text{curl } \underset{\sim}{H} \quad , \qquad (7b)$$

$$\underset{\sim}{E} = \frac{1}{\sigma} \text{curl } \underset{\sim}{H} - \mu \underset{\sim}{u} \times \underset{\sim}{H} \quad , \qquad (7c)$$

$$\underset{\sim}{D} = \frac{\varepsilon}{\sigma} \text{curl } \underset{\sim}{H} - \varepsilon_0 \mu_0 \underset{\sim}{u} \times \underset{\sim}{H} \quad , \qquad (7d)$$

$$\rho_e = \varepsilon_0 \mu_0 (\underset{\sim}{u} \cdot \text{curl } \underset{\sim}{H} - \underset{\sim}{H} \cdot \text{curl } \underset{\sim}{u}) \quad , \qquad (7e)$$

where an inhomogeneity $\underset{\sim}{j} \cdot \nabla(\varepsilon/\sigma)$ was dropped in Eq. 7e.

The fundamental relation of the OM field to the flowfield is therefore given by Eq. 5a, which has the form of a vector diffusion-convection equation. The diffusion term has time-scale $\tau_d \sim \mu\sigma L^2$ and the convection term, $\tau_c \sim L/u$. Hence,

$$\frac{\text{convection-rate}}{\text{diffusion-rate}} = \frac{\tau_d}{\tau_c} \sim \mu\sigma u L \equiv R_M \quad , \qquad (8)$$

where R_M is a magnetic Reynolds number. R_M is then a measure of the relative effect that the flowfield has on the magnetic field. In most cases to be considered in OM, R_M is somewhat less then unity, though not negligible. Consequently, the OM fields can be treated as small perturbations to the ambient field, though still well above the sensitivity limits of present magnetometers.

We remark that, in the MHD approximation, the familiar displacement/conduction current-ratio $\omega\varepsilon/\sigma \sim 10^{-9}/T$ is $<< 1/L$ by Eq. 4 and so is assured small for the lengths L considered here. That

is, we do not enter the electrohydrodynamic regime that obtains when electric relaxation becomes slower than magnetic, viz. $\sigma/\varepsilon \ll 1/\tau_d$ or $L \ll 9/\mu\sigma c \sim 10^{-2}$ meters here.

2.2 THE MAGNETIC FIELD ABOVE THE OCEAN

The utility of airborne observation warrants specific consideration of the field equations above the sea surface. Since the conductivity of air is $\sim 10^{-14}$ times that of seawater, the conduction current is completely negligible there. Thus, within the approximations of Eqs. 3 and 4 all currents are zero, so that curl $\underset{\sim}{H} = 0$ (cf. Eq. 7b) and we may write

$$\underset{\sim}{H} = \text{grad } \Psi \quad . \tag{9}$$

Since div $\underset{\sim}{H}$ = div $\underset{\sim}{B}/\mu_0 = 0$ by Eq. 1b, the potential Ψ satisfies Laplace's equation

$$\Delta\Psi = 0 \quad , \tag{10a}$$

subject to the boundary conditions (Eqs. 6a and 6b), which become here

$$\underset{\sim}{H} \text{ continuous at air/sea interface} \quad , \tag{10b}$$

and subject also to the condition that the field remain finite at infinity.

Therefore, the OM field above the ocean is essentially determined, via Laplace's equation, by the OM field at the surface of the ocean. An immediate corollary is that the altitude dependence of the OM field is fixed by the horizontal variation of the sea surface field. The generality of this feature of the aerofield is somewhat obscured among details in the existing analyses cited in Sec. 1.

For example, consider a plane-wave Fourier component of the OM field at the sea surface,

$$\underset{\sim}{H}_{\text{surface}} = \underset{\sim}{C}\, e^{i\omega t - i\underset{\sim}{k}\cdot\underset{\sim}{x}} \quad , \tag{11a}$$

where $\underset{\sim}{C}$ is Fourier amplitude, ω frequency, and $\underset{\sim}{\kappa}$ horizontal wavevector. The corresponding Fourier transform of the aerofield ($z > 0$) must then have the form $\underset{\sim}{H}_{air} = \underset{\sim}{\nabla}\Psi = \underset{\sim}{C}\, e^{i\omega t - i\underset{\sim}{\kappa}\cdot\underset{\sim}{x} - iqz}$ to satisfy Eqs. 10, wherein Laplace's Eq. 10a requires $\Delta\Psi \propto \kappa^2 + q^2 = 0$, or $q = \pm i\kappa$. Hence, we have at once that

$$\underset{\sim}{H}_{air} = \underset{\sim}{H}_{surface} \cdot e^{-\kappa z} \qquad (z > 0) \quad , \qquad (11b)$$

taking $\mathrm{Re}\underset{\sim}{\kappa}$ (the real part of $\underset{\sim}{\kappa}$) > 0 and dropping the exponentially growing solution. In other words, a sinusoidal surface wave leads to an exponential altitude decrease (cf. Refs. 6 and 8). More generally, in a surface variation consisting of a superposition of Fourier components, the longer wavelength effects tend, ceteris paribus, to reach to higher altitudes.

2.3 THE OCEAN FLOW FIELD

Returning to the sea, we describe its flow field $\underset{\sim}{u}$ by the Navier-Stokes equation

$$\rho \frac{d\underset{\sim}{u}}{dt} = -\underset{\sim}{\nabla}P + \rho(\underset{\sim}{g} - \underset{\sim}{\Omega} \times \underset{\sim}{u}) + \eta\Delta\underset{\sim}{u} + \mu(\underset{\sim}{H} \cdot \underset{\sim}{\nabla})\underset{\sim}{H} \quad , \qquad (12a)$$

wherein ρ is seawater density, P is the sum of kinetic, magnetic, and viscous pressures ($P \equiv p + \frac{1}{2}\mu H^2 - (\zeta + \eta/3)\mathrm{div}\,\underset{\sim}{u}$), $\underset{\sim}{g}$ is earth's gravity (including centripetal acceleration), $\underset{\sim}{\Omega}$ its rotation (twice angular velocity), and η, ζ are shear, bulk viscosities that have been assumed constant. Along with Eq. 12a we have the continuity equation

$$\mathrm{div}\,\underset{\sim}{u} = -\frac{d\ln\rho}{dt} \quad , \qquad (12b)$$

and equations of state and energy as needed.

The salient part of Eq. 12a for OM phenomena is the last term together with the magnetic pressure term. These terms enter via the EM stress tensor on dropping electric components ($E^2/c^2B^2 \sim L^2/c^2T^2 \ll 1$ by Eq. 4) and with μ taken constant (ambiguities for moving magnetic media will not concern us here — cf.

Ref. 13, p. 496). Alternatively, since $\nabla \frac{1}{2}H^2 \equiv \underset{\sim}{H} \times \text{curl}\, \underset{\sim}{H} + (\underset{\sim}{H} \cdot \nabla)\underset{\sim}{H}$, the two terms are equivalent to the Lorentz force density $\rho_e \underset{\sim}{E} + \underset{\sim}{j} \times \underset{\sim}{B} \approx \mu \underset{\sim}{j} \times \underset{\sim}{H}$, to the same approximations as Eqs. 5 through 7. Notice that the $\underset{\sim}{j} \times \underset{\sim}{H}$ form makes clear that a strictly external magnetostatic field ($\text{curl}\, \underset{\sim}{H} \approx \underset{\sim}{j} = 0$) contributes negligible acceleration to Eq. 12a. Hence, aside from any nonstatic part of the ambient fields (e.g., geomagnetic time variations), magnetism will affect the flow only through the flow-induced OM field. Since the latter is expected to be relatively small ($\sim R_M$, cf. the discussion following Eq. 8), we therefore expect the effects of magnetism on flow to be correspondingly small.

Furthermore, the relative size of the magnetic forces in Eq. 12a generally depends on the Alfvén speed A, which gauges the magnetic energy per unit mass. Thus, the ratio of magnetic to inertial terms in Eq. 12a gives

$$\frac{\text{magnetism}}{\text{flow}} \sim \frac{A^2}{u^2} \quad , \qquad \text{where} \quad A^2 \equiv \frac{\mu H^2}{\rho} \quad . \tag{13}$$

Comparison of magnetism with other forces in Eq. 12a can be made in terms of $(A/u)^2$, R_M, and the usual Reynolds number $R_e \equiv uL\rho/\eta$, or various combinations. (For example, from the last two terms in Eq. 12a, magnetism/viscosity $\propto (A/u)^2 \cdot R_e$ or R_H^2/R_M, where $R_H \equiv AL\sqrt{\mu\sigma\rho/\eta}$ is the Hartmann number; we shall see that the latter measures the ratio of magnetic to viscous wave damping.) For the geomagnetic field in ocean water, $A \sim 2 \cdot 10^{-3}$ m/s, which is small compared to most flow speeds of interest here. The already small OM magnetism then has its effect on the flow reduced by the small ratio $(A/u)^2$ of Eq. 13.

Consequently, it seems well justified to ignore the magnetic forces in Eq. 12a. This neglect uncouples Eqs. 12 from Eqs. 5, and the flow description becomes an ordinary hydrodynamic problem that we shall assume to have been solved elsewhere. We are then left to consider Eqs. 5 alone, as outlined in Sec. 3.1 and elaborated in the bulk of this report (Secs. 4 through 6). Because of the potential importance of reciprocal magnetism-flow interactions as propagators of OM waves, we shall also look more closely at the coupled Eqs. 12 and 5 in Sec. 3.2 under various simplifying approximations.

Ref. 13. R. M. Fano, L. J. Chu, and R. B. Adler, Electromagnetic Fields, Energy and Forces, Wiley, New York, NY, 1960.

Table 1 presents some definitions and numerical values of various parameters of importance for ocean magnetic phenomena.

Table 1

Ocean Magnetics Parameters

Symbol	Parameter	Nominal Value*
σ	Ocean electrical conductivity	4
μ	Ocean magnetic permeability	$4\pi \times 10^{-7}$
ε	Ocean dielectric constant	$9 \times 10^{-9}/4\pi$
β	Ocean compressibility	4.5×10^{-10}
η	Ocean shear viscosity	1.5×10^{-3}
c_s	Ocean sound speed	1500
ρ	Ocean density	1025
H_e	Earth magnetic field	5×10^4 (γ)
g	Earth gravity	9.8

*mks units are used throughout, except that magnetic fields are measured in γ (= 10^{-5} G).

3. OVERVIEW OF PHENOMENA

We decompose the magnetic field and the flow field into their uncoupled portions plus hydromagnetically coupled remainders,

$$\underset{\sim}{H} = \underset{\sim}{H}_0 + \underset{\sim}{h} \quad , \qquad \underset{\sim}{u} = \underset{\sim}{u}_0 + \underset{\sim}{v} \quad . \tag{14a,14b}$$

That is, $\underset{\sim}{H}_0$ represents the magnetic field neglecting flow and $\underset{\sim}{u}_0$ the flowfield neglecting magnetism, both of which will ordinarily be assumed as given here.

The OM field proper, $\underset{\sim}{h}$, $\underset{\sim}{v}$, should be small according to the discussions following Eqs. 8 and 13; specifically, we expect the hierarchy

$$\frac{v}{u_0} << \frac{h}{H_0} << 1 \quad . \tag{15}$$

(Or, if $\underset{\sim}{u}_0 \approx 0$, consider the first ratio to be $v/(L/T)$). Therefore, in the first instance one is led to consider the limiting case

$$\underset{\sim}{v} = 0 \quad \text{(OM induction)} \quad , \tag{16a}$$

in which $\underset{\sim}{h}$ is simply induced by the given, purely mechanical, flow $\underset{\sim}{u}_0$. Subsequently we may lift this restriction in order to investigate the important (however unlikely) possibility of significant OM wave propagation. That is, the general case

$$\underset{\sim}{v} \neq 0 \quad \text{(OM radiation)} \tag{16b}$$

admits $\underset{\sim}{h}$ and $\underset{\sim}{v}$ interactions that may conceivably radiate through the ocean.

3.1 VARIETIES OF OM INDUCTION

In the case given by Eq. 16a, the OM field $\underset{\sim}{h}$ is essentially determined via the basic HM Eq. 5a as a function of the given fields $\underset{\sim}{H}_0$, $\underset{\sim}{u}_0$. This gives a straightforward induction problem, which becomes multifarious, however, through the variety of non-hydromagnetic fields $\underset{\sim}{H}_0$ and $\underset{\sim}{u}_0$ that will enter.

The given magnetic field is taken as the sum of earth (e) and magnetized-body (b) fields,

$$\underset{\sim}{H}_0 = \underset{\sim}{H}_e + \underset{\sim}{H}_b \quad , \tag{17}$$

$\underset{\sim}{H}_e$ being the total geomagnetic field and $\underset{\sim}{H}_b$ the proper field of the body when immersed at rest in quiescent seawater.

In general, $\underset{\sim}{H}_e$ consists of the magnetostatic mean earth field, which can be taken as locally uniform over scales of interest here, plus the slight temporal and local variations often called geomagnetic and geologic noise, respectively. (Notice that the noise includes that generated by currents induced in the sea by the geomagnetic noise itself, so that $\underset{\sim}{H}_e$ is not a strictly external field, cf. Eq. 20a below.) The noise is usually well above magnetometer sensitivities and therefore must be considered in the detection of signals such as the OM $\underset{\sim}{h}$ field down to the limits of sensitivity. However, the hydromagnetic effects of the noise are of course much smaller than those of the mean geomagnetic field. Therefore, we can set aside the geomagnetic and geologic noise in the calculation of the OM $\underset{\sim}{h}$ signals, and consider $\underset{\sim}{H}_e$ as constant in space and time.

Similarly, while $\underset{\sim}{H}_b$ in general has a spatial variation that we shall, of course, not ignore, its intrinsic time variations will be assumed minor here. (Notice that, like $\underset{\sim}{H}_e$ above, $\underset{\sim}{H}_b$ includes a part associated with currents induced in the seawater by any intrinsic time variation of $\underset{\sim}{H}_b$ itself, so $\underset{\sim}{H}_b$ too is not a strictly external field, cf. Eq. 20b below.) On that assumption, we can neglect the hydromagnetic effects of the intrinsic time variations in calculating $\underset{\sim}{h}$ and consider $\underset{\sim}{H}_b$ as constant in the body rest frame. There remains, of course, its convective time-variation due to motion of the body through the sea (cf. the last term in Eq. 22a).

The given mechanical field is taken to be composed as

$$\underset{\sim}{u}_0 = \text{"natural" and/or "body-related" motions} \quad , \tag{18}$$

wherein the two classes of motion include

1. The natural motions.

   Surface gravity waves (SW), due to either local winds (sea) or distant storms (swell), (18a)

   Internal gravity waves (IW), (18b)

   Ambient acoustic waves (AW), and (18c)

   Sea currents and tides; (18d)

2. The body-related motions due to passage of a vehicle through the seawater:

   Mean flow, i.e., the relative translation of the seawater and the body-field $\underset{\sim}{H}_b$, (18e)

   Potential flow, caused by hull displacement, (18f)

   Wake flow, from turbulent growth near the body to collapse in far region, and (18g)

   Propagated disturbances, due to body-generated SW, IW, and AW. (18h)

In general, these various motions are not independent, due to hydrodynamic interactions, so that Eq. 18 is a nonadditive combination. However, for simplicity we will consider the idealized situation of negligible interaction. Then Eq. 18 becomes additive, as does Eq. 17, so that the hydromagnetic driving (last term of Eq. 5a) is a sum of binary combinations of each part of $\underset{\sim}{H}_0$ with each of the $\underset{\sim}{u}_0$.

The numerous possible pairs of given motion (Eqs. 18a through 18h) and magnetism (Eq. 17) yield a respectably long list of phenomena to be considered. After a general theoretical development in Sec. 4, each phenomenon will be considered individually in Secs. 5 and 6. But first we will discuss briefly the propagation of purely inductive effects (pseudowaves) versus true OM radiation.

3.2 PSEUDOWAVES AND OM RADIATION

Even in the case $\underset{\sim}{v} = 0$ (Eq. 16a) of pure OM induction notice that there can be propagation of the induced magnetism $\underset{\sim}{h}$

when the inducing flow is a mechanical radiation. That is, if the prescribed $\underset{\sim}{u}_0$ is a propagating flow (SW, IW, or AW), then the purely mechanical waves carry along with them their induced $\underset{\sim}{h}$ fields. Such OM "pseudoradiations" are treated in detail as propagating varieties of pure induction phenomena (Eqs. 18a, b, c, and h, above) in Secs. 4 through 6.

In the case of $\underset{\sim}{v} \neq 0$ (Eq. 16b), however, one has the possibility of the complete OM fields, $\underset{\sim}{h}$ and $\underset{\sim}{v}$, mutually interacting so as to produce a magnetomechanical wave propagation, or true OM radiation. In that case, we have to consider the coupled set of Maxwell-Navier-Stokes equations that we reduced in Sec. 2 essentially to Eqs. 5 and 12 plus subsidiary relations as required. These equations become by virtue of Eqs. 14 and 15 a linearized set coupling $\underset{\sim}{h}$ and $\underset{\sim}{v}$. With $\underset{\sim}{h}$ considered determined in terms of $\underset{\sim}{v}$ by Eqs. 5 and with $\underset{\sim}{g}$, $\underset{\sim}{\Omega}$ specified, Eqs. 12 represent four relations among five unknowns ($\underset{\sim}{v}$ and the OM perturbations in density and pressure, $\delta\rho$ and δp). To complete the system, simple equations of state and/or energy will suffice for the idealized situations (cases 1, 2, and 3, below) considered here. More general cases, of course, would require more detailed considerations of state and energy conservation.

1. Incompressible and Homogeneous Ocean: Under the simplest assumption the state equation is

$$\rho = \text{Constant in Space and Time} \quad .$$

In this case, Eqs. 5 and 12 yield the familiar Alfvén radiation (e.g., Ref. 14). For example, neglecting viscosities and earth rotation in Eq. 12a (Eq. 12b is simple div $\underset{\sim}{u} = 0$) and supposing the unperturbed ocean is at rest, we get the plane-wave dispersion relationship

$$\omega\left(\omega - \frac{ik^2}{\mu\sigma}\right) = k^2A^2\cos^2\theta_{kH}$$

between wave-vector ($\underset{\sim}{k}$) and frequency (ω), with A the Alfvén speed (Eq. 13) and θ_{kH} the angle between $\underset{\sim}{k}$ and $\underset{\sim}{H}_0$. But in the ocean, μ and A are so small that the dissipative term predominates, and

Ref. 14. J. M. Robertson, Hydrodynamics in Theory and Application, Prentice-Hall, NJ, 1965.

$k^2 \approx -i\mu\sigma\omega$ at any sensible frequency (viz., $\omega >> \mu\sigma A^2 \sim 10^{-11}$ Hz). In other words, an Alfvén wave is so highly damped in the ocean that it degenerates to simply a magnetic-diffusion wave (solution of Eq. 5a with $\underset{\sim}{u} = 0$).

2. Incompressible but Inhomogeneous Ocean: If the ocean is treated still as incompressible, but inhomogeneous, we can consider the density a Lagrangian constant, i.e., the equation of state is

$$\frac{d\rho}{dt} = 0 \qquad \text{or} \qquad \frac{\partial\rho}{\partial t} = -(\underset{\sim}{u} \cdot \underset{\sim}{\nabla})\rho \quad .$$

In this case, Eq. 12b is again div $\underset{\sim}{u} = 0$, but Eq. 12a with viscosities and earth rotation neglected involves the added term $\underset{\sim}{g}\delta\rho$, leading to internal gravity-magnetism waves. For example, if the unperturbed state is one of stable vertical (z) stratification, then the above equation linearizes to $(\partial/\partial t + \underset{\sim}{u}_0 \cdot \nabla)\delta\rho = -v_z \, d\rho_0/dz$. For a constant buoyancy frequency N (i.e., $\rho_0 \propto \exp(-N^2 z/g)$) and in the Boussinesq approximation, one obtains the plane-wave dispersion relationship

$$\left(\omega^2 - N^2\sin^2\theta\right)\left(\omega - \frac{ik^2}{\mu\sigma}\right) = \omega A^2 k^2 \cos^2\theta_{kH}$$

where θ is the angle $\underset{\sim}{k}$ makes with the vertical. Here if one neglects the oceanic A and σ as vanishingly small (again for frequencies $>> 10^{-11}$ Hz), one obtains in addition to the degenerate Alfvén (magnetic-diffusion) wave above, the usual internal-gravity modes ($\omega = \pm N \sin\theta$) for constant N. A more complete discussion, which also includes shear flow effects, will be found in Ref. 15.

3. Compressible but Adiabatic Ocean: When one admits compressible, but adiabatic, ocean motions, the linearized equation of state is

$$\rho = \rho_0[1 + \beta(p - p_0)] \qquad \text{or} \qquad \delta\rho = \frac{\delta p}{c_s^2}$$

Ref. 15. N. Rudraiah and M. Venkatachalappa, "Effect of ohmic dissipation on internal Alfvén-gravity waves in a conducting shear flow," J. Fluid Mech., Vol. 62, 1974, p. 705.

where $\beta \equiv 1/\rho_0 c_s^2$ is the compressibility and c_s the sound speed in the sea. In this case Eqs. 5 and 12 yield, in addition to the degenerate Alfvén wave of case 1 and the IW for stratified inhomogeneity of case 2, the magnetosonic radiations of compressible MHD. Neglecting damping and assuming ρ_0 to be uniform, we have for the dispersion relation of the magnetosonic modes

$$\omega^2 = \frac{1}{2} k^2 \left\{ (c_s^2 + A^2) + \left[(c_s^2 + A^2)^2 - 4 c_s^2 A^2 \cos^2\theta_{kH} \right]^{\frac{1}{2}} \right\}.$$

But in the ocean $A^2/c_s^2 \sim 10^{-12}$, so that with very little error the magnetosonic wave is simply the ordinary acoustic compression wave ($\omega^2 = k^2 c_s^2$). More detailed considerations, which also show the very slight MHD effects on damping and acoustic shear waves, will be found in Ref. 16.

From these examples, it will be clear that true OM radiation is not expected to be of significance in the ocean. However, we emphasize that the purely mechanical radiations (SW, IW, and AW) to which the magnetogravity and magnetosonic modes reduce in the ocean are still capable of propagating induced magnetic fields, the OM pseudoradiation referred to above. Thus, for example, ocean compressibility will allow what we will call, in contradistinction to the magnetosonic waves above, the sonomagnetic OM pseudowaves discussed in Subsecs. 5.3 and 6.6.

Ref. 16. G. I. Cohn, "MHD wave phenomena in seawater," Electromagnetics of the Sea, AGARD Conf. Proc. 77, 1970.

4. THEORY OF OM INDUCTION AND USEFUL FORMULAE

In the pure induction case (Eq. 16a) in which the flow is prescribed ($\underset{\sim}{u} = \underset{\sim}{u}_0$), Eqs. 5 alone determine the magnetic field,

$$\underset{\sim}{H} \equiv \underset{\sim}{H}_0 + \underset{\sim}{h} = \underset{\sim}{H}_e + \underset{\sim}{H}_b + \underset{\sim}{h} \tag{19}$$

(cf. Eqs. 14a and 17). By our definition of $\underset{\sim}{H}_0$ as independent of flow, we have $\underset{\sim}{H}_e$ and $\underset{\sim}{H}_h$ satisfying Eqs. 5 in the forms

$$\Delta \underset{\sim}{H}_e = \mu\sigma \frac{\partial \underset{\sim}{H}_e}{\partial t} \quad , \tag{20a}$$

$$\Delta \underset{\sim}{H}_b = \mu\sigma \dot{\underset{\sim}{H}}_b = \mu\sigma \left(\frac{\partial}{\partial t} + \underset{\sim}{V}_b \cdot \underset{\sim}{\nabla} \right) \underset{\sim}{H}_b \quad , \tag{20b}$$

$$\operatorname{div} \underset{\sim}{H}_e = \operatorname{div} \underset{\sim}{H}_b = 0 \quad . \tag{20c}$$

In Eq. 20b, $\dot{\underset{\sim}{H}}_b$ is time derivative in the body rest frame, i.e., $\underset{\sim}{H}_b$ is to be independent also of the mean relative flow of seawater corresponding to

$$\text{arbitrary body velocity} \equiv \underset{\sim}{V}_b(t) \quad . \tag{21}$$

One sees that in general neither $\underset{\sim}{H}_e$ nor $\underset{\sim}{H}_b$ are external fields, i.e., $\Delta \underset{\sim}{H}_{e,b} \neq 0$, since their time variations induce currents in the ocean $\underset{\sim}{j}_{e,b} \approx \operatorname{curl} \underset{\sim}{H}_{e,b} \neq 0$. As indicated in Sec. 3, we simply assume the solutions $\underset{\sim}{H}_{e,b}$ of Eqs. 20 as given for present purposes.

On inserting the decomposition (Eq. 19) for $\underset{\sim}{H}$ into Eqs. 5 and using Eqs. 20, we obtain the determining equations for the OM field,

$$\left(\frac{\partial}{\partial t} - \frac{1}{\mu\sigma} \Delta \right) \underset{\sim}{h} = \operatorname{curl}(\underset{\sim}{u}_0 \times \underset{\sim}{H}) + (\underset{\sim}{V}_b \cdot \underset{\sim}{\nabla}) \underset{\sim}{H}_b \quad , \tag{22a}$$

$$\operatorname{div} \underset{\sim}{h} = 0 \quad , \tag{22b}$$

which are exact within the HM approximation (Eq. 4) and the induction assumption (Eq. 16a).

An approximate form of Eq. 22a will suffice for discussion here. The convective term curl $(\underset{\sim}{u}_0 \times \underset{\sim}{H})$ is expected to be small (cf. Eq. 8), so that we shall set $\underset{\sim}{H} \approx \underset{\sim}{H}_0$ in it. Then, symmetrizing Eq. 22a by vector identities and Eq. 20c, we have

$$\left(\Delta - \mu\sigma \frac{\partial}{\partial t}\right)\underset{\sim}{h} \approx \mu\sigma \, \text{curl}(\underset{\sim}{H}_0 \times \underset{\sim}{u}_0 - \underset{\sim}{H}_b \times \underset{\sim}{V}_b) \quad . \tag{23}$$

Since this is linear in $\underset{\sim}{h}$, we can handle the body magnetization-translation interaction $(\underset{\sim}{H}_b \times \underset{\sim}{V}_b)$ separately from the other interactions $(\underset{\sim}{H}_0 \times \underset{\sim}{u}_0)$ below. In the latter, we usually consider $\underset{\sim}{H}_0 \approx \underset{\sim}{H}_e$ (i.e., $\underset{\sim}{H}_b \ll \underset{\sim}{H}_e$). In line with the remarks following Eq. 17, we treat $\underset{\sim}{H}_e$ as uniform and static and $\underset{\sim}{H}_b$ as intrinsically static, while of course $\underset{\sim}{V}_b$ is spatially invariant. Therefore, when $\underset{\sim}{V}_b$ is steady, both $\underset{\sim}{H}_0 \approx \underset{\sim}{H}_e$ and $\underset{\sim}{V}_b$ can be considered absolute constants. Notice that the flow $\underset{\sim}{u}_0$ is unrestricted (e.g., div $\underset{\sim}{u}_0 \neq 0$) and that $\underset{\sim}{h} \ll \underset{\sim}{H}_b$ is not assumed.

In general, to determine the complete march of magnitude and configuration for the vector field h requires a detailed analysis for each of the many varieties of given flow $\underset{\sim}{u}_0$ (Sec. 3). Various approaches are appropriate for various flows, as indicated briefly below (and in Appendix A). However, before carrying out detailed analyses, one would like to have some estimates, however crude, for the OM fields. Estimates for the sizes, and somewhat for the extents, are readily derived and will be the main subject of the rest of this report.

4.1 LOCAL ESTIMATOR FOR THE SIZE OF OM FIELDS

A rule of thumb for the magnitude of the OM field induced locally follows from a dimensional analysis. Thus, setting $\partial/\partial t \sim 1/T$, $\Delta^2 \sim 1/L^2$, and curl $\sim 1/L$ (cf. Eq. 4) in Eq. 23 with the body term put aside, we get

$$h \sim \frac{\mu\sigma u_0 L H_0}{1 + O(\tau_d/T)} \xrightarrow{\text{for } T \gg \tau_d} R_M \cdot H_0 \tag{24}$$

(cf. Eq. 8). Here L is the flow scale, which is assumed to set the $\underset{\sim}{h}$ field scale. (For the body term in Eq. 23, let $u_0 H_0 \to V_b H_b$ and L be the H_b scale.) The last form in Eq. 24 is the quasi-static limit (rate of change $1/T \ll$ diffusion rate $1/\tau_d$), which will be applicable for most OM induction effects. The opposite

limit, $T \ll \tau_d$ or $L^2 \gg T/\mu\sigma$ for which $h/H_0 \sim R_M T/\tau_d = u_0/(L/T)$, becomes important only for very long wave motions (cf. Sec. 4.3, where one notes that "quasi-static" does not mean "low frequency" for oceanic waves).

Numerically, the estimator (Eq. 24), with $\underset{\sim}{H}_0 \approx \underset{\sim}{H}_e$ and the values in Table 1, reads

$$h \lesssim \frac{1}{4} u_0 L \quad (\text{in } \gamma = 10^{-5} \text{ G}) \tag{25}$$

for u_0 in m/s and L in m. We emphasize that this is only an order-of-magnitude upper limit, and in special cases the field could be much smaller. (For example, for a uniform field $\underset{\sim}{H}_0$ and an incompressible flow $\underset{\sim}{u}_0$ that varies only transversely to $\underset{\sim}{H}_0$, the right-hand side of Eq. 23 vanishes and $\underset{\sim}{h} = 0$.) Nevertheless, Eq. 25 affords a useful rule of thumb when used with proper discretion.

4.2 A THEOREM ON THE EXTENT OF OM FIELDS

For a localized, incompressible flow in the quasi-static limit, an explicit formula for the OM field $\underset{\sim}{h}$ at distant points $\underset{\sim}{R}$ can be derived in terms of the spin angular momentum $\underset{\sim}{S}$ of the flow, as follows.

Equations 23 and 22b, with $\partial/\partial t$ neglected ($T \gg \tau_d$), $\underset{\sim}{H}_0 \approx \underset{\sim}{H}_e$ uniform, div $\underset{\sim}{u}_0 = 0$, and the body term set aside, possess the integral solution

$$\underset{\sim}{h}(\underset{\sim}{R}) = \frac{\mu\sigma}{4\pi} (\underset{\sim}{H}_e \cdot \underset{\sim}{\nabla}) \int d\underset{\sim}{r}\, \underset{\sim}{u}_0 \frac{1}{|\underset{\sim}{R} - \underset{\sim}{r}|} , \tag{26}$$

plus vector harmonics as needed to satisfy boundary conditions (cf. Appendix A). Consider distant field points $\underset{\sim}{R}$ well outside the flow region. Then the integral in Eq. 26 can be approximated by a Maclaurin expansion of $1/|\underset{\sim}{R} - \underset{\sim}{r}|$ as

$$\int d\underset{\sim}{r}\, u_{0i}/|\underset{\sim}{R} - \underset{\sim}{r}| = (1/R) \int d\underset{\sim}{r}\, u_{0i} - (\underset{\sim}{\nabla}\, 1/R)_j \int d\underset{\sim}{r}\, r_j\, u_{0i} + O(1/R^3)$$

in tensor notation. In these integrals, by hypothesis:

1. div $\underset{\sim}{u}_0 = 0$, so that $u_{0i} = \text{div}(r_i \underset{\sim}{u}_0)$ and $r_j u_{0i} = \frac{1}{2}\text{div}(r_i r_j \underset{\sim}{u}_0) + \frac{1}{2}(u_{0i} r_j - u_{0j} r_i)$, by vector identities; and

2. $\underset{\sim}{u}$ is localized, so that the divergence terms give vanishing surface integrals (specifically, we require $\underset{\sim}{u}_0$ to decrease faster than $1/r^4$ asymptotically).

Thus, we get

$$\int d\underset{\sim}{r}\, \underset{\sim}{u}_0 / |\underset{\sim}{R} - \underset{\sim}{r}| \approx \frac{1}{2} (\underset{\sim}{\nabla}\, 1/R) \times \int d\underset{\sim}{r}\, (\underset{\sim}{r} \times \underset{\sim}{u}_0) \quad , \tag{27}$$

in which we recognize the last integral to be $\underset{\sim}{S}/\rho$ for a flow region of total spin $\underset{\sim}{S}$ and homogeneous density ρ. Combining Eqs. 27 and 26 gives then

$$\underset{\sim}{h}(\underset{\sim}{R}) = - \frac{\mu\sigma}{8\pi\rho} (\underset{\sim}{H}_e \cdot \underset{\sim}{\nabla})(\underset{\sim}{S} \times \underset{\sim}{\nabla}) \frac{1}{R} + O\left(\frac{1}{R^4}\right) \tag{28}$$

for sufficiently localized, incompressible, quasi-static flow in approximately homogeneous infinite medium. The presence of the air-sea boundary will modify this, but the complete solution will retain comparable magnitude in general. (An exception is the highly symmetric case where $\underset{\sim}{S}$ and $\underset{\sim}{H}_e$ are both vertical, for which the complete solution includes an image field that exactly cancels Eq. 28 everywhere on the sea surface and, thus, by Eq. 10b gives zero aerofield; cf. Sec. 6.4.)

Therefore, on working out the derivatives in Eq. 27, we have the explicit theorem

$$\underset{\sim}{h}(\underset{\sim}{R}) \approx \frac{\mu\sigma}{8\pi\rho} \underset{\sim}{S} \times [\underset{\sim}{H}_e - 3\hat{\underset{\sim}{R}}(\hat{\underset{\sim}{R}} \cdot \underset{\sim}{H}_e)] \quad \frac{1}{R^3} \tag{29}$$

under the conditions stated above, wherein $\hat{\underset{\sim}{R}} \equiv \underset{\sim}{R}/R$. Notice that this falls off with distance like a dipole field, $\propto 1/R^3$, but of course with a more complicated directional dependence. Its magnitude then may be represented in terms of effective dipole magnitude,

$$|\underset{\sim}{h}(\underset{\sim}{R})| \approx \frac{m_{eff}}{R^3} \quad , \tag{30a}$$

where

$$m_{eff} \sim \frac{\mu\sigma S H_e}{8\pi\rho} \sim R_M \cdot \underset{\sim}{u}_e \cdot \frac{Vol}{8\pi} \quad , \tag{30b}$$

in which Vol denotes the flow region volume. Alternatively, one can write the distant field estimate (Eqs. 30) as

$$h_{(distant)} \sim h_{(local)} \cdot \left(\frac{Vol}{8\pi R^3}\right) \quad , \tag{31}$$

in terms of the local estimator of Eqs. 24 and 25.

The above theorem and its derivation are mathematically analogous to a well-known magnetostatic theorem (Ref. 17, p. 145) expressing the vector potential due to localized, divergenceless currents in terms of their magnetic moment: $\underset{\sim}{A} \propto \int d\underset{\sim}{r}\, \underset{\sim}{j}/|\underset{\sim}{R} - \underset{\sim}{r}| \propto (\underset{\sim}{\nabla}\, 1/R) \times \underset{\sim}{m}$ (cf. Eq. 27). However, there is the important difference that the induced OM currents here are not localized. That is, whereas in the magnetostatic case the exterior current is zero ($\underset{\sim}{H} \propto$ curl $\underset{\sim}{A} \propto$ grad $(\underset{\sim}{m} \cdot \underset{\sim}{\nabla})1/R$, so that $\underset{\sim}{j}$ = curl H = 0), in the induction case here one has from Eqs. 7a and 24 the distant ("return") current

$$\underset{\sim}{j}(R) \approx \left(\frac{\mu\sigma}{8\pi\rho}\right)(\underset{\sim}{H}_e \cdot \underset{\sim}{\nabla})(\underset{\sim}{S} \cdot \underset{\sim}{\nabla})\underset{\sim}{\nabla}\, \frac{1}{R} \sim \frac{m_{eff}}{R^4} \quad , \tag{32}$$

which is nonzero.

The theorem 29 and resulting estimates 30 through 32 will clearly be most useful for localized flows such as an isolated wave crest or the wake of a body traversing the ocean.

Ref. 17. J. D. Jackson, Classical Electrodynamics, 2nd edition, Wiley, New York, NY, 1975.

4.3 FLOW-WAVE INDUCTION OF OM PSEUDOWAVES

At the other extreme from localized flows, consider flow-fields of large spatial extent that can be Fourier space-time transformed into harmonic wave components. In the ocean, familiar examples are various gravity waves and acoustic fields. Then, one has to deal with induction by the transformed flow in Eq. 23 that becomes linear with constant coefficients on setting aside the body term $\underset{\sim}{H}_b \times \underset{\sim}{V}_b$, taking $\underset{\sim}{H}_0 \approx \underset{\sim}{H}_e$ uniform and static, and $\mu\sigma$ constant. Thus, Eq. 23 trar forms to yield the OM field also in harmonic waves:

$$\underset{\sim}{u}_0 \to \underset{\sim}{\tilde{u}}_0(z)e^{i\omega t - i\underset{\sim}{\kappa}\cdot\underset{\sim}{r}} \Rightarrow \underset{\sim}{h} \to \underset{\sim}{\tilde{h}}(z)e^{i\omega t - i\underset{\sim}{\kappa}\cdot\underset{\sim}{r}} \tag{33}$$

for a flow wave of (angular) frequency ω and horizontal wave vector $\underset{\sim}{\kappa}$. This assumes an ocean of infinite, homogeneous horizontal extent, but of course vertical (z) discontinuity or inhomogeneity is allowed for in the amplitudes, $\underset{\sim}{\tilde{u}}_0(z)$ and $\underset{\sim}{\tilde{h}}(z)$. Notice that the OM frequency and wave vector, and correspondingly its phase and group velocities, are identical with those of the flow wave. That is, the induction wave propagates exactly as does the given flow wave. Physically, the magnetism simply rides along on the mechanical wave, whence we call it OM pseudoradiation.

The amplitude of the OM pseudowave (Eq. 33) may be estimated from Eq. 23, just as was done in Eq. 24 and the following discussion, with $T \to 1/\omega$. Thus we have the limiting behaviors

$$\tilde{h} \sim \begin{cases} \tilde{R}_M \cdot H_e & \text{for} \quad \omega L^2 << \dfrac{1}{\mu\sigma} \qquad (34a) \\ \dfrac{\tilde{u}_0}{\omega L} \cdot H_e & \text{for} \quad \omega L^2 >> \dfrac{1}{\mu\sigma} \ , \qquad (34b) \end{cases}$$

where $\tilde{R}_M \equiv \mu\sigma\tilde{u}_0 L$. Except for waves long enough for the vertical scale length to enter, we have $L \sim 1/\kappa$ and $\omega L \sim$ the wave phase speed, $c_{ph} \equiv \omega/\kappa$ (cf. $L/T \to c_{ph}$ below Eq. 24). Equation 34a corresponds to the quasi-static limit in Eq. 24, and Eq. 34b to the nonstationary limit indicated following Eq. 24. Notice that in the latter case the OM field is independent of the ocean parameters μ and σ, except as they delimit the ω-L regime. We emphasize that the quasi-static limit is not generally the same as a low-frequency limit. Rather, for oceanic varieties of wave motion,

Eq. 34a is the short wavelength ($\lambda \equiv 2\pi/\kappa$), high-frequency limit, while Eq. 34b obtains for long, low-frequency waves.

To be specific, the two regimes in Eqs. 34 are delimited by the criterion function $\omega = 1/\mu\sigma L^2$, which is $\gtrsim \kappa^2/\mu\sigma$, whereas all ocean waves have the dispersion relation $\omega = \omega(\underset{\sim}{\kappa})$ increasing less rapidly than κ^2 for all $\underset{\sim}{\kappa}$. Consequently, the quasi-static case (Eq. 34a) is certain to obtain for ω, κ sufficiently above (or λ below) a point ω_0, κ_0 (or λ_0). On the other hand, the opposite limit (Eq. 34b) may or may not obtain at $\omega < \omega_0$, $\lambda > \lambda_0$, depending on the vertical scale length (e.g., see Subsec. 5.1.5. In particular, the dispersion relations for SW on ocean of depth D, for IW on a relatively sharp density change $\delta\rho/\rho$ at depth $d \ll D$, and for AW of constant speed c_s with a hard ocean bottom, are respectively

$$\text{SW:}\quad \omega^2(\underset{\sim}{\kappa}) = g\kappa \tanh \kappa D \quad , \tag{35a}$$

$$\text{IW:}\quad \omega^2(\underset{\sim}{\kappa}) = \frac{g\kappa(\delta\rho/\rho)}{[\coth \kappa d + \coth \kappa(D-d)]} \quad , \tag{35b}$$

$$\text{AW:}\quad \omega^2(\underset{\sim}{\kappa}) = c_s^2 \left[\kappa^2 + \frac{\left(\ell + \tfrac{1}{2}\right)^2 \pi^2}{D^2}\right], \quad (\text{modes } \ell = 0,1,2,\ldots) \quad . \tag{35c}$$

(For the shorter, capillary SW and the small-scale IW, as well as Coriolis effects, see Ref. 18. The hypothetical case of "bound" SW is discussed in Subsec. 5.1.5.) In the three cases (Eqs. 35), one finds for the quasi-static limit above ($\omega > \omega_0$ and $\lambda < \lambda_0 = 2\pi/\sqrt{\mu\sigma\omega_0}$) the values:

$$\text{SW:}\quad \omega_0 = \mu\sigma g D \quad \text{for} \quad D \lesssim 1 \text{ km},$$

$$\omega_0 = (\mu\sigma g^2)^{\frac{1}{3}} \quad \text{for} \quad D \gtrsim 2 \text{ km} \quad ;$$

$$\text{IW:}\quad \omega_0 = \mu\sigma g d\,(\delta\rho/\rho) \quad ;$$

$$\text{AW:}\quad \omega_0 = \mu\sigma c_s^2 \quad .$$

The frequency-wavelength ($\nu \equiv \omega/2\pi$, $\lambda \equiv 2\pi/\kappa$) dispersion curves (Eqs. 35) are illustrated numerically in Fig. 1 for typical

---

Ref. 18. O. M. Phillips, The Dynamics of the Upper Ocean, Cambridge University Press, 1966.

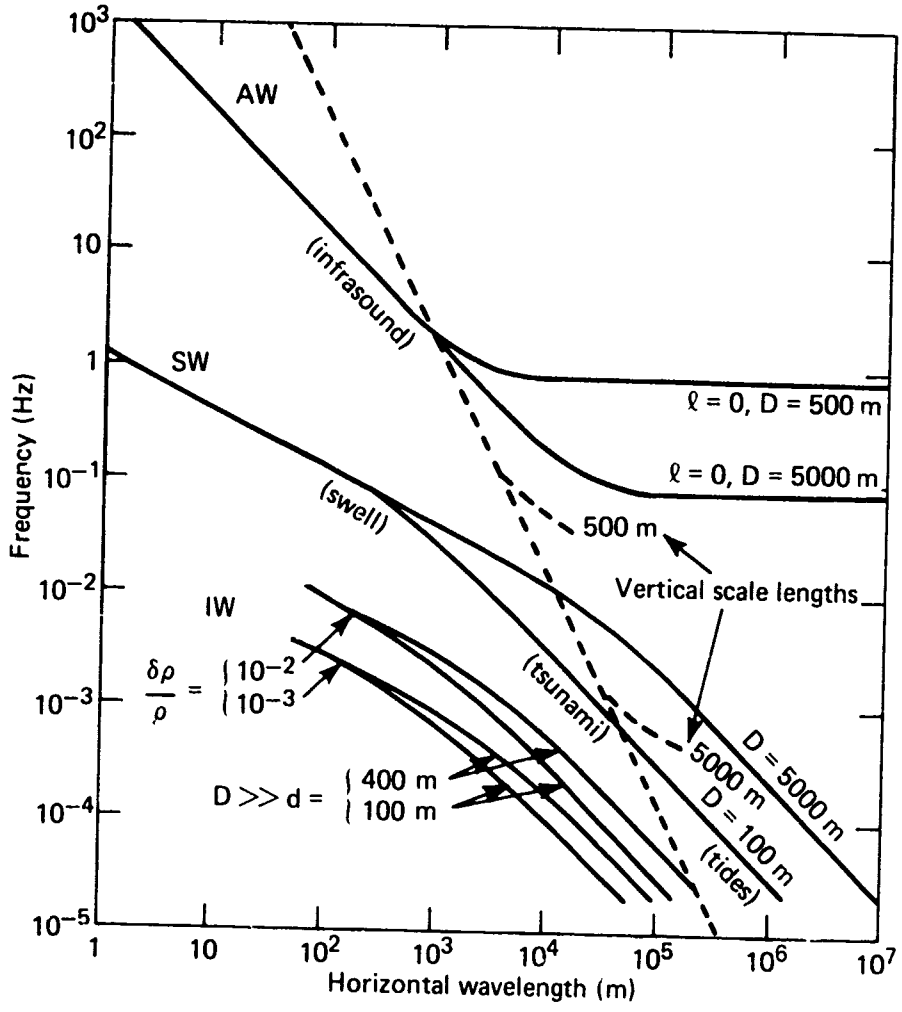

Fig. 1 Ocean Wave Dispersion Curves of Acoustic (AW), Surface (SW), and Internal (IW) Wave Motions for Various Ocean Depths (D), Pycnocline Depths (d), and Density Changes ($\delta\rho/\rho$), Sonic Mode (ℓ), with IW Truncated at Brunt-Vaisala Frequency for a 25-m-Thick Pycnocline. Dashed line separates quasi-static (left) and nonstatic (right) regimes of OM pseudoradiation (cf. Eq. 34a).

ocean parameters. The dashed diagonal line represents the limiting locus (ν_0,λ_0) for the quasi-static approximation (Eq. 34a) to become valid for infinite vertical scale length, while departures from this locus due to finite vertical scale are indicated at $\kappa \leqslant 1/D$ $(\lambda \geqslant 2\pi D)$. One sees that the quasi-static approximation Eq. 34a holds for: (a) all internal waves but those of tidal frequencies; (b) all surface waves to well below the swell band, breaking down only for the rare tsunami or longer waves; and (c) all acoustic waves of audio frequency or higher. The non-static limit (Eq. 34b) can obtain, on the other hand, for deep-water tsunamis, tides, and infrasound.

5. ESTIMATES OF OM INDUCTION BY NATURAL SEA MOTIONS

From the foregoing theory, we will estimate in this section the OM fields induced by the various flows due to natural sea movements, as listed in Eqs. 18a through 18d. Aside from their intrinsic interest (e.g., for ocean wave studies), these naturally induced fields are important as noise background for observations on the body-related OM fields treated in Section 6.

As indicated in the Introduction, the estimates in this section and in Sec. 6 are intended to be simple and clear, rather than precise. When available, more detailed analyses will be cited for more exact results.

5.1 SURFACE WAVES

The OM field induced by the interaction of $\underset{\sim}{H}_e$ with the most common ocean waves, sea and swell, have been discussed by a number of authors (cf. Refs. 4, 6, and 8, and others cited therein). Longer waves such as tsunamis were considered by Larsen (Ref. 9). We can collate and summarize the essential results of these detailed calculations by means of the foregoing theory. First we consider the cases of sea and swell on deep ocean, as well as swell in shelf waters, which come under the quasi-static approximation of Eq. 34a. We then go on to the longer waves for which Eq. 34b obtains.

Linear plane gravity waves of frequency $\omega = 2\pi\nu$, wave vector $\underset{\sim}{\kappa}$, and amplitude $\tilde{a}_\nu$ have flow speed and scale roughly

$$\tilde{u}_0 \sim \frac{\omega \tilde{a}_\nu}{\tanh \kappa D} \qquad \text{and} \qquad L \sim \frac{\tanh \kappa D}{\kappa} \tag{36}$$

near the sea surface ($z = 0$), where of course u_0 is largest. Then one has

$$\tilde{h} \leq H_e \mu \sigma \tilde{a}_\nu \frac{\omega}{\kappa} \sim \frac{1}{4} \tilde{a}_\nu \frac{\omega}{\kappa} \gamma \tag{37}$$

from the quasi-static Eq. 34a, which applies to both swell and sea (Fig. 1).

On the deep ocean ($D > 1/\kappa$, $\omega^2 \approx g\kappa$), $\tilde{u}_0$ decreases $\propto e^{\kappa z}$ below the surface ($z < 0$), and completing the OM solution to fit the boundary condition of Eq. 10b introduces a factor of $\frac{1}{4}$ into the surface field. Then more accurately

$$\tilde{h}_{surface} \approx \frac{1}{10} \frac{\tilde{a}_\nu}{\nu} \text{ in } \gamma \quad , \tag{38}$$

while $\tilde{h}$ decreases essentially exponentially with depth ($\tilde{\propto} 2\kappa z e^{\kappa z}$ for $-z >> 1/\kappa$). At altitudes $z \geq 0$, Eq. 11b with $\kappa = \omega^2/g \approx 4\nu^2$ gives at once, from Eq. 38,

$$\tilde{h}_{air} \approx \frac{1}{10}\left(\frac{\tilde{a}_\nu}{\nu}\right) e^{-4z\nu^2} \ \gamma \text{ (deep water)} \quad . \tag{39a}$$

Detailed analysis modifies these expressions by a directional factor involving the magnetic dip angle (I) and the wave propagation angle (θ_κ) relative to magnetic north, namely,

$$\sqrt{\sin^2 I + \cos^2 I \cos^2 \theta_\kappa} \quad ,$$

which is of order unity, except for east-west waves in the tropics when it approaches zero (cf. Ref. 6). We set aside that case here.

In shallow waters ($\kappa D < 1$, $\omega \approx \kappa\sqrt{gD}$), bottom effects become important. The flow amplitude $\tilde{u}_0$ has little depth variation, and the OM field penetrates to the seabed where it must be made continuous into the conducting sediments. Detailed solutions are given by Larsen (Ref. 9) and numerical results by Klein et al. (Ref. 4). But observe simply that the above estimates remain valid as to order of magnitude provided that instead of $\kappa \approx \omega^2/g$ we use $\kappa \approx \omega/\sqrt{gD}$, according to Eq. 35a. Thus, Eq. 39a becomes

$$\tilde{h}_{air} \sim \left(\frac{\sqrt{D}}{5}\right) \tilde{a}_\nu \, e^{-2z\nu/\sqrt{D}} \ \gamma \text{ (shallow water)} \quad . \tag{39b}$$

Note from Eq. 35a that $\kappa D < 1$ implies $D \lesssim \frac{1}{5} T^2$, which, for periods T up to the longest (20 s) swells, gives $D \lesssim 80$ m, i.e., the shallowest shelf waters.

The above estimates make clear the very few factors that fix the gross field magnitude. The dominant factor is the exponential altitude (and depth) behavior, such that the lowest frequency

waves can be larger, since $a_v \propto 1/\nu^2$ for given steepness $(2a_v/\lambda)$. Thus, the lowest frequency waves also tend to induce OM fields of the most sizable amplitude. More precise statements require specification of the wave power spectrum, which depends on local winds and distant storms. Representative spectra for the corresponding sea waves and ocean swells are sketched in Fig. 2. We stress, however, that the actual spectra obtaining in varied environments remain the major uncertainty in applications.

5.1.1 Swell

Ocean swell consists of long, not very steep waves that have run faster and farther (i.e., $c_{ph} = \sqrt{g\kappa} \propto \sqrt{\lambda}$ and less dissipation) than their shorter, steeper siblings from a storm center. At a distant site, typical swell then exceeds sea waves in the important low-frequency regime when local winds are below gale strength (speeds $\leq$ 25 knots, cf. Fig. 2). More detailed comparison of swell and sea will be made in Sec. 5.1.3.

The swell has a relatively narrow-band spectrum, periods $T \sim$ 10-20 s (Fig. 2). Swell wave-steepness, $\delta \equiv 2a_v/\lambda$, is far below the ideal limit (1/7), or even the observed wind-wave limits ($\leq 1/10$). A nominal steepness might be $\delta \leq 1\%$, in which case $a_v \sim \delta \cdot T^2 \leq$ 1-4 m (cf. $\lambda \sim$ 160-640 m). In any event, from Eqs. 38 and 39a we have

$$\text{Swell:} \quad \begin{cases} \tilde{h}_{surface} \approx a \cdot \frac{T}{10} \leq 1\ \gamma \ , & (40) \\ \tilde{h}_{air} \approx a \cdot \frac{T}{10} \cdot e^{-4z/T^2} \leq e^{-z/(25\ \text{to}\ 100)}\ \gamma \ , & (41) \end{cases}$$

with $T \sim$ 10-20 s and $a \leq$ 1 m.

Thus, for example, a magnetometer of sensitivity $10^{-4}\ \gamma$ could register swell-induced OM up to altitudes of order

$$z_{max} \sim 2.4T^2 \sim 200 \text{ m to } 1 \text{ km} \qquad (42)$$

when $a \sim$ 1 m and $T \sim$ 10-20 s (and to depths of similar order).

We note that in the case of shallow-water, long-period swell (Eq. 39b above), Eqs. 40 and 41 are multiplied by a factor $2\sqrt{D}/T < 1$ and the exponent in Eq. 41 is divided by the same factor.

Thus, the OM field becomes smaller and less extensive ($\to 0$ as $D \to 0$) for the shallower shelf waters.

5.1.2 Sea

The rms OM field induced by a random sea-wave field is determined by ensemble-averaging Eqs. 38 and 39a appropriately. Since $\tilde{h} \propto a_\nu$, this means

$$h_{rms} = \left[\frac{1}{2}\int_0^\infty d\omega\ S(\omega)\left(\frac{\tilde{h}}{a}\right)^2\right]^{\frac{1}{2}}$$

where $S(\omega)$ is the power spectrum of wave amplitudes a_ω, and the factor $\frac{1}{2}$ arises from time averaging. Sea spectra are relatively broadband (Fig. 2) and vary with wind speed (W), fetch, and duration. As an upper limit, one can consider a fully arisen sea (long fetch and duration, so only W remains as a parameter) and adopt one of the simple phenomenological spectra that have been proposed. In general, these spectra fall exponentially with de-

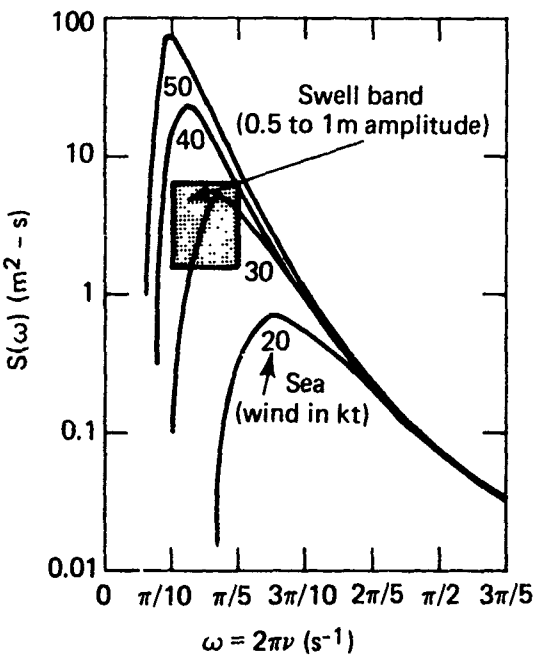

Fig. 2 Sea and Swell Wave Spectra for Pierson-Moskowitz (Ref. 19) Seas and Typical Deep-Ocean Swells

creasing ω, competing with the opposite exponentiation in $\tilde{h}$ (Eq. 39). The essential result is a weakened altitude fall-off for h_{rms} as compared with $\tilde{h}$. Thus, the spectral forms discussed by Pierson and Moskowitz (Ref. 19) and the resulting asymptotic behavior of h_{rms} are, aside from algebraic factors,

$$S(\omega) \propto e^{-b/\omega^n} \Rightarrow h_{rms} \tilde{\propto} e^{-b' z^m} \quad ,$$

according to the integral approximation given below. Here $m \equiv n/(n+2)$ is always < 1 and therefore h_{rms} exponentiates less rapidly than the components $\tilde{h}$ in Eq. 39a.

For more specific results, we will adopt the generally accepted spectrum recommended by Pierson and Moskowitz,

$$S(\omega) = \left(\frac{0.8}{\omega^5}\right) \exp\left(\frac{-\beta g^4}{W^4 \omega^4}\right) m^2 - s \quad ,$$

where $\beta \equiv 0.74$. The older Neumann spectrum has been used in earlier detailed calculations, which are summarized into simple formulae at the end of this section.

Evaluation of the integral for h_{rms} at the surface ($z = 0$) is elementary, while that at sufficient altitude can be approximated by the general asymptotic formula

$$\int_0^\infty d\omega g(\omega) e^{-f(\omega)} \sim \left[\frac{2\pi}{f''(\omega_0)}\right]^{\frac{1}{2}} g(\omega_0) e^{-f(\omega_0)}$$

in which ω_0 is the solution of $f'(\omega_0) = 0$. In this way we derive the useful simple estimators

Sea:

$$h_{rms}(z = 0) \leqslant \left(\frac{W_K}{30}\right)^3 \gamma \tag{43}$$

$$h_{rms}\left(z > \frac{1}{\alpha}\right) \leqslant \left(\frac{W_K}{30}\right)^3 \cdot (\alpha z)^{\frac{1}{3}} e^{-(\alpha z)^{\frac{2}{3}}} \gamma \tag{44}$$

Ref. 19. W. J. Pierson, Jr., and L. Moskowitz, "A proposed spectral form for fully developed wind seas based on the similarity theory of S. A. Kitaigorodskii," J. Geophys. Res., Vol. 69, 1964, p. 5181.

where $\alpha \equiv (3/2)^{3/2}\sqrt{\beta}\ gW^2 = (7.65/W_K)^2$ per m and W_K is wind speed in knots (K). Notice that Eq. 44 usually obtains at reasonable altitude. since $z > 1/\alpha \leqslant 10$ m for subgale winds, becoming only ~40 m for a whole gale ($W_K \sim 50$). One may interpolate roughly between $z = 0$ (Eq. 43) and $z > 1/\alpha$ (Eq. 44).

For sea, therefore, a magnetometer of sensitivity 10^{-4} γ could register the induced field to altitudes (or depths) given roughly by

$$\left|z_{max}\right| \sim \frac{1}{2} W_K^2 \cdot \left[1 + \frac{1}{2} \ln\left(\frac{W_K}{30}\right)\right] \tag{45}$$

for winds from a gentle breeze up to hurricane strengths. The height (Eq. 45) exceeds 1 km only for strong gales and decreases rapidly for lesser winds.

In comparison with the Person-Moskowitz sea, the Neumann spectrum $S(\omega) \propto \omega^{-6} \exp(-2g^2/W^2\omega^2)$ gives a more extensive field. By the methods above, we can derive formulae corresponding to Eqs. 43, 44, and 45, viz.:

$$h_{rms}(z = 0) \leqslant \left(\frac{W_K}{25}\right)^{\frac{7}{2}} ;$$

$$h_{rms}\left(z > \frac{1}{\alpha'}\right) \leqslant \left(\frac{W_K}{25}\right)^{\frac{7}{2}} \cdot (\alpha' z)^{\frac{3}{4}} e^{-(\alpha' z)^{\frac{1}{2}}}$$

where $\alpha' \equiv 4g/W^2 = (12.2/W_K)^2$ per m; and $\left|z_{max}\right| \sim W_K^2 \cdot [1 + \ln(W_K/25)]$.

5.1.3 Swell versus Sea

Comparison of Eqs. 40, 41, and 42 for "typical" swell and Eqs. 43, 44, and 45 for a "full" sea shows that it requires a gale for the OM field induced by sea to exceed in size and extent that induced by swell, if present. That is, the relative steepness (δ up to 10%) of sea waves is more than offset by the low-frequency content of ocean swell, unless a gale develops. Notice further that, by its nature, swell is widespread in contrast to localized high-sea conditions. Thus, swell also tends to dominate sea in horizontal extent over the ocean.

Figure 3 illustrates the swell- and sea-induced OM field magnitudes given by Eqs. 41 and 44 as functions of altitude. Curves at depth display similar behavior, except that $\tilde{h}$ is increased by a factor $\sim 2\kappa|z| = 8|z|/T^2$ at depths $|z| \gtrsim 1/\kappa \approx T^2/4$, where, however, exponential decrease also becomes dominant. More detailed curves will be found, for example, in Ref. 4. However, Fig. 3 is sufficient to show the sizes and relative regimes of swell and sea OM. As indicated in the figure caption, Neumann sea spectra considerably overestimate the OM field at altitude relative to Pierson-Moskowitz sea spectra estimates.

5.1.4 Large Wave Crests

We have so far considered linearized wave theory. Waves of finite height (Ref. 20, Sec. 250) contain higher harmonics, but these are of relative size $\kappa a = \pi\delta << 1$ even for the steepest sea waves. Thus, the finite amplitude harmonics introduce negligible corrections to the preceding formulae. However, nonlinear waves do not superpose additively, and hence, in a high sea, chance combination of waves can form individual wave crests of exceptional height.

An isolated high crest will produce an excess contribution to the OM field through its associated mean flow. Naturally, this cannot be treated by the plane wave theory as above. Instead, the crest OM field may be estimated by the localized flow theory of Sec. 4.2. From Ref. 20, the crest possesses a mean flow $\bar{u}_0 = \kappa^2 a^2 c_{ph} e^{2\kappa z}$ ($z \leq 0$, $c_{ph} = \omega/\kappa$) with scale-length $L \sim 1/\kappa$, so that its magnetic Reynolds number is $R_M \sim \mu\sigma a^2\omega$ over a depth $\sim 1/2\kappa$ and a horizontal area $\sim(\pi/\kappa)L_{cr}$ where L_{cr} is the transverse crest length; i.e., Vol $\sim \pi L_{cr}/2\kappa^2$ in Eqs. 30 and 31. According to Eq. 24, this flow in the earth field induces a local OM field that is $\sim\kappa a << 1$ times the linear wave result of Eq. 38. However, at distances $R >> L_{cr}$, the field falls off as $1/R^3$ according to Eqs. 30, instead of exponentially as in Eq. 39. Further, since it varies $\propto a^2$ instead of linearly with amplitude as in Eqs. 38 and 39, it is possible for an exceptionally high crest to exceed the overall sea in the higher altitude OM field.

The crest flow induces currents whose effective dipole moment is $m_{eff} \sim H_e\mu\sigma a^2\omega L_{cr}/16\kappa^2$ according to Eq. 30b with the above R_M and Vol expressions. For a deep sea ($\omega^2 \approx g\kappa$) then $m_{eff} \sim \frac{1}{4}\mu\sigma g H_e \cdot (a^2 L_{cr}/4\omega\kappa)$, cf. Eq. 38. Hence, at ranges $R >> L_{cr}$, we have from Eq. 30a

---

Ref. 20. H. Lamb, Hydrodynamics (1932), 6th edition, Dover, 1945.

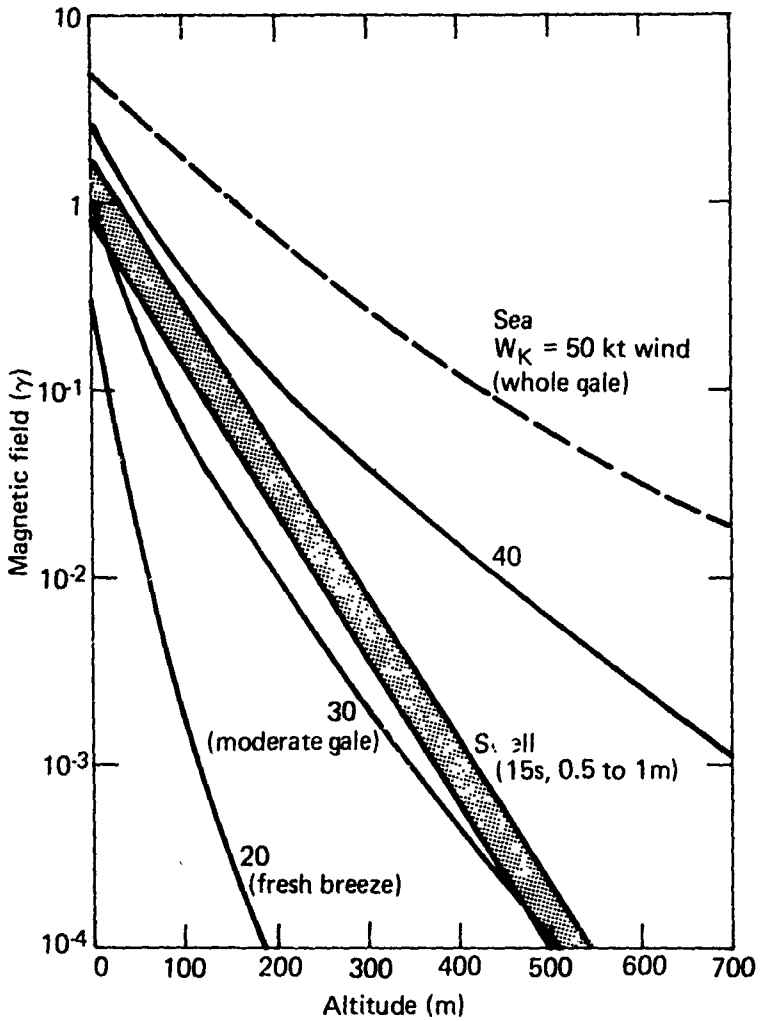

Fig. 3 OM Field Estimates for Pierson-Moskowitz Seas and Deep-Ocean Swells. Dashed-line (whole-gale) sea is rarely fully arisen. Note: Neumann-sea OM would be much larger, e.g. the fresh-breeze OM would approach the moderate-gale curve shown, while fresh-gale (37-kt) OM would lie near the whole-gale curve.

$$\text{Crest:}\quad h \sim \frac{1}{10}\,\frac{a}{\nu}\cdot\left(\frac{aL_{cr}}{4\kappa R^3}\right)\,\gamma\ , \tag{46}$$

where the factor $(aL_{cr}/4\kappa R^3) \propto 1/R^3$ now replaces the exponential factor in Eq. 39.

Again, for numerical illustration we assume sensitivity $10^{-4}\ \gamma$ and find the maximum range

$$R_{max} \sim 4(a^2L_{cr})^{\frac{1}{3}}\ T \leqslant 1\ \text{km}\ , \tag{47}$$

where the upper limit assumes a long $T \sim 20$ s, an $L_{cr} \sim 1/\kappa \sim 100$ m, and a crest height $a \sim 3$ m which might occur occasionally in a sea state of about 6 ($W_K \sim 30$ knots). Thus, an isolated high crest can sometimes produce an OM field exceeding that of swell at altitudes ~ 1 km. Notice that, since the crest moves at speed c_{ph}, its OM field is like that of the effective dipole moving at speed $\sim\frac{1}{2}T$ m/s $\sim T$ knots.

5.1.5 Long Waves

We turn briefly to low-frequency, long-wavelength SW, for which the nonstatic limit of Eq. 34b can become applicable (cf. Fig. 1). Aside from the tides, long ocean waves are rare, i.e., large seismic sea waves (tsunamis) occur approximately once a year. Nevertheless, the HM effects of both tides and tsunamis have been analyzed and compared with observation by Larsen (Refs. 9 and 21). As the numerical results of his detailed analyses are readily estimated as to order of magnitude from our theory, we shall do so for completeness. Our estimates will not include the finer effects due to sediment and/or mantle conductivities (of significance only for the longest waves), for which see Ref. 9 (Table 1). Note that his "induction parameter" Q is essentially our $\omega\tau_d$.

A deep-ocean tsunami falls under the nonstatic regime of Fig. 1. Hence, Eq. 34b and the following discussion, together with $L \sim 1/\kappa$, $\tilde{u}_0 \sim ag\kappa/\omega$ (see Eq. 39b), and $\omega/\kappa \equiv c_{ph} \approx \sqrt{gD}$ (Eq. 35a), gives at once

---

Ref. 21. J. C. Larsen, "Electric and magnetic fields induced by deep sea tides," Geophys. J. Roy. Astron. Soc., Vol. 16, 1968, p. 47.

$$\frac{h}{H_e} \sim \frac{\tilde{u}_0}{c_{ph}} \sim \frac{a}{D} \quad , \tag{48}$$

which is simply the tsunami-amplitude/ocean-depth ratio. For $a \sim 0.2$ m, $D \sim 5$ km, and $H_e \sim \frac{1}{2} \cdot 10^5$ γ, this yields OM field magnitudes of $h \sim 2$ γ, as were obtained in Ref. 9.

A shallow-water tsunami, on the other hand, falls into the quasi-static regime of Fig. 1. Then Eq. 39b applies and

$$h \sim \frac{1}{5} a\sqrt{D}\ \gamma \quad . \tag{49}$$

Thus, for $a \sim 0.2$ m and $D \sim 200$ m, we get $h \sim 0.6$ γ, as in Ref. 9.

The tides considered as free waves (e.g., in the Atlantic or Pacific basins) of frequency $\nu \leq 2 \cdot 10^{-5}$ Hz have, from Eq. 35b,

$$\frac{h}{H_e} \sim \frac{\kappa\tilde{u}_0}{\omega} = \frac{\tilde{u}_0}{c_{ph}} \sim \frac{a}{D} \quad , \tag{50}$$

the same as for the deep-water tsunami. Modifications due to boundary effects, such as proximity to an ocean island, are calculated in Ref. 21.

All of these OM fields are very large scale, comparable to that of the long SW (>100 km, cf. Fig. 1), both horizontally and vertically from sea bottom to the air above the sea surface. Thus, locally they appear as periodic geomagnetic noise components.

5.1.6 Bound Waves

It is possible that a high-frequency system of bound waves may be carried along by a single "carrier" wave (of frequency ω_c, speed c_c) in the case of nonlinear deep-water waves (cf. Ref. 22). In such an event, the bound waves have a constant speed c_c and their $\omega(\underset{\sim}{\kappa})$ dispersion relation becomes

$$\omega = c_c \kappa \propto \frac{1}{\lambda} \qquad (\omega > \omega_c) \quad ,$$

Ref. 22. H. C. Yuen and B. M. Lake, "Reply to comments of G. Roskes," Phys. Fluids, Vol. 19, 1976, p. 767.

which is steeper than the dispersion curve for the usually assumed free-wave spectrum ("sea" in Fig. 1). Thus, the quasi-static estimator of Eq. 34a remains applicable, leading as above to Eqs. 38 and 39 times the factor c_c/c. For example, for deep water the bound-wave spectrum would contribute the high-frequency hydromagnetic amplitudes

$$\tilde{h}_{air} \approx \left(\frac{\omega}{\omega_c}\right) \times \text{Eq. 39a} \quad .$$

As a result, for a sea spectrum containing bound waves, the rms hydromagnetism estimates of Subsec. 5.1.2 may increase as follows: Eq. 43 for the surface field by $\approx c_c/W$ and Eq. 44 at $z > 1/\alpha$ by $\sim c_c/W\ (\alpha z/2)^{1/6}$, provided these correction factors exceed unity; otherwise the change is negligible. However, typical sea spectra have little contribution at wave speeds $\gtrsim$ wind speed (i.e., $\omega \approx g/c \lesssim g/W$ in Fig. 2), so that one expects $c_c < W$. Therefore, the existence of bound waves would have little effect on the sea-induced hydromagnetism curves of Fig. 3.

5.2 INTERNAL WAVES

Buoyancy waves on a density stratification (pycnocline) within the ocean generate OM fields that are usually smaller than the SW-induced fields above. However, for observations with a magnetometer towed in the vicinity of the pycnocline, the IW-induced magnetism can become significant. IW magnetic fields have been calculated by Beal and Weaver (Ref. 7) for a sharp pycnocline and in a recent extension of their work (Podney, Ref. 8) for the other extreme of an exponentially stratified ocean. In general, the OM field due to IW can be estimated readily much as for SW above. Thus, the quasi-static Eq. 34a (with parameters from Table 1) gives

$$\tilde{h} \sim H_e \mu\sigma \frac{\tilde{u}}{\kappa} \sim \frac{1}{4} \frac{\tilde{u}}{\kappa} \quad (\text{in } \gamma) \quad , \tag{51}$$

applicable to any IW of supratidal frequency (cf. Fig. 1).

For the sharp pycnocline model of Beal and Weaver, we have $\tilde{u}/\kappa \sim \tilde{a}\omega/\kappa = \tilde{a}c_{ph}$, where $c_{ph} = \sqrt{g(\delta\rho/\rho)}/\sqrt{\kappa + \kappa \coth \kappa d}$ for deep ocean ($D > 1/\kappa$) from Eq. 35b. Boundary conditions (Eq. 10b) together with directional dependence (cf. Eqs. 39 and following) introduce a factor $\sim \frac{1}{2}(\pm\frac{1}{4})$, so that Eq. 51 yields roughly

$$\tilde{h}_{\text{pycnocline}} \sim \frac{1}{10}\sqrt{g\left(\frac{\delta\rho}{\rho}\right)} \cdot a \cdot \begin{cases} \sqrt{\lambda/4\pi} & \text{for } \lambda \leqslant 2\pi d\ , \quad (52a) \\ \sqrt{d} & \text{for } \lambda \gtrsim 2\pi d\ . \quad (52b) \end{cases}$$

(Away from the pycnocline, $\tilde{h}$ decreases essentially exponentially with a scale length of $1/\kappa$.) Numerically, for pycnocline depth $d = 100$ m and density step $\delta\rho/\rho < 10^{-2}$, one finds near the pycnocline

$$\frac{\tilde{h}}{a} \leqslant \text{few-tenths } \gamma/\text{m} \qquad (53)$$

for IW of a wavelength $\lambda > 1$ km, and $\propto \sqrt{\lambda}$ less for $\lambda < 1$ km (cf. Beal and Weaver's numerical example).

For the exponentially stratified model, Podney (Ref 8) chooses to express $\tilde{h}$ in terms of the IW horizontal flow at the surface his $v_{k0,n}$ $(n=1,2,\ldots)$. Since $\tilde{u} \sim (\kappa D/n\pi) \cdot v_{k0,n}$, Eq. 51 yields

$$\tilde{h} \sim \frac{1}{4\pi} D\, v_{k0,1} \sim 1\ \gamma \qquad (54)$$

for the numerical example $D = 1000$ m, $v_{k0} = 1$ cm/s of Podney, in rough agreement with his detailed calculations.

The more detailed behavior of the OM field can be seen from the model calculations of Beal and Weaver, and Podney. However, Eqs. 52 and 54 display clearly the essential factors that determine the size of the IW magnetic field.

In a stratified fluid there can also exist internal shock waves, or hydraulic jumps (Ref. 23), analogous to the well-known SW phenomena (e.g., bores and solitary waves, cf. Lamb, Ref. 20, pp. 280 and 423). Typical of earlier observation in the Straits of Gibraltar and in Massachusetts Bay are the detailed measurements of Hunkins and Fliegel in Ref. 24. A nominal example has an

---

Ref. 23. C. H. Su, "Hydraulic jumps in an incompressible stratified fluid," J. Fluid Mech., Vol. 73, 1976, p. 33.

Ref. 24. K. Hunkins and M. Fliegel, "Internal Undular Surges in Seneca Lake: A Natural Occurrence of Solitons," J. Geophys. Res., Vol. 78, 1973, p. 539.

amplitude of ~10 m, speed of ~$\frac{1}{2}$ m/s, and time scale of ~10 min, which leads via Eq. 25 to the estimate

$$h_{jump} \sim \text{few gamma}$$

for this transient hydromagnetic field.

5.3 ACOUSTIC WAVES

Sound in the sea generates a hydromagnetic field by virtue of the interaction of the acoustic seawater motions with the earth's magnetic field. This acoustic OM field is carried along with the sound wave, thereby radiating through the ocean as a pseudowave induction field. We shall refer to the field as sonomagnetism, to distinguish it from the magnetosonic radiations of compressible MHD. The difference is that sonomagnetism propagates purely mechanically via the acoustic forces, whereas magnetosonics involves in addition the magnetic action back on the fluid motions. In the ocean, that reaction is very small (cf. the discussion following Eq. 13), and so magnetosonic modes collapse to ordinary sound waves (Ref. 16). (Note however that for sonic damping, rather than propagation, magnetic forces become more important than viscosity at infrasonic frequencies. That is, the Hartmann number given in the discussion following Eq. 13 with $L \sim 1/\kappa = c_s/\omega$ becomes $R_H \sim 1/\nu$ for the ocean parameters of Table 1, so that magnetic/viscous damping > 1 for $\nu \leq 1$ Hz. This happens to correspond roughly to the transition frequency of Eq. 55 below.) Thus, the sound wave here will be taken as prescribed by the usual acoustic equations (Ref. 25) for an assumed homogeneous ocean.

Sonomagnetism was discussed theoretically by Kontorovich (Ref. 26) for plane sound waves in an infinite ocean, with brief consideration of reflection-transmission at the air-sea interface. We can recapitulate his results from our theory and discuss in addition the effect of finite ocean depth. The latter is necessary particularly for infrasonic frequencies, since in that regime the wavelength can become comparable to depth (cf. Fig. 1), and also the ambient sonomagnetism will become largest.

Ref. 25. H. Lamb, The Dynamical Theory of Sound (1925), 2nd edition, Dover, 1960.

Ref. 26. V. M. Kontorovich, "Magnetohydrodynamics of the Ocean," Problems of MHD and Plasma Dynamics II, 2nd Conf. on Theoret. and Appl. MHD, Riga, USSR, 1960.

For a plane sound wave in infinite ocean, the sonomagnetic pseudowave has identical frequency, wavelength, and velocity as the sound. But its amplitude (and phase) depend markedly on whether the frequency (ν) is above or below the rate of magnetic diffusion, i.e., closer to the quasi-static or nonstatic limits, Eqs. 34a or 34b, respectively. The transition frequency is (see the discussion following Eq. 35c)

$$\nu_0 \equiv \frac{\omega_0}{2\pi} = \frac{\mu\sigma c_s^{\,2}}{2\pi} \approx 2\text{Hz} \quad , \tag{55}$$

for the ocean parameters of Table 1. With $L \sim 1/\kappa$, $\omega = \kappa c_s$, and by continuity (Eq. 12b) $\tilde{u}_0 \sim (\omega/\kappa)\ \tilde{\delta\rho}/\rho = c_s\beta\ \tilde{\delta P}$, Eqs. 34 yield the OM amplitude estimate

$$\tilde{h} \sim \begin{cases} H_e \cdot \beta \cdot \tilde{\delta P} \cdot \dfrac{\nu_0}{\nu} & (\nu \gg \nu_0) \qquad (56a) \\ H_e \cdot \beta \cdot \tilde{\delta P} & (\nu \ll \nu_0) \qquad (56b) \end{cases}$$

where $\beta \equiv 1/\rho c_s^{\,2}$ is seawater compressibility and $\tilde{\delta P}$ the acoustic pressure amplitude.

An exact expression for the OM field is easily derived from the basic Eq. 23 for infinite plane waves, viz.,

$$\underset{\sim}{\tilde{h}} = \left[\underset{\sim}{H}_e - (\underset{\sim}{H}_e \cdot \underset{\sim}{\kappa})\ \frac{\underset{\sim}{\kappa}}{\kappa^2}\right] \cdot \beta \cdot \tilde{\delta P} \cdot \frac{\nu_0}{\nu_0 - i\nu} \quad ,$$

which displays the dependence on field (H_e) and propagation (κ) directions and the general frequency behavior

$$\left[1 + \left(\frac{\nu}{\nu_0}\right)^2\right]^{-\frac{1}{2}} \exp i\left(\tan^{-1}\frac{\nu}{\nu_0}\right) \quad .$$

For example, a total field magnetometer would measure amplitude $|\underset{\sim}{\tilde{h}} \cdot \underset{\sim}{H}_e/H_e| = H_e \cdot \beta \cdot \tilde{\delta P}\ \sin^2\theta/\sqrt{1 + (\nu/\nu_0)^2}$ (cf. Eqs. 56), where θ is the angle of sound propagation with respect to the earth field. In general, the phase difference between the sonomagnetic and

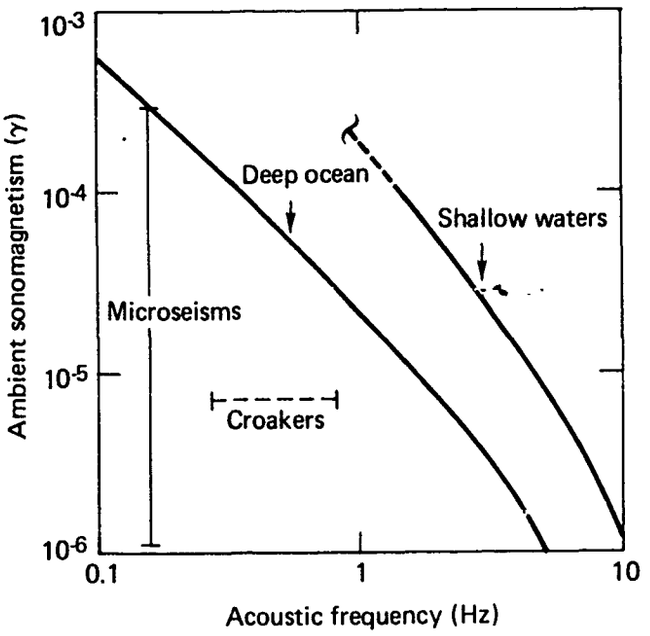

Fig. 4 Ambient Sonomagnetic Spectra for Typical Ocean Noises (Ref. 27) and a Chesapeake Bay Fish (Croakers, Ref. 28).

acoustic waves, $\tan^{-1}(\nu/\nu_0)$, is 90° in the regime of Eq. 56a and 0° in that of Eq. 56b. For the sonomagnetic field amplitude, we can rewrite Eqs. 56, using Eq. 55 and the parameters of Table 1, as

$$\tilde{h} \sim 10^{(S-86)/20} \cdot (2^2 + \nu^2)^{-\frac{1}{2}} \gamma \quad , \tag{57}$$

in terms of the acoustic intensity measure, S dB re 1 Pa, for which $\delta\tilde{P} = 10^{S/20}$.

According to Eq. 57, ambient sound levels in the ocean (Ref. 27) produce the sonomagnetic "noise" amplitudes shown in Fig. 4. These are order-of-magnitude estimates only and for the

Ref. 27. G. M. Wenz, "Acoustic ambient noise in the ocean: spectra and sources," J. Acoust. Soc. Am., Vol. 34, 1962, p. 1936.

infinite-ocean plane wave approximation. Thus, it applies for widespread, distant sources, with no specific account of sea-air and seabed reflections, channeling, etc. (See Sec. 6 regarding strong, local sources at shallow submergences.) For such conditions, Fig. 4 shows that ambient sonomagnetism is detectable with magnetometer sensitivities of $\sim 10^{-4}$ $\gamma/\sqrt{\text{Hz}}$ only in the far infrasonic regime.

We may note that, for a noise souce at great distances (R) such that its radiation approximates a plane wave at the magnetometer, the sonomagnetic transmission loss-factor is the square root of the sonic factor (Ref. 28), i.e., $\underset{\sim}{h} \propto 1/R$ for spherical spreading, $1/\sqrt{R}$ for cylindrical, etc. This obtains because $\underset{\sim}{h} \propto$ sound amplitude, not intensity, in Eq. 56.

We briefly consider boundary influences. The sea-air and seabed interfaces are included in the dispersion relation of Fig. 1, from which we see that the transition frequency ν_0 of Eq. 55 differs little from $D = \infty$ up to $D \sim 500$ m. (In shelf waters of $D \sim 100$ m, ν_0 increases to ~ 5 Hz.) In general, the sonomagnetic field can be constructed as a particular integral $\underset{\sim}{h}_P$ of our basic Eq. 23 (with $\underset{\sim}{V}_b = 0$) plus a complementary solution $\underset{\sim}{h}_c$ chosen to satisfy the boundary conditions. Now, using the acoustic wave equation $(\Delta + \omega^2/c_s^2)\underset{\sim}{u}_0 = 0$, one can see that the Ansatz $\underset{\sim}{h}_P = -\mu\sigma/(i\omega\mu\sigma + \omega^2/c_s^2) \cdot \text{curl}(\underset{\sim}{H}_e \times \underset{\sim}{u}_0)$ satisfies Eq. 23, as well as Eq. 22b. Therefore, $\underset{\sim}{h}_c$ is that transverse-wave solution of the homogeneous vector Helmholtz equation $((\Delta - i\omega\mu\sigma)\underset{\sim}{h}_c = 0$, cf. Eq. 23 with the right-hand side zero) determined through the boundary conditions (Eqs. 6a and 6b) by the value of $\underset{\sim}{h}_P$ at the interfaces.

For example, at the air-sea surface ($z = 0$) we find for the acoustic modes of Eq. 35c that

$$\underset{\sim}{h}_P(z=0) = \frac{1}{2} \sin 2\alpha \cdot \left[(\underset{\sim}{H}_e \cdot \hat{z})\underset{\sim}{\hat{\kappa}} + (\underset{\sim}{H}_e \cdot \underset{\sim}{\hat{\kappa}})\hat{z} \right] \frac{\beta \delta P}{i + \nu/\nu_0} e^{i(\omega t - \underset{\sim}{\kappa} \cdot \underset{\sim}{r})} , \quad (58)$$

where $\alpha \equiv \tan^{-1} \kappa D/(\ell + \frac{1}{2})\pi$ contains the depth (D) and mode (ℓ) dependence. In terms of the acoustic cutoff frequencies $\nu_c \equiv (2\ell + 1)c_s/4D$ (cf. Fig. 1 and Eq. 35c with $\kappa \to 0$), we have $\frac{1}{2} \sin 2\alpha = (\nu_c/\nu)\sqrt{1 - (\nu_c/\nu)^2}$ which has a broad maximum at frequency $\nu = \sqrt{2}\ \nu_c$. Thus for $\nu \gtrsim \nu_c$ to $\nu \sim$ several ν_c, Eq. 58 and also the $\underset{\sim}{h}$ determined through it are comparable with the infinite plane-wave expression given following Eqs. 56. Therefore, in that infrasonic

Ref. 28. R. J. Urick, Principles of Underwater Sound, McGraw-Hill, NY, 1975.

regime the complete sonomagnetic field is still fairly estimated by Eqs. 56 and 57 when air-sea boundary effects are included.

The unique feature of the sonomagnetic pseudowave vis-à-vis the acoustic wave, however, is that it extends into the air above the sea where the transmitted sound is negligible. As stressed in Subsec. 2.2, a surface field of the form $\propto e^{i\omega t - i\underset{\sim}{\kappa}\cdot\underset{\sim}{r}}$ as in Eq. 58 (see also Eq. 11a) leads to an aerofield (cf. Eq. 11b)

$$\underset{\sim}{h}_{air} = \underset{\sim}{h}(z=0) \cdot e^{-\kappa z} \propto e^{i\omega t - i\underset{\sim}{\kappa}\cdot\underset{\sim}{r} - \kappa z} . \qquad (59a)$$

That is, the sonomagnetic aerofield looks like a surface wave (pseudo "ground wave") with altitude penetration measured by

$$\text{Scale height} = \frac{1}{\kappa} \sim \frac{D}{(\ell + \frac{1}{2})\pi} \qquad (59b)$$

near the optimum frequency $\nu \sim \sqrt{2}\ \nu_c$. Thus, on deep ocean and for ν in the 0.1 to 1 Hz band, the sonomagnetic field has a scale height of $\sim$ kms. This is much greater than for other ocean-wave OM in that frequency regime (viz., $\gtrsim 10$ times the scale height for long (20 s) swells, cf. Eq. 41) simply because infrasound wavelengths are relatively long (Fig. 1). Thus, although in the sea sonomagnetism is smaller than SW-generated fields, in the air it can remain detectable to altitudes beyond the limit for such fields. For example, microseismic sound (Fig. 4) might in principle be studied free of surface-wave noise through the high-altitude sonomagnetic field.

5.4 SEA CURRENTS

Ocean circulations interacting with the earth's magnetostatic field have long been recognized as sources of considerable electromagnetic perturbations, over and above those effects induced in a static ocean by temporal variations in the earth's field. In 1968, Bullard and Parker (Ref. 5) reviewed both types of oceanic induction, though with emphasis on the latter. The time-variation effects may be regarded as the ocean environment contribution to geomagnetic noise and will not be considered further here. The other, sea-current effects are discussed for a simple model of major ocean streams in Subsec. 4 of Ref. 5, with further references therein. Later references are cited in this subsection.

Sea-current OM fields can be estimated from Eqs. 24 and 25,

$$h \leq \frac{1}{4} u_0 L \quad (\gamma) \quad , \tag{60}$$

given the current speed and scale, u_0 and L. Of particular interest to observers has been the electric field, $\underset{\sim}{E} \approx \text{curl } \underset{\sim}{h}/\sigma - \mu \underset{\sim}{u}_0 \times H_e$, by Eq. 7c in the present approximation ($h << H_e$, $\underset{\sim}{H}_e$ uniform), or sometimes only that part measured by electrodes moving with the seawater, the "geomagnetic electrokinetic" (GEK) field, $\underset{\sim}{E}' \approx \text{curl } \underset{\sim}{h}/\sigma$. Generally, one can estimate these electric fields, using $|\text{curl } \underset{\sim}{h}| \approx h/L$ and Eq. 24, as

$$E \sim \mu H_e u_0 \sim \frac{1}{2} 10^{-4} u_0 \quad (\text{V/m}) \quad , \tag{61}$$

which involves only the current speed, not scale.

In the open ocean, Ekman currents driven by winds of ~10 knots may have surface speed $u_0 \sim 10^{-1}$ m/s and can extend to depths up to $\sim 10^2$ m, in which case

$$h \leq 1 \ \gamma \quad , \qquad E \leq \frac{1}{20} \ \mu\text{V/cm} \quad . \tag{62}$$

Detailed analysis in Ref. 29 confirms this OM estimate. Open ocean tidal currents have comparable speed and therefore electric field. For example, Harvey (Ref. 30) measured E as ~ 0.014 μV/cm at the lunar semidiurnal tidal frequency.

Major open ocean streams can have higher speeds and larger OM effects. For example, the equatorial countercurrent (eastward) has u_0 up to 1 m/s and depth $\sim 10^2$ m, so that

$$h \leq 25 \ \gamma \quad , \qquad E \leq \frac{1}{2} \ \mu\text{V/cm} \quad . \tag{63}$$

Ref. 29. G. A. Burtsyev, "Magnetohydrodynamics of sea currents," Fiz. Atmosf. Okeana, Vol. 11, 1975, p. 1084

Ref. 30. R. R. Harvey, "Derivation of oceanic water motions from measurement of the vertical electric field," J. Geophys. Res., Vol. 79, 1974, p. 4512.

(Cf. Bullard-Parker's simple model calculation in Ref. 5.) Thus, Rommel and McCleave (Ref. 31) quote their unpublished data predicting up to 0.46 μV/cm in the Gulf Stream and von Arx (corrected) figures of ~0.1 μV/cm in other Atlantic currents.

Boundary currents on eastern margins of the ocean, e.g., the California current, tend to be sluggish and relative shallow. Thus, typically $u_0 \sim 1/10$ m/s and $L < 500$ m, so that

$$h < 10\ \gamma\ , \qquad E < \frac{1}{20}\ \mu V/cm \tag{64}$$

are generous upper limits.

Western boundary currents, on the other hand, are fast and deep enough to produce considerably larger OM fields. For example, the Florida current of the Gulf Stream is geostrophically driven to speed u_0 of ~ 1 to 3 m/s with a draft of ~ 1 to 1.5 km, so that

$$h \leq 10^{2 \text{ or } 3}\ \gamma\ , \qquad E \leq 1\ \mu V/cm\ . \tag{65}$$

All of the above sea currents are very large scale, with widths typically ~100 km. Thus, the induced OM field h is correspondingly extensive, comparable to the scale of geologic anomalies to the earth's dipole field.

On a smaller scale, one may consider the Langmuir circulation, consisting of a wind-induced array of pairs of opposing helical current cells. For windspeeds ≥ 5 m/s, the cell widths are 5 to 50 m (Ref. 32), and typical current speeds are ~ cm/s (Ref. 33). Thus, the OM field forms a periodic spatial pattern of wavelength (λ) twice the cell width, or

$$h \leq 10^{-2 \text{ to } -1}\ \gamma \quad \text{with} \quad \lambda \sim 10^{1 \text{ to } 2}\ m\ . \tag{66}$$

Ref. 31. S. A. Rommel, Jr., and J. D. McCleave, "Oceanic electric fields: Perception by American eels?" Science, Vol. 176, 1972, p. 1233.

Ref. 32. T. Gammelsrød, "Instability of Couette flow in a rotating fluid and origin of Langmuir circulations," J. Geophys. Res., Vol. 80, 1975, p. 5069.

Ref. 33. N. E. J. Boston, A. Maratos, J. A. Galt, and E. D. Traganza, "A measurement of nearshore Langmuir circulation," Naval Postgraduate School Report NPS-58Bb75041, 1975.

An exact calculation (unpublished) for a simple model of the Langmuir cells finds h reduced by a factor ~ (cell-height/cell-width)^2, which can be an order of magnitude or more. Note that by Eqs. 11 the field pattern (Eq. 66) extends into the air with

$$\text{Scale height} = \frac{\lambda}{2\pi} < 15 \text{ m} \quad , \tag{67}$$

so the Langmuir circulation OM effects are correspondingly confined to the neighborhood of the sea surface.

6. ESTIMATES OF OM INDUCTION BY BODY-RELATED SEA MOTIONS

The size and extent of the OM fields induced by seawater motions related to the passage of a body through the ocean, as listed in Eqs. 18e through 18h, are now estimated from the theory of Sec. 4. As indicated there, the basic Eq. 23 is driven by a body magnetization-translation ($\underset{\sim}{H}_b \times \underset{\sim}{V}_b$) interaction and by various geomagnetic-flow ($\underset{\sim}{H}_e \times \underset{\sim}{u}_0$) interactions. Here $\underset{\sim}{u}_0$ will be seawater disturbances caused by the body, each treated separately (cf. the discussion following Eqs. 18) and in isolation from the natural sea motions considered in Sec. 5. As there, clarity and simplicity are chosen over precision, but some detailed analyses that elaborate our estimates will be cited.

We begin (Subsec. 6.1) with the magnetization-translation interaction, simply a mean-flow effect, assuming a constant body motion and magnetization but with no important restrictions on the ocean model (uniform conductivity and of course the HM approximation (Eq. 4)). Then the flow effects due to finite body displacement are taken up, under the assumption of a homogeneous and incompressible ocean. We first consider (Subsec. 6.2) the potential flow around a moving body at large Reynolds number. In an Oseen-like approximation for the OM field, the potential flow effect will be seen homologous to the mean flow effect. We estimate next (Subsec. 6.3) wake-flow effects in uniform or stratified ocean via the theorem of Subsec. 4.2. Brief consideration is given (Subsec. 6.4) of the OM effects radiated via surface wave generation by a moving body. We then go on to other OM pseudoradiations that arise by virtue of the inhomogeneity and the compressibility of the ocean. Inhomogeneity introduces propagated induction via internal waves (Subsec. 6.5) generated by a body moving through stratified ocean. Finally, compressibility (Subsec. 6.6) allows acoustic waves that induce sonomagnetic radiation accompanying sound emissions from the body.

6.1 MEAN FLOW

Consider the hydromagnetic effect that arises simply from the translation through the ocean of the magnetostatic field of a moving magnetized vehicle. That is, we set aside until later any actual seawater disturbances due to the finite displacement of the

body. We are then left with just the "disembodied" magnetostatic field $\underset{\sim}{H}_b$ sweeping through the seawater and thereby inducing motional electromotive forces, eddy currents, and magnetic fields. Or from the point of view of the moving body, we have a mean flow $(-\underset{\sim}{V}_b)$ of seawater through the magnetostatic field $(\underset{\sim}{H}_b)$ that induces these hydromagnetic phenomena.

The mean flow effect is described mathematically by Eq. 23 with $\underset{\sim}{u}_0$ set equal to zero. We assume a constant body velocity $\underset{\sim}{V}_b$ so that, in the steady state, $\partial\underset{\sim}{h}/\partial t = -(\underset{\sim}{V}_b \cdot \underset{\sim}{\nabla})\underset{\sim}{h}$ on the left-hand side of Eq. 23. The spatial dependence in Eq. 23 devolves solely from $\underset{\sim}{H}_b$ on the right-hand side, and that field varies algebraically with distance (R) from the body (cf. the multipole expansion of magnetostatics). Thus, the magnetic Reynolds number for the mean flow is, by Eq. 8, $R_M \sim \mu\sigma V_b R$, and the first (diffusion) term dominates on the left-hand side of Eq. 23 for ranges

$$R << R_v \equiv \frac{1}{\mu\sigma V_b} \sim 2 \cdot \frac{10^5}{V_b} \quad . \tag{68}$$

That is, the quasi-static approximation (cf. Eq. 24) obtains, and we have the OM estimate

$$h \sim \mu\sigma V_b \, RH_b \sim \frac{\mu\sigma V_b \, m_b}{R^2} \tag{69}$$

in terms of the magnetic dipole moment of the body, i.e., with $H_b \sim m_b/R^3$. The outstanding feature of the result of Eq. 69 is its monopolar range behavior, i.e., $1/R^2$ falloff, as compared with the dipolar $1/R^3$ behavior of H_b. Of course this is restricted to ranges of Eq. 68 and to an infinite ocean. However, we see below that the $1/R^2$ behavior persists to all distances in the wake of the body and in a finite ocean, with boundary effects mainly introducing complicated angular and directional dependence (cf. Eq. 71, below). Thus, Eq. 69 will roughly estimate the size and extent behind the body of this nonisotropic but monopole-like OM field.

Numerically, Eq. 69 may be evaluated by using $\underset{\sim}{m}_b \equiv \int d\tau \, \underset{\sim}{M}_b \sim V_M \cdot M_b$ where V_M is the volume of magnetic matter in the body and $\underset{\sim}{M}_b$ its magnetization. (For example, a steel shell with a thickness/diameter ratio δ would have m_b in $\gamma - m^3 \sim 10^6 \cdot \delta \cdot$ remanent magnetization in gauss $\cdot$ body displacement in tons.) However, it is more perspicuous to measure h relative to H_b from Eqs. 68 and 69 as

$$\frac{h}{H_b} \sim \frac{R}{R_v} \quad \text{for} \quad R << R_v \approx \left(\frac{400}{V_b(\text{in kt})}\right)\text{km} \quad . \tag{70}$$

Thus, h represents a small correction to H_b that increases with distance. It appears that at $R \sim R_v$ (i.e., $R_m \sim 1$) we might have $h \sim H_b$. However, there the second term on the right-hand side of Eq. 23 becomes important, i.e., the quasi-static approximation breaks down, and more detailed considerations become necessary.

The complete analysis* of Eq. 23 for a body of arbitrary magnetization and shape includes as a particular case the zero-displacement mean flow effect. More recently, the latter case for a point dipole in a uniform flow has also been given by Semenov (Ref. 34), in the context of the solar wind influence on the earth dipole field. These analyses show that at great distances ($R \gtrsim R_v$) the magnetic field is swept back to form a paraboloidal wake behind the body, analogously to Oseen's solution for the hydrodynamic, low Re flow about a sphere (Lamb, Ref. 20, p. 613). In particular, our analysis shows that at $R > R_v$ outside the wake the OM field approaches exponentially the negative of the body field, i.e., $\underset{\sim}{h} \to -\underset{\sim}{H}_b$, so that the total field $\underset{\sim}{H} = \underset{\sim}{H}_b + \underset{\sim}{h} = 0$ there. On the other hand, at distances $R > R_v$ within the wake the OM field retains the $1/R^2$ behavior of Eq. 69, plus a $1/R$ behavior modified by a small factor involving the downstream angle in the wake. The result is that in a downstream "tail" h now remains $\sim 1/R^2$ as in Eq. 69 at all ranges. Thus in the far wake ($R >> R_v$) the total field is essentially just the OM contribution, i.e., $h >> H_b$, so that $\underset{\sim}{H} = \underset{\sim}{H}_b + \underset{\sim}{h} \approx \underset{\sim}{h}$. The two paraboloidally separated regions of different behavior of the OM field are as depicted in Fig. 5 of Subsec. 6.2 (with m_0 from the unified analysis equalling $\underset{\sim}{m}_b$ here).

An infinite ocean, or plasma in Semenov's case, is assumed in the above. Otherwise, the only noteworthy restriction is that the motion $\underset{\sim}{V}_b$ and the moment $\underset{\sim}{m}_b$ be constant (cf. Ref. 34 for oscillating or precessing $\underset{\sim}{m}_b$).

Air-sea boundary effects have been calculated in the unified analysis quoted in the next subsection.* For example, for a body with vertical moment $\underset{\sim}{m}_b$ moving with horizontal velocity $\underset{\sim}{V}_b$ at depth d below the surface, one finds the results given in Eqs. 79 and 80, below, except with m_0 there replaced by m_b. That is, the OM field both in the sea and in the air above has the form (for $R << R_v$)

$$h = \frac{1}{2}\{\cdots\} \times \frac{\mu\sigma V_b m_b}{R^2} \quad , \tag{71}$$

*This will be the subject of a report now in preparation by J. F. Bird.

Ref. 34. V. S. Semenov, "Three-dimensional dipole in a uniform flow of conducting fluid," Geomagn. Aeron., Vol. 15, 1975, p. 419 (APL/JHU translation 2776).

in which $\{\cdots\}$ is a complicated vector function of magnitude ~ unity. Thus, the configuration of the OM field is determined by $\{\cdots\}$, as depicted in Figs. 6 and 7 in the next subsection. The size and extent of the field, however, remains roughly ($\sim\frac{1}{2}$) as estimated in Eq. 69.

6.2 POTENTIAL FLOW

Now consider the hydromagnetic interaction between the flow around the hull of a moving body and the local magnetic field. In the ocean, the hull flow may be taken as a potential flow, since the Reynolds number (Re) is large for dimensions and speeds of interest here. That is, $Re \equiv Lu\,\rho/\eta = R_M \cdot \rho/\eta\mu\sigma$ by Eq. 8, which in seawater (Table 1) gives $Re \sim 10^{11} \cdot R_M$, so that $Re >> 1$ for any R_M that will result in significant OM fields (cf. Eq. 24). The local magnetism in the ocean may be taken as a constant uniform earth field (cf. the discussion following Eq. 17), ignoring any body magnetic field. That is, for typical body magnetization one has $H_b/H_e \sim m_b/H_e R^3 \sim (M_b/H_e)(V_M/R^3)$ (cf. the discussion preceding Eq. 70), which is small everywhere excepting possibly in the immediate vicinity of a thick-hulled ferromagnetic body. But in the latter case, one will also have $H_b >> h$ near the hull so that the OM field is swamped by the body field. In any event, we will confine our attention here to distances outside a few body diameters.

The potential flow interaction with the geomagnetic field is described by Eq. 23 with the right-hand side forcing term

$$\text{curl}(\underset{\sim}{H}_0 \times \underset{\sim}{u}_0) \rightarrow -(\underset{\sim}{H}_e \cdot \underset{\sim}{\nabla})\underset{\sim}{\nabla}\,\Phi \tag{72}$$

where Φ is the flow potential. Now, notice that the body term in Eq. 23 treated earlier can be written

$$-\text{curl}(\underset{\sim}{H}_b \times \underset{\sim}{V}_b) = -(\underset{\sim}{V}_b \cdot \underset{\sim}{\nabla})\underset{\sim}{\nabla}\,\Psi_M \quad , \tag{73}$$

in terms of the scalar magnetic potential Ψ_M to the body field $\underset{\sim}{H}_b$. One sees at once that the potential flow effect is homologous to the mean flow effect. In general, one can show (Bird, in preparation) that the potential flow OM is equivalent, within an Oseen-like approximation, to a "mean flow" OM due to "translation" $\underset{\sim}{V}_b = \underset{\sim}{H}_e$ of a "magnetization" source $\text{div}\,\underset{\sim}{M} = \rho(\underset{\sim}{r})$, when the potential flow is represented by a distribution $\rho(\underset{\sim}{r})$ of sources and sinks.

In particular, a Rankine ovoid model for the flow gives a very simple homology relation between potential and mean flow effects. The ovoid potential at sufficient distances R is that of a source-sink dipole which we may compare with a magnetic dipole potential:

$$\Phi \approx s^2a^3(\underset{\sim}{V}_b \cdot \underset{\sim}{\nabla})\frac{1}{R} \quad , \qquad \Psi_M \approx (\underset{\sim}{m}_b \cdot \underset{\sim}{\nabla})\frac{1}{R} \quad , \tag{74}$$

where a and s are functions of body length L and diameter D (Ref. 14, with its m = our s) such that $s^2a^3 \approx LD^2/16$ for a slender body (L >> D) or for a sphere (L = D) and an overestimate by at most 13% for intermediate L/D ratios. From Eq. 74 and a commutation of operators, one sees Eq. 72 is equivalent to Eq. 73, only with $s^2a^3\underset{\sim}{H}_e$ replacing $\underset{\sim}{m}_b$. Therefore, for the ovoid and at R >> a, the potential flow OM is identical with that arising from mean flow $\underset{\sim}{V}_b$ past a "hydromagnetic moment"

$$\underset{\sim}{m}_{hm} \equiv s^2a^3\underset{\sim}{H}_e \geq \frac{1}{16} LD^2 \underset{\sim}{H}_e \quad . \tag{75}$$

Notice that m_{hm} depends only on body displacement and earth field. The purely hydromagnetic effect (Eq. 75) should not be confused with similar excluded-volume effects of magnetostatics.

We may compare m_{hm} with m_b as estimated preceding Eq. 70 to find $\underset{\sim}{m}_{hm} \geq (H_e/f_M \cdot M_b)\underset{\sim}{m}_b$ where f_M is the fraction of total body volume that is magnetic. Thus, as somewhat of a numerical coincidence, a typical ocean vehicle with $f_M \leq 10^{-3}$ and $M_b \leq 10^3$ gauss has

$$m_{hm} \geq m_b \Rightarrow \text{potential flow OM} \geq \text{mean flow OM} \quad . \tag{76}$$

In the limit of a nonmagnetic body, of course, the latter is absent, but the potential flow OM always persists.

The combined potential and mean flow effects for a moving magnetized body in the above ovoid-dipole approximation can now be seen to be equivalent to the magnetization-translation interaction for an effective dipole

$$\underset{\sim}{m}_0 \equiv \underset{\sim}{m}_b + \underset{\sim}{m}_{hm} \quad . \tag{77}$$

Hence, the combined OM field is given as in Eq. 69 with Eq. 68,

$$h \sim \frac{\mu\sigma V_b m_0}{R^2} \quad \text{for} \quad R \ll R_v \ . \tag{78}$$

Again, for $R \gtrsim R_v$ the field h is formed into two paraboloidally separated regions as depicted in Fig. 5, with the OM behavior as described in Subsec. 6.1, only with $\underset{\sim}{m}_b$ generalized to $\underset{\sim}{m}_0$. Thus, in the outer region $\underset{\sim}{h} \to -\underset{\sim}{H}_0$ exponentially, where $\underset{\sim}{H}_0$ is the field due to the effective dipole $\underset{\sim}{m}_0$ of Eq. 77, so that the total field $\underset{\sim}{H} = \underset{\sim}{H}_e + \underset{\sim}{H}_b + \underset{\sim}{h} = \underset{\sim}{H}_e - \underset{\sim}{H}_{hm}$ there with the dipolar $\underset{\sim}{H}_{hm}$ due to $\underset{\sim}{m}_{hm}$. (Note that the body field $\underset{\sim}{H}_b$ is still cancelled in the outer region as in Subsec. 6.1.) On the other hand, in the paraboloidal wake, $\underset{\sim}{h}$ retains the monopole-like behavior of the inner region given in Eq. 78.

Complete details of the OM field will be given in the unified analysis to be published (Bird, in preparation). The special cases of spherical bodies with $\underset{\sim}{H}_e = 0$, $\underset{\sim}{m}_b \parallel (-)\underset{\sim}{V}_b$ and with $\underset{\sim}{H}_e \parallel \underset{\sim}{m}_b \parallel (-\underset{\sim}{V}_b)$ were treated earlier by Ludford and Murray (Ref. 35) and by Bois (Ref. 36), respectively. These are included as degenerate forms of our analysis, which considers nonparallel $\underset{\sim}{H}_e$, $\underset{\sim}{V}_b$, and $\underset{\sim}{m}_b$, nonspherical body, nondipolar $\underset{\sim}{H}_b$, and bounded media (see below). The solution was obtained by an Oseen-like approximation, in addition to the usual HM and incompressibility assumptions and constant $\underset{\sim}{V}_b$, $\underset{\sim}{H}_b$, $\underset{\sim}{H}_e$ simplifications.

The air-sea boundary does not greatly change the estimate of Eq. 78, but mainly the detailed configuration of the OM field as indicated at the end of Subsec. 6.1. To begin with, the effect of the air-sea surface on the potential flow is accounted for by adding to the ovoid potential in Eq. 74 its image potential (Ref. 14). Then the solution of Eqs. 23 and 22b with the superposed potentials is found that satisfies the boundary conditions of Eqs. 6. Of course in the present, finite-displacement case, one must also consider the body-sea boundary. The latter introduces in $\underset{\sim}{h}$ terms $\propto 1/R^4$, which become negligible away from the body. If the body is submerged by more than a few times its dimensions, this body-sea effect is unimportant at the air-sea boundary. In that case, the latter independently determines the far-field effects via Eq. 10b.

Ref. 35. G. S. S. Ludford and J. D. Murray, "On the flow of a conducting fluid past a magnetized sphere," J. Fluid Mech., Vol. 7, 1960, p. 516.

Ref. 36. P.-A. Bois, "Influence sur quelques types de champs magnétiques de l'écoulement d'un fluide conducteur autour d'une sphère," J. Méc., Vol. 9, No. 35, 1970.

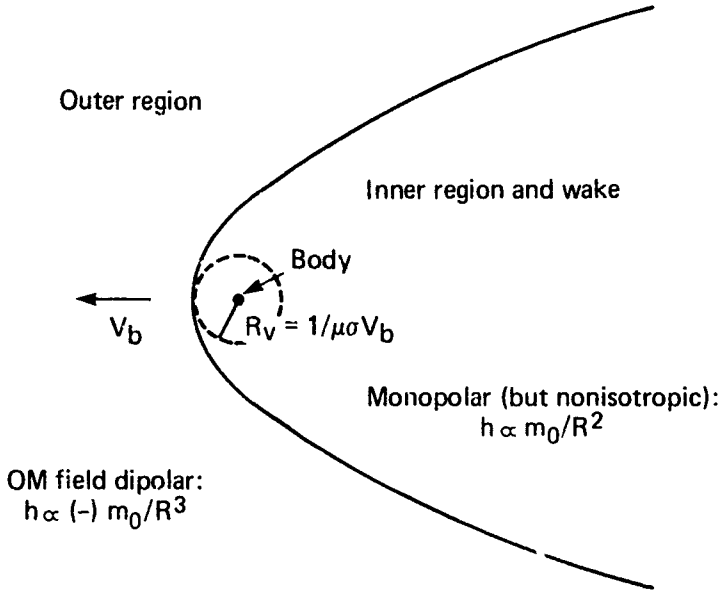

Fig. 5 Hydromagnetic Field Regions and Wake for Body Velocity (V_b) in a Medium of Magnetic Diffusivity ($1/\mu\sigma$) (cf. Table 1), Leading to Length Scale R_V (Eq. 68). The OM field (h) for effective magnetic dipole (m_0, cf. Eq. 77) is indicated as a function of range (R).

The complete solution within the inner region and paraboloidal wake of Fig. 5 (which are quite extensive in the ocean — cf. R_V in Eq. 68) is detailed for such a submerged body by Bird (in preparation). For example, in the case of a vertical effective moment $\underset{\sim}{m}_0$ and horizontal velocity $\underset{\sim}{V}_b$, one finds the following formulae:

1. Within the sea, excepting horizontal ranges comparable with body and/or measurement depths,

$$\underset{\sim}{h} \approx \frac{1}{2} \left[\hat{R} \cos\phi(1 + \cos\theta) - \hat{\theta} \cos\phi \sin\theta + \hat{\phi} \sin\phi\right] \cdot \frac{\mu\sigma V_b m_0}{R^2} \quad ; \tag{79}$$

2. In the air overhead, excepting ranges comparable with body depth,

$$\underset{\sim}{h} \approx \frac{1}{2}\left[\frac{\hat{R} \cos\phi \sin\theta - \hat{\theta} \cos\phi + \hat{\phi} \sin\phi}{1 + \cos\theta}\right] \cdot \frac{\mu\sigma V_b m_0}{R^2} \quad . \tag{80}$$

In these formulae, R, θ, ϕ are spherical polar coordinates centered on the body, with the polar axis vertically up, azimuth ϕ measured relative to direction of body motion, and $\hat{R}$, $\hat{\theta}$, $\hat{\phi}$ unit coordinate vectors. Field configurations calculated from Eqs. 79 and 80 are shown in Figs. 6 and 7.

Aside from the involved angular and directional dependence as illustrated for this example, Eqs. 79 and 80 show that the overall size and extent of the OM field due to combined potential flow and mean flow effects remain roughly as estimated by Eq. 78.

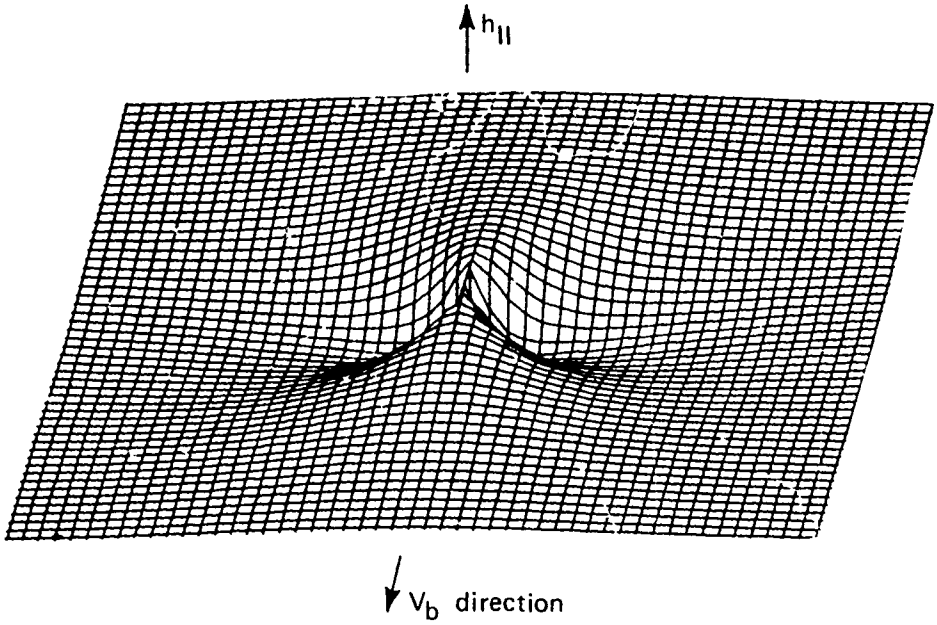

Fig. 6 Potential Flow and/or Mean Flow Hydromagnetic Configuration in the Sea. Spatial pattern of the OM field parallel to motion ($h \parallel V_b$) in the horizontal plane centered at a body (grid units $\sqrt{\mu\sigma V_b m_0/\gamma}$).

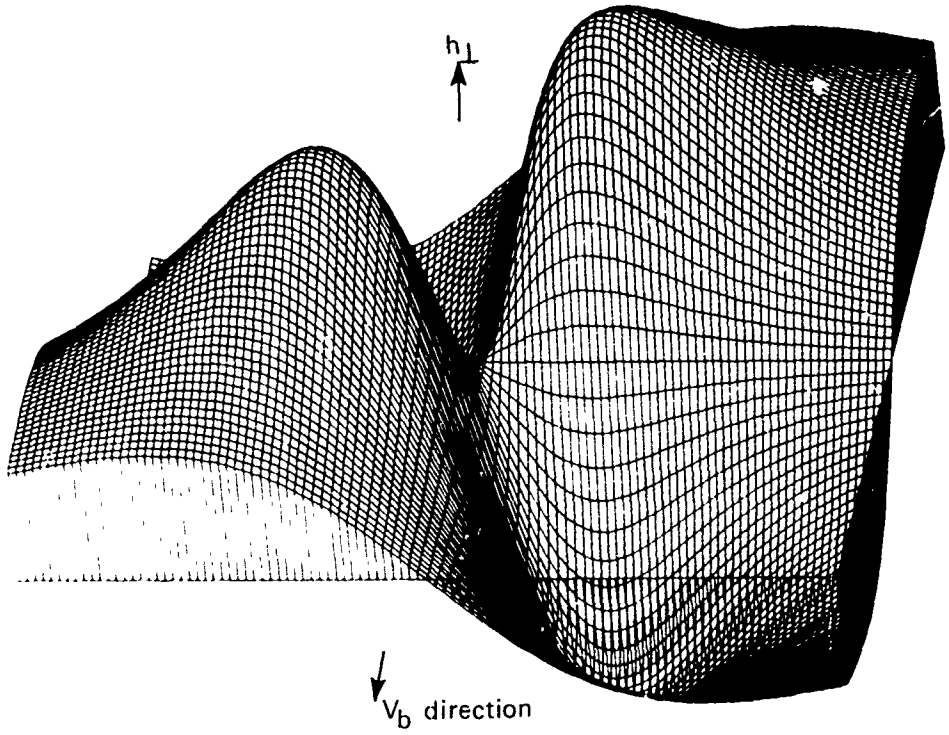

Fig. 7 Potential Flow and/or Mean Flow Hydromagnetic Configuration in the Air. Spatial pattern of the OM field perpendicular to motion ($h \perp V_b$) in a plane at altitude 15 grid units centered above a body submerged 1 unit. (Grid scale 1/2 that of Fig. 6).

6.3 WAKE FLOW

Hydromagnetism in the wake of a moving body will be considered induced by a constant uniform earth field, neglecting any body field. The OM effect is then determined by the character of the wake flow, i.e., whether the body is self-propelled or towed, on the surface or submerged, in a homogeneous or stratified ocean, etc. However, estimates of the OM field via Subsecs. 4.1 and 4.2 will require only a general, phenomenological description of the wake-flow magnitude and scale (cf. Eq. 25).

In general (cf. Wu, Ref. 37), for the large $Re \sim 10^{11}\ R_M$ indicated earlier (Subsec. 6.2), the wake may be divided into three regions: (a) near wake, (b) turbulent far wake, and (c) laminar far wake. Farther downstream, a submerged body moving in stratified fluid may develop a region of (d) large distant eddies (Ref. 38). In addition to these localized disturbances, of course, there can be radiated disturbances (IW, SW, AW), that will be considered later (Subsecs. 6.4 through 6.6).

The near wake extending some few body diameters D downstream, typically, has transverse scale $\sim D$ and flow speed $\leqslant V_b$. The local OM field is then $\leqslant H_e \mu\sigma V_b D \sim \frac{1}{4} V_b D$ by Eqs. 24 and 25, while at distant points it is given by Eq. 31 as

$$h \leqslant \frac{H_e \mu\sigma V_b D^4}{8\pi R^3} \qquad (R >> D) \quad . \tag{81}$$

This may be compared with the potential flow effect, Eq. 79 with $m_0 \sim (1/10) D^2 L H_e$ and $L \gtrsim D$, to obtain

$$\frac{\text{near wake OM}}{\text{potential flow OM}} \leqslant \frac{D^2}{LR} \leq \frac{D}{R} \quad , \tag{82}$$

which is small since $R >> D$.

The far wake develops in a complex fashion, particularly in stratified flow (Refs. 39, 40, and 41), but generally the wake-flow magnitude decreases and its scale increases, eventually collapsing vertically in stratified fluid. In any event, the turbulent far wake generates random OM fields of approximately zero

---

Ref. 37. T. Y. Wu, "Cavity and wake flows," Ann. Rev. Fluid Mech., Vol. 4, 1972, p. 243.

Ref. 38. H.-P. Pao and T. W. Kao, "Vortex structure in the wake of a sphere," Phys. Fluids, Vol. 20, 1977, p. 187.

Ref. 39. R. J. Hartman and H. W. Lewis, "Wake collapse in a stratified fluid: linear treatment," J. Fluid Mech., Vol. 51, 1972, p. 613.

Ref. 40. R. J. Hartman, "The development of a partially mixed region in a stratified shear flow," J. Fluid Mech., Vol. 71, 1975, p. 407.

Ref. 41. T. W. Kao, "Principal stage of wake collapse in a stratified fluid: two-dimensional theory," Phys. Fluids, Vol. 19, 1976, p. 1071.

mean, but of rms size comparable to that estimated for the near wake. The laminar far wake developed by relaminarization further downstream becomes of course part of the distant potential flow already discussed in Subsec. 4.2.

Finally, consider the possibility of large eddies persisting farther downstream, as indicated by the experiment of Pao and Kao (Ref. 38), in stratified fluid of small Richardson number ($Ri \equiv N^2D^2/V_b^2$ where N is buoyancy frequency). If such eddies are produced in the wake collapse, we may suppose them to be slowly rotating, spheroidal vortices, with vertical size ~D, horizontal size perhaps an order of magnitude greater, and angular velocity $\omega \sim N$. In that case, Eqs. 24 and 25 yield $h \lesssim ND^2$, or compared to the near wake estimates above,

$$\frac{\text{eddy OM}}{\text{near wake OM}} \lesssim \frac{DN}{V_b} \equiv \sqrt{Ri} \quad , \tag{83}$$

which is small for $Ri << 1$. Nevertheless, since these putative eddies are very distant from the moving body and large compared to it, their OM field configuration may retain interest.

For example, modeling the eddy as a spherical vortex of radius a with its spin vector parallel to $\underset{\sim}{H}_e$, one can use the detailed solution given in Ref. 13, Subsec. 9.9. In this case, the vector $\underset{\sim}{h}$ is purely horizontal, azimuthally directed, with magnitude $h = H_e\mu\sigma\omega\, a^2(\sin 2\theta/10) \cdot \{(R/a)^2$ for $R \lesssim a$, $(a/R)^3$ for $R \gtrsim a\}$ where θ is angle from vertical. Thus, the size of h is as estimated above (Eq. 83), only now for a sphere and with a factor $\lesssim 1/10$ introduced by the spherical boundary condition, viz., at most $h \lesssim \omega a^2/40$ at $R = a$. The fall off $\propto 1/R^3$ outside the vortex is as expected from the theorem of Subsec. 4.2. The detailed field configurations in horizontal planes passing through and near the spherical vortex are illustrated in Fig. 8 (plane at a/5 above or below vortex center) and in Fig. 9 (plane at 2a/5 above or below vortex edge). Modifications due to air-sea boundary effects are small, as long as the eddy is submerged more than a few radii. However, we note that this vertical-spin-vertical-field example is exceptional in that its OM field in the air above the sea is identically zero (cf. following Eq. 28).

More general cases of arbitrary eddy shape, spin, and field direction will have field configurations outside the eddy given by the theorem of Eq. 29.

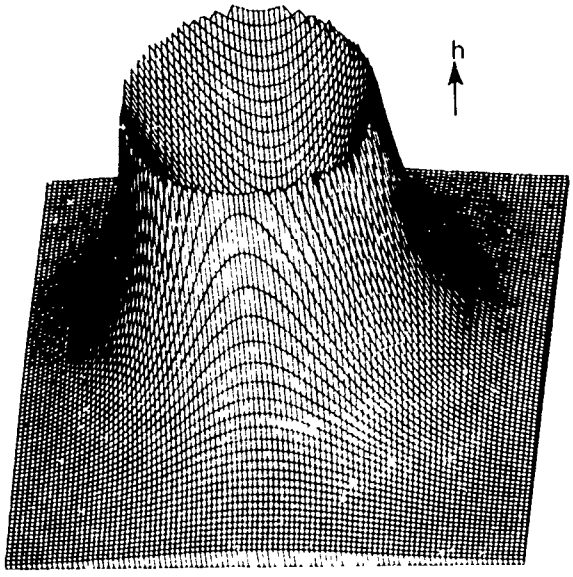

Fig. 8 Vortex Hydromagnetism in Plane Through Spherical Eddy: Spatial Configuration of Total OM Field Over Planes of Rotational Motion Located 1/10 Eddy-Diameter Above or Below Eddy Center.

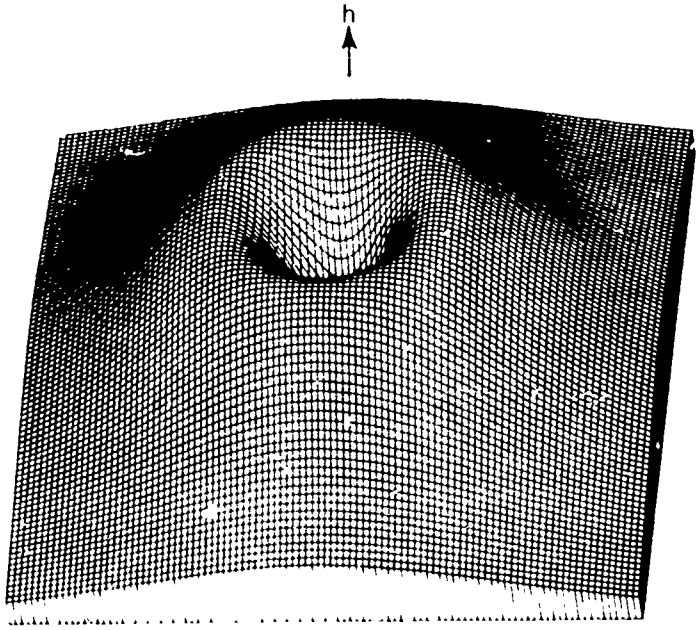

Fig. 9 Vortex Hydromagnetism Above or Below Spherical Eddy: Spatial Configuration of Total OM Field in Planes or Rotation at 1/5 Eddy-Diameter Away from the Eddy Top or Bottom Boundaries.

6.4 SURFACE WAVES

The OM field due to body-generated SW is estimated using Subsec. 4.3, somewhat as we did for natural SW at the beginning of Subsec. 5.1. In the present case, however, for constant body motion $\underset{\sim}{V}_b$, a stationary (in body frame) wave system will develop such that the frequency ω of each Fourier component with wave vector $\underset{\sim}{\kappa}$ satisfies

$$\omega = \underset{\sim}{\kappa} \cdot \underset{\sim}{V}_b \equiv \kappa V_b \cos \theta_{\kappa V} \quad . \tag{84}$$

Equation 84, together with the dispersion relation Eq. 35a, delimits the permissible waves, as detailed below. However, for any ordinary body speed v_b, Eq. 84 alone will suffice to estimate the OM field. That is, Eq. 84 plots as a line of slope -45° and ordinate intercept $V_b \cos \theta_{\kappa V}$ in Fig. 1, which, as long as $V_b \leq 10^2$ m/s, will always intersect the SW dispersion curves well within the quasi-static regime. Hence, Eq. 34a applies with $\tilde{u} \sim \tilde{a}\omega/\tanh \kappa D$ and $L \sim (\tanh \kappa D)/\kappa$ (Subsec. 5.1) to give $\tilde{h} \leq H_e \mu\sigma\tilde{a}\omega/\kappa$. Then Eq. 84 yields at once

$$\tilde{h} \leq H_e \mu\sigma V_b \cos \theta_{\kappa V} \tilde{a} \quad , \tag{85}$$

as an upper limit on the OM amplitude in terms of plane SW amplitude $\tilde{a}$.

A limitation for Eq. 84 to be compatible with the dispersion Eq. 35a, which says that $\omega \leq \kappa\sqrt{gD}$, is the requirement

$$V_b \cos \theta_{\kappa V} \leq \sqrt{gD} \quad . \tag{86}$$

For most usual speeds and depths, $V_b^2/D \leq g$ so that this condition is fulfilled for all angles $\theta_{\kappa V}$. Furthermore, ordinarily $V_b^2/D << g$ so that $\omega << \kappa\sqrt{gD}$, i.e., the deep-water approximation is applicable (cf. Eq. 87, below). Only for very fast motion in very shallow water ($V_b^2/D > g$) is the above restriction important, in which case it limits the range of $\theta_{\kappa V}$ (see below).

In the ordinary case ($V_b^2/D << g$), more accurate formulae for the OM field analogous to those in Subsec. 5.1 are readily obtained. The only difference here is that Eq. 84 combined with the deep-water dispersion relation $\omega^2 \approx \kappa g$ determines

$$\kappa \approx \frac{g}{V_b^2 \cos^2 \theta_{\kappa V}} \quad \text{and} \quad \omega \approx \frac{g}{V_b \cos \theta_{\kappa V}} \tag{87}$$

Notice these give lower bounds ($\kappa \geq g/V_b^2$, $\omega \geq g/V_b$) attained for plane-wave propagation along the direction of body motion ($\theta_{\kappa V} = 0$). The first element of Eq. 87 shows that the body-generated SW are short compared to depth ($\kappa D \geq gD/V_b^2 >> 1$) and the deep-water approximation is quite good. Also, the quasi-static approximation of Eq. 34a ($\omega/\kappa^2 << 1/\mu\sigma$) is verified from Eq. 87 to be adequate for $V_b < (g/\mu\sigma)^{1/3} \sec \theta_{\kappa V}$, which is assured in the ocean (Table 1) for $V_b \leq 10^2$ m/s (cf. above). Therefore, just as in Eq. 38 and the discussion following Eq. 39, only with ν therein given by Eq. 87, we have

$$\tilde{h}_{\text{surface}} \approx \frac{1}{16} \tilde{a} V_b \cdot \{I, \theta_\kappa, \theta_V\} \leq \frac{1}{16} \tilde{a} V_b \quad \text{in } \gamma \tag{88}$$

where $\{I, \theta_\kappa, \theta_V\} \equiv \cos(\theta_\kappa - \theta_V) \sqrt{\sin^2 I + \cos^2 I \cos^2 \theta_\kappa}$ in terms of dip angle I and compass angles θ_κ, θ_V of wave propagation and body motion, respectively, so $|\theta_{\kappa V}| = |\theta_\kappa - \theta_V|$. Equation 88 gives the OM plane-wave component at the air-sea interface in terms of the plane SW amplitude $\tilde{a}$. The altitude (or depth) variation is exponential (or predominantly so) corresponding to Eq. 39 and following. However, in the present case one sees from Eq. 87 that

$$\text{vertical scale} \sim \frac{1}{\kappa} \leq \frac{V_b^2}{g} \tag{89}$$

is typically small (i.e., the body-induced SW are short) so that the OM field is essentially restricted to the near-surface region. There Eq. 88 will give a fair estimate of the OM field.

In the fast-shallow situation ($V_b^2/D > g$), we saw that the permissible wave solutions are restricted to the directions $\cos \theta_{\kappa V} \leq \sqrt{gD}/V_b$ (cf. also Ref. 20, p. 440). However, Eq. 88 with this restriction remains a fair estimate, as does Eq. 89 well within the allowed directions. For $\theta_{\kappa V}$ approaching the cut-off angle θ_c, the scale by Eqs. 35a and 84 becomes $1/\kappa \propto 1/\sqrt{\theta_{\kappa V} - \theta_c} \to \infty$, but the OM amplitude remains bounded in accord with Eqs. 85 and 86, viz., $\tilde{h} \leftrightarrows H_e \mu\sigma \sqrt{gD}\, \tilde{a}$ (cf. Eq. 39b).

For a simple illustration, consider the one-dimensional ($\theta_\kappa = \theta V = 0$) SW generated by a cylinder of radius b moving at submerged depth d in deep water. According to Dagan (Ref. 42), linear

Ref. 42. G. Dagan, "Free-surface gravity flow past a submerged cylinder," J. Fluid Mech., Vol. 49, 1971, p. 179.

wave theory is valid for $d \geq 5b$, in which case the wave amplitude is $\tilde{a} = 4\pi b^2 \kappa e^{-\kappa d}$ (Ref. 20, p. 412). Then Eq. 88 with Eq. 87 gives

$$\tilde{h} \approx \left(\frac{\pi b^2 g}{4V_b}\right) \exp\left(\frac{-gd}{V_b^2}\right) \quad , \qquad (d \geq 5b) \quad , \tag{90}$$

which depends on cylinder size b and depth d as one might expect. The body-speed dependence is such that the OM field is a maximum for $V_b = \sqrt{2gd}$, giving $\tilde{h}_{max} \approx b^2/\sqrt{d}\ \gamma \leq \frac{1}{2}b^{3/2}\ \gamma$ for $d \geq 5b$, from Eq. 90. For moderate depths ($2.5b \leq d \leq 5b$), the same formulae hold with d replaced by a larger effective depth; for shallower depths ($0 < d < 2.5b$), nonlinearities modify the SW significantly (Ref. 42).

Realistic two-dimensional wave systems require Fourier integration of Eq. 88 to determine the OM field $\underline{h}$. Of course, h may be estimated from a knowledge of the dominant SW amplitudes. The intricacies of wave patterns (Ref. 43) will be reflected in correspondingly complex configurations of the OM field. However, perhaps the major difference from one-dimensional models is that the SW amplitudes $\tilde{a}$ fall off with distance from the source, except possibly in any singular directions.

For example, Kelvin ship-wave patterns as sketched in Fig. 10 consist of transverse ($\sqrt{2/3} \leq \cos\theta_{KV} \leq 1$) and lateral ($0 \leq \cos\theta_{KV} \leq \sqrt{2/3}$) systems of equal amplitude (Ref. 20, p. 436). However, the transverse waves being longer, they have larger R_M ($\propto \tilde{u}/\kappa \propto \omega/\kappa \propto \cos\theta_{KV}$, by Eq. 87) and therefore tend to contribute more to the size (and extent away from the surface) of the OM field. Mathematically, one sees in Eq. 88 that the angle factor $\{I, \theta_K, \theta_V\}$ is larger for transverse plane waves than for lateral, excepting east-west ship headings ($\theta_V \sim \pm\pi/2$) in the tropics ($I \sim 0$). Particularly in polar regions, or for more north-south ship headings elsewhere, the transverse waves dominate in the OM effect, giving

$$\tilde{h} \sim \frac{1}{16}\tilde{a}\, V_b \sin I\ \gamma \quad . \tag{91}$$

Of course, the plane-wave amplitudes $\tilde{a}$, and thus $\tilde{h}$, must be determined from the usual two-dimensional circular wave solutions. However, well within the wake and far downstream, the transverse system looks like plane waves of slowly decreasing amplitude,

---

Ref. 43. C. Hunter, "On the calculation of wave patterns," J. Fluid Mech., Vol. 53, 1972, p. 637.

$$\tilde{a} \propto R^{-\frac{1}{2}} \qquad (\theta_{\kappa V} \approx 0) \tag{92}$$

at horizontal ranges R in given direction (Ref. 20, p. 436), and the OM field falls off correspondingly. We remark that in the cusp directions, the wave height decreases more slowly,

$$a \propto R_c^{-\frac{1}{3}} \qquad (\cos^2 \theta_{\kappa V} = \frac{2}{3}\ , \quad \theta_{\kappa V} \approx \pm 35°) \tag{93}$$

for a (not its Fourier amplitude $\tilde{a}$) as a function of distance R_c along a cusp (Ref. 44). Hence, h can fall off slowly. However, more elaborate analysis is necessary to include the singular directions (Eq. 93)

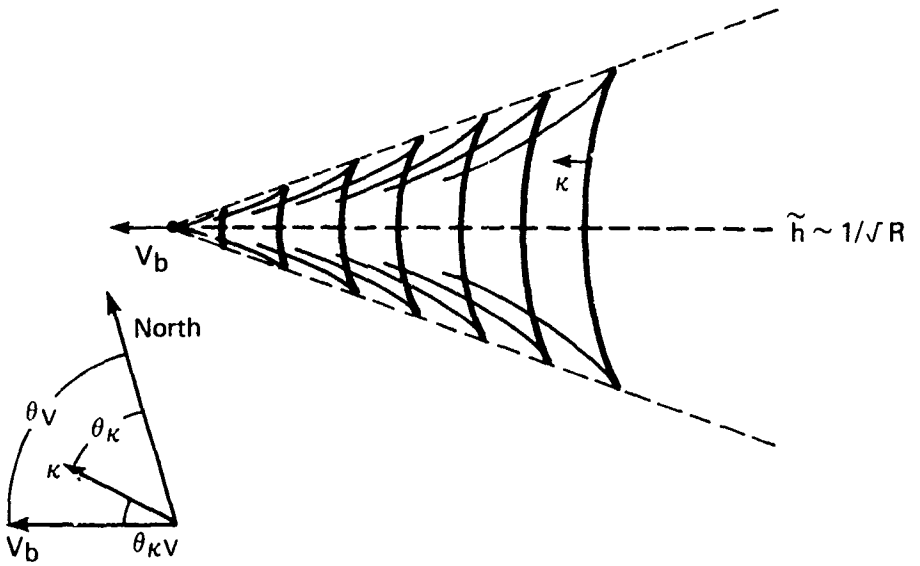

Fig. 10 Kelvin Ship-Wave Hydromagnetism: h Contributed Largely by Lateral Waves (bold wavefronts, propagation vector κ) From Body Surface Movement (V_b), with Asymptotic Range (R) Dependence Indicated (cf. Eq. 90). Inset shows direction angles of text (cf. Eqs. 84 and 88).

Ref. 44. F. Ursell, "On Kelvin's shipwave pattern," J. Fluid Mech., Vol. 8, 1960, p. 418.

6.5 INTERNAL WAVES

In stratified ocean, a moving body generates IW whose OM effects can be estimated as for the SW above. IW motion is in general three dimensional and vertically inhomogeneous, but its horizontal dependence may usefully be expanded in plane waves ω, $\underset{\sim}{\kappa}$. Then for constant body motion $\underset{\sim}{V}_b$, again one has a wave system stationary in the body frame that satisfies Eq. 84 as before. Since the IW curves in Fig. 1 lie considerably below the SW ones, the compatibility condition between Eq. 84 and the IW dispersion Eq. 35b will be more restrictive than in the case of SW (see below). By the same token, however, the allowed IW a fortiori fall further than did the SW within the quasi-static regime of Fig. 1. Hence, Eq. 34a with Eq. 84 gives as above immediately

$$\tilde{h}(z) \leq H_e \mu \sigma V_b \cos \theta_{\kappa V} \tilde{a}_I(z) \tag{94}$$

for the OM amplitude due to a plane IW, in terms of its azimuth $\theta_{\kappa V}$ in the horizontal plane corresponding to vetical coordinate z and its amplitude $a_I(z)$.

The restriction imposed by the IW dispersion relation can be seen from Fig. 1, again imagining there the -45° line (Eq. 84). It intersects the IW curves only if it does not exceed the limit for long IW, for which the thin thermocline of Eq. 35b is most apt, giving $\omega \leq \kappa\sqrt{g(\delta\rho/\rho)d}$. Therefore, from Eq. 84,

$$V_b \cos \theta_{\kappa V} \leq \sqrt{g(\delta\rho/\rho)d} \sim \text{few m/s} \tag{95}$$

for typical pycnocline depth d and density change $\delta\rho/\rho$ (Table 1) in ocean of depth $D >> d$. (For finite D, Eq. 95 is reduced by $\sqrt{1 - d/D}$.) Thus, only for slowly moving bodies or for very deep, strong pycnoclines is there no serious restriction. Otherwise, Eq. 95 delimits permissible IW propagation angles $\theta_{\kappa V}$ for all $V_b > \sqrt{g(\delta\rho/\rho)}$ (cf. Ref. 20, p. 416 for the one-dimensional case, $\theta_{\kappa V} = 0$).

To illustrate the more detailed behavior, we may consider various limiting cases that arise as $V_b \cos \theta_{\kappa V}$ is decreased from its limit (Eq. 95). One sees from Fig. 1 that, as the -45° line of Eq. 84 is lowered, it intersects the IW curves initially in the long-wave ($1/\kappa \geq d$) region; then, for $V_b \cos \theta_{\kappa V}$ somewhat below the limit of Eq. 95, in an intermediate wavelength ($\epsilon << 1/\kappa \leq d$) region, provided the pycnocline structure so allows (i.e., width

ε << depth d); and ultimately in the short-wave ($1/\kappa < \varepsilon$) region where the IW dispersion curve becomes bounded by the buoyancy frequency, i.e., $\omega^2 \leq N^2 \sim g(\delta\rho/\rho)/\varepsilon$ (cf. Ref. 18).

For the long waves with $V_b \cos\theta_{\kappa V} \approx \sqrt{g(\delta\rho/\rho)d}$, i.e., near the cutoff angles (θ_c) indicated by Eq. 95, the dispersion Eq. 35b together with Eq. 84 gives that

$$\kappa^2 \approx \frac{6}{Dd} \tan\theta_c \cdot |\theta_{\kappa V} - \theta_c| \ , \quad (\theta_{\kappa V} \approx \theta_c) \ , \tag{96a}$$

again for D >> d. Thus, κ (and ω) $\to 0$ as $\theta_{\kappa V} \to \theta_c$, while Eqs. 94 and 95 with the values of Table 1 yield

$$\tilde{h}(z) \leq \sqrt{(\delta\rho/\rho)d} \cdot \tilde{a}_I(z)\ \gamma \ , \quad (\theta_{\kappa V} \to \theta_c) \tag{96b}$$

as the absolute upper bound on the OM amplitude.

For the solutions with $V_b \cos\theta_{\kappa V}$ somewhat smaller, but not so much as to vitiate the thin pycnocline approximation, say $\sqrt{g(\delta\rho/\rho)\varepsilon} << V_b \cos\theta_{\kappa V} \leq \sqrt{g(\delta\rho/\rho)d/2}$ (assuming ε << d), the dispersion relation is the $\kappa d \geq 1$ form of Eq. 35b, i.e., $\omega \approx \sqrt{\kappa g(\delta\rho/\rho)/2}$. This together with Eq. 84 determines (cf. Eq. 87)

$$\kappa \approx \frac{g(\delta\rho/\rho)}{2V_b^2 \cos^2\theta_{\kappa V}} \quad \text{and} \quad \omega \approx \frac{g(\delta\rho/\rho)}{2V_b \cos\theta_{\kappa V}} \ , \tag{97a}$$

which with the above limits on $V_b \cos\theta_{\kappa V}$ span the wavelength and frequency ranges

$$\varepsilon << \frac{1}{\kappa} \leq d \quad \text{and} \quad \sqrt{\varepsilon/2d}\ N \leq \omega << N \tag{97b}$$

indicated earlier. Observe from Eqs. 97 that the quasi-static approximation of Eq. 34a ($\omega L^2 \leq \omega/\kappa^2 << 1/\mu\sigma$) is assured for d << $(2/\mu^2\sigma^2 g(\delta\rho/\rho))^{1/3}$, which is at least $\sim 10^4$ m.

This range of $V_b \cos\theta_{\kappa V}$ leading to Eq. 97b covers the bulk of the admissible IW for a thin pycnocline (ε << d). For such waves, Beal and Weaver's work (Ref. 7), which led to Eq. 52 above except with $c_{ph} = \omega/\kappa = V_b \cos\theta_{\kappa V}$ here by Eq. 84, gives the (±50%) estimate

$$\tilde{h} \sim \frac{1}{10} V_b \cos\theta_{\kappa V} \tilde{a}_I \approx \frac{1}{4} \sqrt{(\delta\rho/\rho)/\kappa}\ \tilde{a}_I\ \gamma \ \text{(at pycnocline)} \tag{97c}$$

using Eq. 97a. Away from the pycnocline, $\tilde{h}$ falls essentially exponentially with

$$\text{vertical scale} \sim \frac{1}{\kappa} \leqslant d \quad . \tag{97d}$$

In Eqs. 97c and 97d, κ varies according to Eqs. 97a and 97b.

Eventually, IW with $V_b \cos \theta_{\kappa V} \leqslant \sqrt{g(\delta\rho/\rho)\varepsilon}$ enter as higher modes if the pycnocline is sharp ($\varepsilon << d$), or in place of the above "thin-thermocline" mode if it is diffuse ($\varepsilon \sim d$). In either event, these waves have scale length $\leqslant$ pycnocline thickness, so details of the stratification assume importance. However, one can roughly estimate the OM field from the general properties of the IW modes. Their spatial variation is dominated by the shorter of the two lengths given in Phillips (Ref. 18, Sec. 5.2), the horizontal $\ell_h \sim 1/\kappa$ for $\omega \sim N$ and the vertical $\ell_z \sim \ell_h/\sqrt{N^2/\omega^2 - 1} \sim \omega/N\kappa$ for $\omega << N$. Thus, one can write for the scale length in the mode with $\kappa = \kappa_n$,

$$\ell_n \sim \frac{\omega}{N\kappa_n} \qquad \text{(mode n)} \quad . \tag{98a}$$

Then from the quasi-static Eq. 34a with $L \sim \ell_n$ there, one has directly

$$\tilde{h}(z) \leqslant H_e \mu\sigma \ell_n \tilde{u}_I(z) \approx \frac{1}{4} \ell_n \tilde{u}_I(z) \gamma \tag{98b}$$

for an upper limit on the OM amplitude due to the IW mode n with velocity amplitude $\tilde{u}_I(z)$.

The direction angle $\theta_{\kappa V}$ for these higher modes by Eqs. 84 and 98a satisfy

$$\cos \theta_{\kappa V} = \frac{\omega}{V_b \kappa_n} \sim \frac{N}{V_b} \ell_n \text{ (mode n)} \quad . \tag{99}$$

This represents a quantization of $\theta_{\kappa V}$ that can have import for the extent of the OM field, as discussed later. For the OM size, however, Eq. 99 simply reproduces the estimate of Eq. 98b with $\tilde{u}_I \to \omega\tilde{a}_I$, using Eq. 94 corrected by a factor $\kappa\ell_n \sim \omega/N$ to include the cases $\ell_z << \ell_h$ encountered here. Note that by assumption above $V_b \cos \theta_{\kappa V} \leqslant \sqrt{g(\delta\rho/\rho)\varepsilon}$, which by Eq. 99 implies $\ell_n \leqslant \varepsilon$ as we have indicated. Also notice that in the limiting extreme of an infinite

ocean, in which case $d \to \infty$, Eq. 95 no longer restricts but instead is replaced by $V_b \cos \theta_{\kappa V} \leqslant N\epsilon$.

To determine the full extent and configuration of the OM field requires a detailed analysis equivalent to superimposing (via multiple Fourier integration and with proper selection to fit the boundary conditions, e.g., Eq. 10b) the various IW solutions we have estimated. In special cases, however, some estimate of the range behavior is easily obtained. For example, in a thin-thermocline approximation the dominant IW displacement at the interface behaves asymptotically like a plane wave of amplitude

$$\tilde{\varepsilon}_I \propto \frac{1}{\sqrt{\rho}}$$

at large horizontal ranges ρ, according to Hudimac (Ref. 45, Eq. 44). Then the OM field behaves similarly by Eqs. 96b or 97c. At the other extreme, in an infinitely thick constant-N thermocline, the IW flow velocity behaves asymptotically like a plane wave of amplitude

$$\tilde{u}_I \propto \frac{1}{R}$$

at large radial distances R, according to Miles (Ref. 46, Eqs. 6.12 and 6.13). In this case, Eq. 98b (with $\ell_n \sim$ Miles' $1/k \equiv V_b/N$) gives similar range behavior for the OM field. More generally, however, the IW mode structure has to be taken into account.

The quantization of the IW into discrete modes can lead to singular behavior in preferred directions. Consider the field at large distances in or near the pycnocline, which corresponds to small κ in the Fourier inversion, and therefore to large ℓ_h above. Thus, the higher modes for which $\ell_h \gg \ell_z$ contribute largely to this asymptotic field. For such modes the scale length is $\ell_n \approx \ell_z$. Now ℓ_z is determined by the boundary conditions at the air-sea surface and seabed (Ref. 18). Therefore, from Eq. 99 the mode angle $\theta_{\kappa V}$ is also essentially fixed, viz.,

$$\cos \theta_{\kappa V} = \cos \theta(n) \sim \frac{N}{V_b} \ell_z(n) \quad \text{(mode n)} \quad . \tag{100}$$

Ref. 45. A. A. Hudimac, "Ship waves in a stratified ocean," J. Fluid Mech., Vol. 11, 1961, p. 229.

Ref. 46. J. W. Miles, "Internal waves generated by a horizontally moving source," Geophys. Fluid Dyn., Vol. 2, 1971, p. 63.

As a consequence, each higher mode yields via Fourier inversion an asymptotic field contribution that is predominantly in the reciprocal direction

$$\phi(n) = \frac{\pi}{2} - \theta(n) \quad , \tag{101}$$

where ϕ is the field-point horizontal azimuth, measured from the downstream ($-\underset{\sim}{V}_b$) direction. (Briefly, Eq. 101 arises from Eq. 100 as follows: in cylindrical polar coordinates ρ, ϕ, z with z axis vertical, $\underset{\sim}{h}(\rho,\phi,z) \equiv \int d\underset{\sim}{\kappa} e^{i\kappa\rho \cos(\theta_{\kappa V} + \phi)} \underset{\sim}{\tilde{h}}(z)$ goes by Eq. 100 to $\int \kappa d\kappa \, e^{i\kappa\rho \cos(\theta(n) + \phi)} \underset{\sim}{\tilde{h}}_n(z)$ whose horizontal asymptote ($\rho \to \infty$) is predominantly along the direction for which $\cos(\phi + \theta(n)) = 0$.) Notice that as the mode n increases so that $\ell_z(n)$ decreases, $\theta(n) \to \pi/2$ by Eq. 100, so that $\phi(n) \to 0$, by Eq. 101. That is, the higher modes contribute asymptotically mainly within the downstream cone

$$\phi < \phi(1) \sim \sin^{-1} \frac{N\ell_z(1)}{V_b} \quad , \tag{102}$$

which for a given stratified ocean varies inversely with V_b, as depicted by the stippled region in Fig. 11.

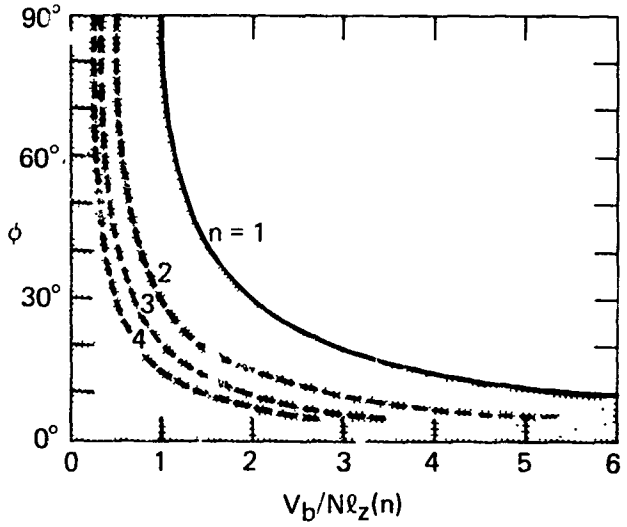

Fig. 11 Singular Wedge of Internal-Wave Wake of Horizontal Azimuth (ϕ) as a Function of Body Velocity (V_b) in Units of Brunt-Vaisala Frequency (N) Times Vertical Scale of n^{th} Mode ($\ell_z(n)$). In general, all singular rays lie in the stippled region defined by the lowest mode (n = 1); for the special case of the exponentially stratified ocean model, singular rays for higher modes (n = 2, 3, 4 . . .) are determined by the dashed curves.

We may illustrate, and also summarize the essential origins of the singular behavior, by considering an exponentially stratified ocean (N = constant and $\epsilon = D$). In that case we have the exact relations,

$$\text{Dispersion:} \qquad \omega^2 = \frac{N^2\kappa^2}{k^2} = \frac{N^2\kappa^2}{\kappa^2 + k_z^2} \quad ,$$

$$\text{Stationarity:} \qquad \omega = \kappa V_b \cos\theta_{\kappa V} \quad ,$$

$$\text{Boundary conditions:} \qquad k_z = \frac{n\pi}{\epsilon} \quad , \quad (n = 1,2,\ldots) \quad ,$$

which yield $\cos\theta_{\kappa V} = (N\epsilon/V_b)/\sqrt{\kappa^2\epsilon^2 + n^2\pi^2}$ (cf. Eq. 39). Then for $\rho \to \infty$ ($\kappa \to 0$), we have for all n

$$\text{Asymptotically:} \qquad \cos\theta(n) = \frac{N\epsilon}{V_b n\pi} \quad ,$$

cf Eq. 100, and by the argument above the corresponding

$$\text{Singular directions:} \qquad \phi(n) = \sin^{-1}\left(\frac{N\epsilon}{V_b n\pi}\right) \quad ,$$

whence our estimate for the downstream limiting cone now becomes exact (Eq. 102). In this ocean model, the above results obtain for all the modes ($n \geq 1$), as indicated by the dashed curves in Fig. 11. These preferred directions were earlier derived by R. I. Joseph from detailed calculations for the N = constant, $\epsilon = D$ model.

6.6 ACOUSTIC WAVES

The compressibility of seawater (Table 1) allows sound radiation to propagate with phase speed $c_s \approx 1500$ m/s, so that

$$V_b \ll c_s \qquad (103)$$

for any normal ocean body motion. Hence, in contrast to the SW and IW cases above, the stationarity condition, Eq. 84, and the

AW dispersion relation, Eq. 35c, from which $\omega \leq \kappa V_b$ and $\omega \geq \kappa c_s$, respectively, are incompatible. That is, in Fig. 1 the line given by Eq. 84 lies far below the AW curve, and they cannot intersect. Physically, no stationary wave system develops, because that requires a relative Doppler shift in the body frame of unity (i.e., frequency zero), whereas the maximum shift for AW is $V_b/c_s \ll$ unity, by Eq. 103. For the OM field induced by AW, therefore, the body is relevant solely as an approximately stationary source of sound, which once emitted propagates as free AW through the ocean. We thus neglect the body motion V_b entirely below.

The sonomagnetic pseudowave emitted along with the AW by virtue of the interaction between acoustic velocities and earth's magnetic field was discussed for plane waves in Subsec. 5.3. At great distances from a radiating body such that the AW is effectively plane, the results are directly applicable. In particular, we may use the simple OM estimates of Eqs. 56 and 57 for an infinite ocean, the more accurate Eq. 58 and its following discussion for air-sea and seabed boundary effects, and Eqs. 59 for the OM aerofield behavior. Of course, the AW intensity level $S \equiv 20 \log \delta P$ in Eqs. 57 and 58 is that existing at the observation point. It is reduced from that at the source position by losses, mainly the transmission loss with proper allowance for channeling (cf. the discussion following Eq. 57). At near-to-moderate distances from the sound-emitting body, however, the acoustic and sonomagnetic waves cannot be considered simply plane. Instead, more complex fields are radiated as determined by source and boundary geometries.

In general, the sonomagnetic field equations consist of our basic Eqs. 22 for $\underset{\sim}{h}$ (with $\underset{\sim}{H} \approx \underset{\sim}{H}_e$, $\underset{\sim}{V}_b \approx 0$, and $\underset{\sim}{u}_0 \equiv \underset{\sim}{\nabla}\phi_s$) and the usual wave equation for the acoustic potential ϕ_s. For simple harmonic emissions of frequency ω, these involve acoustic and magnetic propagation constants,

$$k_s \equiv \frac{\omega}{c_s} \quad \text{and} \quad k_m \equiv \sqrt{-i\mu\sigma\omega} \quad , \tag{104}$$

respectively. Thus, the field equations read

$$(\Delta + k_m^2)\underset{\sim}{h} = \mu\sigma \, \text{curl}(\underset{\sim}{H}_e \times \underset{\sim}{\nabla}\phi_s) \quad , \tag{105a}$$

$$\text{div} \, \underset{\sim}{h} = 0 \quad , \tag{105b}$$

$$(\Delta + k_s^2)\phi_s = Q \quad , \tag{105c}$$

for any sonic source distribution Q. Equations 105 are subject to the magnetic boundary conditions (Eqs. 6) and appropriate acoustic ones. For given Q, the sonic field is determined separately via Eq. 105c, so we may assume it to be known and express $\underset{\sim}{h}$ in terms of ϕ_s as follows. First, we derive a particular integral by writing $\underset{\sim}{h}_p = \mu\sigma \operatorname{curl}(\underset{\sim}{H}_e \times \underset{\sim}{\nabla}\psi)$, which identically satisfies Eq. 105b and also satisfies Eq. 105a if $(\Delta + k_m^2)\psi = \phi_s$. From the similarity of this to Eq. 105c, it is easy to find the solution $\psi = (\phi_s - \phi_m)/(k_m^2 - k_s^2)$ where ϕ_m is the same function as ϕ_s only with $k_s \to k_m$ in it, i.e., $(\Delta + k_m^2)\phi_m = Q$. Thus, a particular integral of Eqs. 105a and 105b is

$$\underset{\sim}{h}_p = \frac{-\mu\sigma \operatorname{curl}[\underset{\sim}{H}_e \times \underset{\sim}{\nabla}(\phi_s - \phi_m)]}{k_s^2 - k_m^2} \tag{106}$$

where $\phi_m \equiv \phi_{s\to m}$. For a monopole Q (cf. below), $\phi_{s,m}$ are just the Green's functions for the Helmholtz operators $(\Delta + k_{s,m}^2)$, respectively, given by Appendix B, Eqs. B.3 and B.5. We can now write the complete solution for the sonomagnetic field as

$$\underset{\sim}{h} = \begin{cases} \underset{\sim}{h}_p + \underset{\sim}{h}_c & \text{(within ocean)} \qquad (107a) \\ \underset{\sim}{h}_{a,b} & \text{(above, below ocean)} \qquad (107b) \end{cases}$$

where $\underset{\sim}{h}_a = \underset{\sim}{\nabla}\Psi$ with $\Delta\Psi = 0$ (Subsec. 2.2), $\underset{\sim}{h}_b$ depends on seabed conductivity, and $\underset{\sim}{h}_c$ is the complementary integral of the homogeneous form of Eq. 105a, $(\Delta + k_m^2)\underset{\sim}{h}_c = 0$, with div $\underset{\sim}{h}_c = 0$ (eq. 105b). Thus, $\underset{\sim}{h}_{a,b,c}$ can be expanded in known functions - $\underset{\sim}{h}_a$ via Ψ in harmonic functions, $\underset{\sim}{h}_c$ in the transverse waves of the vector Helmholtz equation, and $\underset{\sim}{h}_b$ similarly as appropriate (Ref. 47) - and finally determined via the boundary conditions.

For general illustration, we consider a monopole source in a semi-infinite homogeneous ocean. Because the superposition principle is valid for both acoustics and sonomagnetics, the effects of any more general source can be built up as a sum of the monopole effects. Also, for a source whose submergence is shallow relative to the ocean depth, the seabed boundary is of minor importance for the OM field near the body, so only the air-sea boundary need be considered. Inhomogeneities of scale greater than the source and/or

Ref. 47. P. M. Morse and H. Feshbach, Methods of Theoretical Physics, McGraw-Hill, New York, NY, 1953.

the observation depth will also be unimportant; small-scale inhomogeneity, which would greatly complicate the acoustic and consequent sonomagnetic fields, is for simplicity assumed absent.

A monopole emits AW with purely radially directed acoustic velocities $\underset{\sim}{u}_0$ which interact with the earth's field $\underset{\sim}{H}_e$ to induce electrical current in loops with a common axis, along $\underset{\sim}{H}_e$. The air-sea boundary may be idealized as a perfectly reflecting plane for the AW, equivalent to placing an image monopole above the surface which also induces current loops about $\underset{\sim}{H}_e$. Thus physically one sees that the sonomagnetic field is closely related to the familiar electromagnetic radiation generated by magnetic dipoles oriented along $\underset{\sim}{H}_e$, albeit in the sonomagnetic case we have to deal with an infinite distribution of finite-sized loops. The main difference is that the sonomagnetic field will involve the acoustic propagation constant in addition to the (low-frequency) electromagnetic one, k_s and k_m of Eq. 104. That is, the sonomagnetic field solution will take a form analogous to the Sommerfeld integrals for low-frequency EM radiation from submerged radio antennae, but in terms of both k_s and k_m instead of only k_m.

The sonomagnetic field of the monopole is calculated in detail in Appendix B for the case of vertical $\underset{\sim}{H}_e$ — appropriate near the earth's north or south poles (indicated as + and −, respectively, below). The resulting $\underset{\sim}{h}$ field is given via Eqs. (107) with $\underset{\sim}{h}_b$ irrelevant here, $\underset{\sim}{h}_p$ determined by Eq. 106 from the $\phi_{s,m}$ of Appendix B, and aerofield $\underset{\sim}{h}_a$ and complementary function $\underset{\sim}{h}_c$ of the form

$$\underset{\sim}{h}_{a,c} = C_{\pm}(S_1,\omega) \cdot e^{i\omega t} \cdot \underset{\sim}{I}_{a,c}(\omega,d,\rho,z) \quad . \tag{108}$$

Here, $C_{\pm}$ is a constant depending on source intensity S_1 (in db re 1μPa at 1 m) and frequency ω, with $|C_{\pm}| \approx 10^{-5.2+S_1/20}/\nu^2\sqrt{\nu^2+\nu_0^2}$ in γ - m^3 for typical ocean parameters (Table 1) and $\nu_0 \approx 2$ Hz (Eq. 55). The $\underset{\sim}{I}_{a,c}$ are Sommerfeld-like integrals of dimensions $1/m^3$ that vary with source frequency and depth (ω,d) and the cylindrical coordinates (ρ horizontal, z vertical). These integrals are not amenable to closed-form evaluation, except for various field-region approximations as given in Appendix B.

Since the outstanding feature of the sonomagnetic field vis-à-vis the sonic field is that the former extends into the air above the sea (cf. the end of Subsec. 5.3), consider the aerofield $\underset{\sim}{h}_a$ and in particular its measure by a total field magnetometer, $\underset{\sim}{h}_a \cdot \hat{\underset{\sim}{H}}_e \approx \underset{\sim}{h}_a \cdot \hat{\underset{\sim}{z}}$ in the polar regions. Inserting parameters from

Table 1 into Eqs. B.16 through B.20 gives the following simple approximations. At close ranges above a shallow source (ρ,z,d $\ll 240/\nu$ and $180/\sqrt{\nu}$), we have the nonpropagating

$$\text{Near aerofield: } \underset{\sim}{h}_a \cdot \hat{\underset{\sim}{H}}_e \approx \alpha \cdot e^{i\omega t} \quad , \tag{109a}$$

$$|\alpha| \approx 10^{-10.6+S_1/20} \frac{(z+d)d}{\nu R^3} \gamma \quad , \tag{109b}$$

where $z(\geq 0)$ is altitude above sea and $R \equiv \sqrt{\rho^2 + (z+d)^2}$ is range from source (parameters S_1,d,$\nu = \omega/2\pi$). This is largest directly overhead on the surface ($\rho = z = 0, |\alpha| \approx 10^{-10.6+S_1/20}/\nu d$). Still nearly overhead only now at high altitudes ($z \gg 240/\nu$ and $180/\sqrt{\nu}$), $|\alpha|$ goes over from the $\sim 1/(z+d)^2$ of Eq. 109b to $\sim 1/z^4$ (Eq. B.17).

On the other hand, at far horizontal ranges but low altitudes ($\rho \gg 240/\nu$ and $180/\sqrt{\nu}$, z $\ll$ these values, and $d \leqslant \rho$), we have the propagating

$$\text{Far aerofield: } \underset{\sim}{h}_a \cdot \hat{\underset{\sim}{H}}_e \approx \beta \cdot e^{i(\omega t - k_s \rho)} \quad , \tag{110a}$$

a circular wave traveling at the speed $\omega/k_s = c_s$ of sound. Its amplitude is

$$|\beta| \approx 10^{-10.6+S_1/20} F_s(\nu) \cdot \frac{d}{\rho^2} \text{ in } \gamma \quad , \tag{110b}$$

where ρ is horizontal range from the source (S_1,d) and $F_s(\nu)$ is defined in Eqs. B.20 and plotted in Fig. 12, showing a broad maximum at $\nu \sim 1$ Hz. The limiting frequency behavior is $F_s(\nu) \approx \nu_0/\nu$ for $\nu \gg \nu_0$ and $2\sqrt{\nu/\nu_0}$ for $\nu \ll \nu_0$, where ν_0 is the transition frequency (≈ 2 Hz) of Eq. 55. Therefore, the sonomagnetic pseudowave propagating at sound speed according to Eqs. 110 is greatest for monopoles of infrasonic frequency at deep submergence (as long as $d \leqslant \rho$), and of course for high intensity S_1, but falls off rapidly with range ρ. For a monopole source $S_1 = 180$ dB at $\nu \sim 2$ Hz and $d \sim 10^2$ m, Eq. 110b yields wave amplitude $|\beta| \sim 2/\rho^2\ \gamma$.

More realistic acoustic sources than the monopole are included in the detailed sonomagnetic theory to be presented in a subsequent report of this series. For example, the dipole sonomagnetic pseudowave can exceed Eqs. 110 by as much as $\sqrt{3}/k_s d$, so that in the numerical example above the aerofield amplitude can increase to $|\beta| \sim 10/\rho^2\ \gamma$, now independently of the submergence depth d.

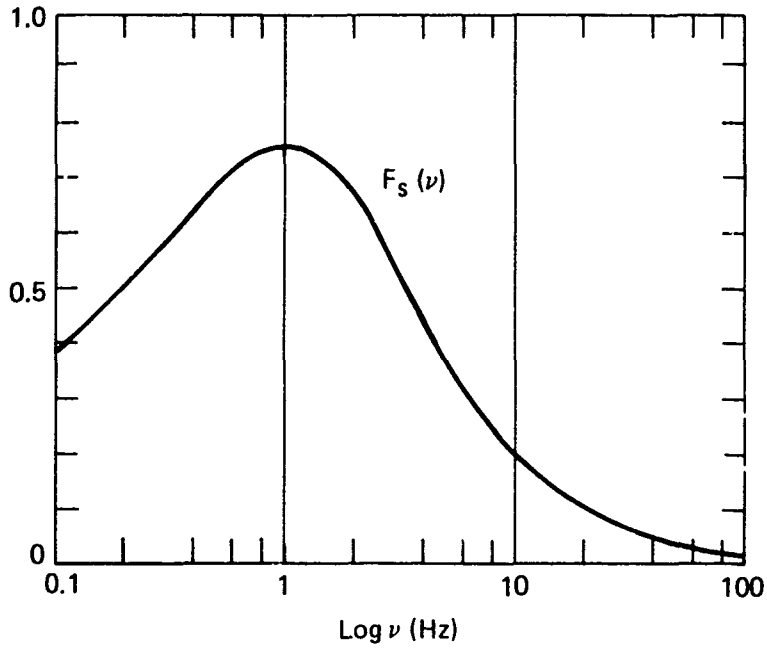

Fig. 12 Sonomagnetic Frequency Response Function: $F_S(\nu)$ as a Function of Frequency (ν) for Far-Field Pseudoradiation of Eqs.110.

7. CONCLUSION

This survey substantiates the general conjecture that the great majority of OM phenomena are reliably estimated from the rule of thumb:

$$h \sim R_M H_e \leq \frac{1}{4} u_0 L \quad (\text{in } \gamma) \quad , \tag{111}$$

for the OM field magnitude h in the quasi-static approximation of Eqs. 24, 25, or 34a. The notable exceptions are long SW (Subsec. 5.1.5) and infrasonic AW (Subsecs. 5.3 and 6.6), for which however the equally simple approximation Eq. 34b is applicable.

The broad conclusion to be drawn from the detailed estimates of Secs. 5 and 6 is that OM fields are typically of the order of magnitude of gammas or less. Despite this inherent weakness of ocean magnetism, however, even the smaller OM fields are considerable relative to current SQUID (Superconducting Quantum Interference Device) magnetometer sensitivities (10^{-4} $\gamma/\sqrt{\text{Hz}}$ or better, cf. Refs. 48 and 49). Thus in magnetic measurements in the ocean environment, all the OM fields considered are potential contributors. Of course the detectability of any one OM effect, in isolation from the others regarded as "noise," depends on the uniqueness of its particular spatial or temporal characteristics.

The OM field extents and their detailed spatial-temporal configurations vary considerably, with features of special interest from case to case. The survey character of this report makes it unfeasible to summarize all of our results here with proper regard to the assumptions and restrictions made in each case. It is preferable to refer to the detailed discussion in the relevant subsections of Secs. 5 and 6. The glossary of major symbols given on the following pages will facilitate use of the estimation formulae we have derived.

Ref. 48. J. Clarke, "Josephson junction detectors," Science, Vol. 184, 1974, p. 1235.

Ref. 49. J. Clarke, "Principles and limitations of SQUIDs," Bull. Am. Phys. Soc., Vol. 22, 1977, p. 86.

GLOSSARY OF MAJOR SYMBOLS

General: $\underset{\sim}{(\ )}$ denotes vector, $\underset{\sim}{\hat{(\ )}}$ unit vector, $\tilde{(\ )}$ Fourier amplitude

a	wave amplitude (subscripts: ν ⇒ at frequency ν, I ⇒ internal wave)
AW	acoustic wave
b	subscript denoting body quantity
c_{ph}	wave phase speed
c_s	sound speed
d	pycnocline depth, or body depth (Sec. 6)
D	ocean depth, or body diameter (Sec. 6)
E	electric field
$F_s(\nu)$	sonomagnetic frequency function (Fig. 12)
g	gravitational acceleration
h	induced magnetic field
H	total magnetic field (subscripts: 0 ⇒ ambient, e ⇒ earth, b ⇒ body)
I	magnetic dip angle
IW	internal wave
j	electric current density
k	wave-vector magnitude (subscripts: s ⇒ sound, m ⇒ magnetic)
ℓ	acoustic mode number
ℓ_n	scale length of IW mode n
L	length scale, or body length (Sec. 6)
m	magnetic dipole moment (subscripts: b ⇒ body, hm ⇒ hydromagnetic, 0 ⇒ combination)

N	buoyancy frequency (Brunt-Vaisala)
OM	ocean magnetic
P	pressure
R	radial distance
Re	Reynolds number
R_M	magnetic Reynolds number (Eq. 8)
R_v	radius of diffusion region for body of velocity V (Fig. 5)
S	acoustic intensity level, or spin (Subsec. 4.2), wave spectrum (Subsec. 5.1.2)
S_1	acoustic intensity level at 1 m from source in db re 1μPa
SM	sonomagnetic
SW	surface wave
T	time scale (period for waves)
u	flow speed
v	hydromagnetic perturbation to the flow
V_b	body speed
W_K	Wind speed (subscript: K => in knots)
z	vertical coordinate
β	compressibility
γ	unit of magnetism (= 10^{-5} G)
ε	pycnocline thickness, or dielectric constant (Sec. 2)
η	shear viscosity
θ	polar angle
$\theta_{\kappa V}$	angle between wave vector and body velocity
κ	horizontal wave vector magnitude

λ	wavelength
μ	magnetic permeability
ν	circular frequency
ν_0	acoustic transition frequency ($\approx$ 2 Hz)
ρ	water density, or horizontal range
σ	electrical conductivity
τ_d	magnetic diffusion time
ϕ	azimuthal angle
ϕ_s	acoustic potential
Φ	flow potential
Ψ	magnetic scalar potential
ω	angular frequency

Appendix A
FORMAL HYDROMAGNETIC SOLUTIONS IN QUASI-STATIC LIMIT

When the hydromagnetic rate of change ($\partial/\partial t \sim 1/T$ in Eqs. 22) is slow relative to the rate of magnetic diffusion ($1/\tau_d$ of Eq. 8), the describing Eqs. 22 become

$$\Delta \underset{\sim}{h} \approx \mu\sigma \, \mathrm{curl}(\underset{\sim}{H}_0 \times \underset{\sim}{u}_0) \quad , \qquad \mathrm{div}\, \underset{\sim}{h} = 0 \quad , \qquad \text{(A.1a,A.1b)}$$

in the approximation of Eq. 23 and omitting a body field and/or velocity. Thus for slow temporal variations, time enters only parametrically in Eqs. A.1. The first is a vector Poisson equation (Ref. 47, Chap. XIV); using its Green's function $1/|\underset{\sim}{r} - \underset{\sim}{r}'|$ (i.e., $\Delta\, 1/|\underset{\sim}{r} - \underset{\sim}{r}'| = -4\pi\delta(\underset{\sim}{r} - \underset{\sim}{r}')$), one can write at once the particular integral

$$\underset{\sim}{h}_p(\underset{\sim}{r}) = \frac{\mu\sigma}{4\pi} \int \frac{d\underset{\sim}{r}'}{|\underset{\sim}{r} - \underset{\sim}{r}'|} \, \mathrm{curl}' \, (\underset{\sim}{u}_0 \times \underset{\sim}{H}_0)' \quad . \qquad \text{(A.2)}$$

By a parts integration (with $\underset{\sim}{u}_0$ assumed to fall rapidly enough with distance) and from the reciprocity property $(\partial/\partial \underset{\sim}{r} + \partial/\partial \underset{\sim}{r}')\, 1/|\underset{\sim}{r} - \underset{\sim}{r}'| = 0$, Eq. A.2 becomes

$$\underset{\sim}{h}_p(\underset{\sim}{r}) = \frac{\mu\sigma}{4\pi} \, \mathrm{curl} \left[\int \frac{d\underset{\sim}{r}' \, (\underset{\sim}{u}_0 \times \underset{\sim}{H}_0)'}{|\underset{\sim}{r} - \underset{\sim}{r}'|} \right] \quad , \qquad \text{(A.3)}$$

which evidently also satisfies Eq. A.1b. On the assumptions of uniform ambient field ($\underset{\sim}{H}_0$ = constant) and incompressible flow ($\mathrm{div}\, \underset{\sim}{u}_0 = 0$), the use of vector identities and reciprocity with parts integration as above further reduces Eq. A.3 to

$$\underset{\sim}{h}_p(\underset{\sim}{r}) = \frac{\mu\sigma}{4\pi} \, (\underset{\sim}{H}_0 \cdot \underset{\sim}{\nabla}) \int \frac{d\underset{\sim}{r}' \, \underset{\sim}{u}_0(\underset{\sim}{r}')}{|\underset{\sim}{r} - \underset{\sim}{r}'|} \quad , \qquad \text{(A.4)}$$

corresponding to Eq. 26 as given in the text.

In the quasi-static approximation and on the above assumptions, Eq. A.4 thus gives the complete formal solution of the hydromagnetic Eqs. 22 ($\approx$ Eqs. A.1) for an infinite medium. (Recall

that other hydromagnetic variables are given in terms of $\underset{\sim}{h}$ via Eqs. 7.) In the case of a bounded medium, the solution is modified to satisfy boundary conditions by adding to Eq. A.4 a suitable linear combination of complementary solutions of the homogeneous form of Eqs. A.1, i.e., the divergenceless vector harmonics that satisfy the vector Laplace equation ($\Delta\underset{\sim}{h} = \text{div}\ \underset{\sim}{h} = 0$, cf. Ref. 47, p. 1784).

In the quasi-static limit, an alternative method of solution is available that determines $\underset{\sim}{h}$ in two stages, instead of directly via the hydromagnetic Eqs. 5 through 7 (or 22 and 7). Since the first stage of solution involves scalar Poisson and Laplace equations, the method can have particular advantage for the application of boundary conditions. The second stage then determines $\underset{\sim}{h}$ via a Biot-Savart or vector potential type integration.

Thus, returning to Maxwell's equations with $\partial/\partial t$ neglected, one has from Eq. 1a that curl $\underset{\sim}{E} = 0$, so that

$$\underset{\sim}{E} = -\nabla\phi \tag{A.5}$$

in terms of an electrostatic potential ϕ. Taking the divergence of Eq. A.5 and using Eq. 7c of the text yields

$$\Delta\phi = \mu\ \text{div}(\underset{\sim}{u} \times \underset{\sim}{H}) \approx \mu\underset{\sim}{H}_0 \cdot \text{curl}\ \underset{\sim}{u}_0 \quad , \tag{A.6}$$

the latter form holding on present assumptions ($\underset{\sim}{u} \approx \underset{\sim}{u}_0$, $\underset{\sim}{H} \approx \underset{\sim}{H}_0 =$ constant). The approximate Eq. A.6 is a scalar Poisson equation, provided the unperturbed flow is rotational (curl $\underset{\sim}{u}_0 \neq 0$) and has some vorticity along the magnetic field ($\underset{\sim}{H}_0 \cdot$ curl $\underset{\sim}{u}_0 \neq 0$). Otherwise, notably for any irrotational flows, it becomes simply the Laplace equation.

In any event, with given right-hand side and appropriate boundary conditions in Eq. A.6, its solution ϕ determines $\underset{\sim}{E}$ via Eq. A.5 and thence the current

$$\underset{\sim}{j} \approx \sigma(-\nabla\phi + \mu\underset{\sim}{u}_0 \times \underset{\sim}{H}_0) \tag{A.7}$$

by the modified Ohm's law (Eq. 2a, and see the discussion following Eq. 4 of the text). Finally, the hydromagnetic field follows from Eq. 7b (with $\underset{\sim}{H}$ = constant) in the integral form

$$\underset{\sim}{h}(\underset{\sim}{r}) = \frac{1}{4\pi}\int d\underset{\sim}{r}'\ \underset{\sim}{j}' \times \nabla'\ \frac{1}{|\underset{\sim}{r} - \underset{\sim}{r}'|} \quad . \tag{A.8}$$

One may verify that Eq. A.8 upon insertion of Eq. A.7 reduces to the infinite medium Eq. A.3, above, by use of the vector identity (with Eq. A.5) $\nabla\phi \times \nabla 1/|\underset{\sim}{r} - \underset{\sim}{r}'| = \text{curl}\,(\underset{\sim}{E}/|\underset{\sim}{r} - \underset{\sim}{r}'|)$ and the integral theorem $\int d\underset{\sim}{r}'\ \text{curl}'\ (\underset{\sim}{E}'/|\underset{\sim}{r} - \underset{\sim}{r}'|) = \int d\underset{\sim}{\sigma}' \times \underset{\sim}{E}'/|\underset{\sim}{r} - \underset{\sim}{r}'| = 0$ for field falling off adequately at infinity, and then rearranging the remaining portion of Eq. A.8 by use of the reciprocity property.

Appendix B

SONOMAGNETISM INDUCED BY SUBMERGED ACOUSTIC MONOPOLE

The sonomagnetic field Eqs. 105 are solved by the method of Eqs. 106 and 107, and the discussion following thereafter, for a simple harmonic acoustic monopole submerged in a semi-infinite homogeneous ocean, whose surface is approximated as a perfect sound reflector. Thus, the source term in Eq. 105c is a monopole at depth z = -d and its negative image in the air-sea surface (z = 0) at altitude z = +d,

$$Q = -4\pi K e^{i\omega t} \left[\delta(\underset{\sim}{r} + \hat{\underset{\sim}{z}}d) - \delta(\underset{\sim}{r} - \hat{\underset{\sim}{z}}d)\right] \quad . \tag{B.1}$$

The strength coefficient K can be expressed via acoustic relations (Lamb, Ref. 25) in terms of the source intensity level S_1 (in dB re 1 μPa) at unit distance from the source in the absence of boundary reflections,

$$K = \frac{ic^2}{\omega} \cdot \beta P \cdot 10^{-11+S_1/20} \quad , \tag{B.2}$$

where c_s is sound speed, β compressibility of seawater, and P ambient pressure. Notice that the last factor in Eq. B.2 contains unit length, so K has dimensions of length^3/time. The solution of Eqs. 105c and B.1 for the acoustic potential ϕ_s is composed of spherical waves from the source and its image,

$$\phi_s = K\left(\frac{e^{i\omega t - ik_s r}}{r} - \frac{e^{i\omega t - ik_s r'}}{r'}\right) \quad , \tag{B.3}$$

in which r is distance from source and r′ from its image,

$$r \equiv \sqrt{\rho^2 + (z+d)^2} \quad , \qquad r' \equiv \sqrt{\rho^2 + (z-d)^2} \quad , \tag{B.4}$$

in cylindrical coordinates ρ, with z centered at the air-sea surface directly above the source (at ρ = 0, z = -d). The magnetic potential function ϕ_m used to construct the particular integral $\underset{\sim}{h}_p$ in Eq. 106.

$$\phi_m = \phi_s \quad \text{with} \quad k_s \to k_m \quad , \tag{B.5}$$

follows at once from Eq. B.3. The propagation constants k_s, k_m are as defined in Eq. 104. The $\underset{\sim}{h}_p$ given in Eqs. B.3 through B.5 and 106 is related to the complementary $\underset{\sim}{h}_c$ and the aerofield $\underset{\sim}{h}_a$ by the boundary condition Eq. 10b at the air-sea interface,

$$\underset{\sim}{h}_a = \underset{\sim}{h}_c + \underset{\sim}{h}_p \quad \text{at} \quad z = 0 \ , \tag{B.6}$$

which finally determines the complete solution, Eqs. 107.

We consider specifically the case of vertical earth field,

$$\underset{\sim}{H}_e = - (\pm) \, \hat{\underset{\sim}{z}} H_e \tag{B.7}$$

approximately applicable in Arctic and Antarctic regions (+ and −, respectively, here and below). Our problem then possesses azimuthal symmetry, so that the expansions of $\underset{\sim}{h}_a$ and $\underset{\sim}{h}_c$ indicated following Eqs. 107 become

$$\underset{\sim}{h}_a = \nabla\Psi \ , \qquad \Psi = \int_0^\infty dq \; A(q) \; J_0(q\rho) e^{i\omega t - qz} \tag{B.8a, B.8b}$$

in the usual cylindrical harmonics, and

$$\underset{\sim}{h}_c = \text{curlcurl} \; \hat{\underset{\sim}{z}} \Phi \ , \tag{B.9a}$$

$$\Phi = \int_0^\infty dq \; C(q) \; J_0(q\rho) e^{i\omega t + \sqrt{q^2 - k_m^2}\, z} \tag{B.9b}$$

in the vector-wave solutions of Morse and Feshbach (Ref. 47, p. 1823). Here A(q), C(q) are coefficients to be determined, J_0 are Bessel functions, and the positive root $\sqrt{q^2 - k_m^2}$ is intended since $z \leq 0$ in the sea. As to $\underset{\sim}{h}_p$, at the air-sea surface Eq. 106 with Eqs. B. 3 through B.5 reduces for the geometry of Eq. B.7 to the form

$$\underset{\sim}{h}_p \; (\text{at } z = 0) = \pm \hat{\underset{\sim}{\rho}} \; \frac{\mu\sigma H_e 2K}{k_s^2 - k_m^2} \, e^{i\omega t} \, \frac{\partial^2}{\partial\rho \, \partial d} \left(\frac{e^{-ik_s r_0} - e^{-ik_m r_0}}{r_0} \right) \tag{B.10}$$

where $\hat{\underset{\sim}{\rho}}$ is the unit cylindrical radial vector and $r_0 \equiv \sqrt{\rho^2 + d^2}$.

Upon inserting Eqs. B.8 through B.10 into Eq. B.6 and using the Fourier-Bessel theorem, one determines that

$$C(q) = -\frac{A(q)}{c_i} \quad , \tag{B.11a}$$

$$A(q) = \frac{q^2}{q + \sqrt{q^2 - k_m^2}} \left(\mp \frac{\mu\sigma H_e 2K}{k_s^2 - k_m^2} \right) \left(e^{-d\sqrt{q^2-k_s^2}} - e^{-d\sqrt{q^2-k_m^2}} \right). \tag{B.11b}$$

Putting these coefficients into Eqs. B.8 and B.9 gives the complete solution to our problem in terms of quadratures that are somewhat analogous in form to the Sommerfeld integrals of electromagnetic theory for submerged radio antennae. For example, the aerofield scalar potential is from Eqs. B.8 and B.11:

$$\Psi = -C_{\pm} e^{i\omega t} \int_0^{\infty} dq \, \frac{q^2}{q + u_m} J_0(q\rho) e^{-qz} \left(e^{-u_s d} - e^{-u_m d} \right), \tag{B.12a}$$

$$C_{\pm} \equiv \pm 2\mu\sigma H_e \frac{K}{k_s^2 - k_m^2} \quad , \tag{B.12b}$$

$$u_m \equiv \sqrt{q^2 - k_m^2} \quad \text{and} \quad u_s \equiv \sqrt{q^2 - k_s^2} \quad . \tag{B.12c}$$

Notice that the integral in Eq. B.12a is similar to that for the magnetic aerofield radiated from a submerged, low-frequency, vertical magnetic dipole (cf. Sinha and Bhattacharya, Ref. 50, Eqs. 3, 4, 12, and 13) but more complicated by the appearance of u_s as well as u_m in the integrand. In general, the integrals for the EM case have not been evaluated in closed form. Therefore, a fortiori in the sonomagnetic case we must turn to approximate evaluation.

Consider that component of the magnetic field in air which would be registered by a total field magnetometer,

$$h_{ae} \equiv \underset{\sim}{h}_a \cdot \hat{\underset{\sim}{H}}_e = \underset{\sim}{h}_a \cdot \hat{\underset{\sim}{z}} \tag{B.13}$$

for the present case (Eq. B.7). From Eqs. B.12a and B.8,

Ref. 50. A. K. Sinha and P. K. Bhattacharya, "Vertical magnetic dipole buried inside a homogeneous earth," Radio Sci., Vol. 1, 1966, p. 379.

$$h_{ae} = C_{\pm} e^{i\omega t} \int_0^{\infty} dq \, \frac{q^3}{q + u_m} J_0(q\rho) e^{-qz} \left(e^{-u_s d} - e^{-u_m d} \right). \quad \text{(B.14)}$$

In terms of sonic and magnetic scale lengths

$$\ell_s \equiv \frac{1}{k_s} \approx \frac{240}{\nu} \quad , \qquad \ell_m \equiv \frac{1}{|k_m|} \approx \frac{180}{\sqrt{\nu}} \quad , \quad \text{(B.15)}$$

there are several regimes of range coordinates ρ, z, and depth d for which we can give simple approximations to Eq. B.14.

1. Very close above shallow source ($\rho, z, d << \ell_m, \ell_s$):

$$h_{ae} \approx e^{i\omega t} \cdot C_{\pm} \cdot (k_m^2 - k_s^2) \cdot \frac{(z + d)d}{4R^3} \quad , \quad \text{(B.16)}$$

in which $C_{\pm} \cdot (k_m^2 - k_s^2)$, via Eqs. B.12b and B.2, is determined by source strength. The regime of Eq. B.16 includes the point on the sea surface directly above the source,

$$h_{ae}(\rho=0, z=0) \approx e^{i\omega t} \left(\mp \frac{1}{2} \mu\sigma H_e K \right) \cdot \frac{1}{d} \quad ,$$

provided now only that the source be shallow enough ($d << \ell_m, \ell_s$).

2. High altitude, directly overhead ($z >> \ell_m, \ell_s$ but $\rho, d \leq \ell_m, \ell_s$):

$$h_{ae} \approx e^{i\omega t} \cdot C_{\pm} \cdot \left(\frac{6}{ik_m} \right) \left(\frac{e^{-ik_s d} - e^{-ik_m d}}{z^4} \right), \quad \text{(B.17)}$$

which is the same fall-off with height ($1/z^4$) as the "quasi-near" electromagnetic field of a vertical magnetic dipole.

3. Far horizontal ranges at low altitude ($\rho >> \ell_m, \ell_s$, $z << \ell_m, \ell_s$):

$$h_{ae} \approx e^{i\omega t - ik_s \rho} \cdot C_{\pm} \left(\frac{ik_s^3 d}{k_s + \sqrt{k_s^2 - k_m^2}} \right) \cdot \frac{1}{\rho^2} \quad . \quad \text{(B.18)}$$

This far-field circular wave reduces over measurement distances that are small compared to the range ($\delta\rho << \rho$) to a plane wave $\propto e^{i(\omega t - k_s x)}$ where $x \equiv \delta\rho$. The wave amplitude is from Eqs. B.18, B.12b, and B.2,

$$|h_{ae}| \approx H_e \cdot \beta P \cdot 10^{-11+S_1/20} \cdot F_s(\nu) \cdot \frac{d}{\rho^2} \quad , \qquad \text{(B.19)}$$

in which the frequency behavior is contained in the function

$$F_s(\nu) \equiv \frac{2(\nu_0/\nu)}{x_\nu} \left(1 + x_\nu + \sqrt{2}\,\sqrt{1 + x_\nu}\right)^{-\frac{1}{2}} \quad , \qquad \text{(B.20a)}$$

$$x_\nu \equiv \sqrt{1 + (\nu_0/\nu)^2} \quad , \qquad \text{(B.20b)}$$

$$\nu_0 \equiv \frac{\mu\sigma c_s^{\,2}}{2\pi} \approx 2 \text{ Hz} \quad , \qquad \text{(B.20c)}$$

the last being the transition frequency of Eq. 55, at which $k_s = |k_m|$.

REFERENCES

1. K. C. Maclure, R. A. Hafer, and J. T. Weaver, "Magnetic variations produced by ocean swell," Nature, Vol. 204, 1964, p. 1290.

2. Ye. M. Groskaya, R. G. Skrynnikov, and G. V. Sokolov, "Magnetic field variations induced by the motion of sea waves in shallow water," Geomagn. Aeron., Vol. 12, 1972, p. 131 (translation).

3. N. A. Cochrane and S. P. Srivastava, "Tidal influence on electric and magnetic fields recorded at coastal sites in Nova Scotia, Canada," J. Atmos. Terr. Phys., Vol. 36, 1974, p. 49.

4. M. Klein, P. Louvet, and P. Morat, "Measurement of electromagnetic effects generated by swell," Physics of the Earth and Planetary Interiors, Vol. 10, 1975, p. 49.

5. E. C. Bullard and R. L. Parker, "Electromagnetic induction in the ocean," Chap. 18, Vol. 4, The Sea, Wiley-Interscience, New York, NY, 1970.

6. J. T. Weaver, "Magnetic variations associated with ocean waves and swell," J. Geophys. Res., Vol. 70, 1965, p. 1921.

7. H. T. Beal and J. T. Weaver, "Calculations of magnetic variations induced by internal ocean waves," J. Geophys. Res., Vol. 75, 1970, p. 6846.

8. W. Podney, "Electromagnetic fields generated by ocean waves," J. Geophys. Res., Vol. 80, 1975, p. 2977.

9. J. C. Larsen, "The electromagnetic field of long and intermediate water waves," J. Marine Res., Vol. 29, 1971, p. 28.

10. V. V. Akindonov, V. I. Naryshkin, and A. M. Ryazantsev, "Electromagnetic waves in sea water (Review)," Radioteknika i Elektronika, Vol. 21, No. 1, English translation in Radioeng. Electron. Phys., Vol. 21, No. 1, May 1976.

11. P. H. Roberts, An Introduction to Magnetohydrodynamics, American Elsevier, New York, NY, 1967.

12. A. Sommerfeld, Electrodynamics, Academic Press, New York, NY, 1952.

13. R. M. Fano, L. J. Chu, and R. B. Adler, Electromagnetic Fields, Energy and Forces, Wiley, New York, NY, 1960.

14. J. M. Robertson, Hydrodynamics in Theory and Application, Prentice-Hall, NJ, 1965.

15. N. Rudraiah and M. Venkatachalappa, "Effect of ohmic dissipation on internal Alfvén-gravity waves in a conducting shear flow," J. Fluid Mech., Vol. 62, 1974, p. 705.

16. G. I. Cohn, "MHD wave phenomena in seawater," Electromagnetics of the Sea, AGARD Conf. Proc. 77, 1970.

17. J. D. Jackson, Classical Electrodynamics, 2nd edition, Wiley, New York, NY, 1975.

18. O. M. Phillips, The Dynamics of the Upper Ocean, Cambridge University Press, 1966.

19. W. J. Pierson, Jr., and L. Moskowitz, "A proposed spectral form for fully developed wind seas based on the similarity theory of S. A. Kitaigorodskii," J. Geophys. Res., Vol. 69, 1964, p. 5181.

20. H. Lamb, Hydrodynamics (1932), 6th edition, Dover, 1945.

21. J. C. Larsen, "Electric and magnetic fields induced by deep sea tides," Geophys. J. Roy. Aston. Soc., Vol. 16, 1968, p. 47.

22. H. C. Yuen and B. M. Lake, "Reply to comments of G. Roskes," Phys. Fluids, Vol. 19, 1976, p. 767.

23. C. H. Su, "Hydraulic jumps in an incompressible stratified fluid," J. Fluid Mech., Vol. 73, 1976, p. 33.

24. K. Hunkins and M. Fliegel, "Internal Undular Surges in Seneca Lake: A Natural Occurrence of Solitons," J. Geophys. Res., Vol. 78, 1973, p. 539.

25. H. Lamb, The Dynamical Theory of Sound (1925), 2nd edition, Dover, 1960.

26. V. M. Kontorovich, "Magnetohydrodynamics of the Ocean," Problems of MHD and Plasma Dynamics II, 2nd Conf. on Theoret. and Appl. MHD, Riga. USSR, 1960.

27. G. M. Wenz, "Acoustic ambient noise in the ocean: spectra and sources," J. Acoust. Soc. Am., Vol. 34, 1962, p. 1936.

28. R. J. Urick, Principles of Underwater Sound, McGraw-Hill, NY, 1975.

29. G. A. Burtsyev, "Magnetohydrodynamics of sea currents," Fiz. Atmosf. Okeana, Vol. 11, 1975, p. 1084.

30. R. R. Harvey, "Derivation of oceanic water motions from measurement of the vertical electric field," J. Geophys. Res., Vol. 79, 1974, p. 4512.

31. S. A. Rommel, Jr., and J. D. McCleave, "Oceanic electric fields: Perception by American eels?" Science, Vol. 176, 1972, p. 1233.

32. T. Gammelsrød, "Instability of Couette flow in a rotating fluid and origin of Langmuir circulations," J. Geophys. Res., Vol. 80, 1975, p. 5069.

33. N. E. J. Boston, A. Maratos, J. A. Galt, and E. D. Traganza, "A measurement of nearshore Langmuir circulation," Naval Postgraduate School Report NPS-58Bb75041, 1975.

34. V. S. Semenov, "Three-dimensional dipole in a uniform flow of conducting fluid," Geomagn. Aeron., Vol. 15, 1975, p. 419 (APL/JHU translation 2776).

35. G. S. S. Ludford and J. D. Murray, "On the flow of a conducting fluid past a magnetized sphere," J. Fluid Mech., Vol. 7, 1960, p. 516.

36. P.-A. Bois, "Influence sur quelques types de champs magnétiques de l'écoulement d'un fluide conducteur autour d'une sphère," J. Méc., Vol. 9, No. 35, 1970.

37. T. Y. Wu, "Cavity and wake flows," Ann. Rev. Fluid Mech., Vol. 4, 1972, p. 243.

38. H.-P. Pao and T. W. Kao, "Vortex structure in the wake of a sphere," Phys. Fluids, Vol. 20, 1977, p. 187.

39. R. J. Hartman and H. W. Lewis, "Wake collapse in a stratified fluid: linear treatment," J. Fluid Mech., Vol. 51, 1972, p. 613.

40. R. J. Hartman, "The development of a partially mixed region in a stratified shear flow," J. Fluid Mech., Vol. 71, 1975, p. 407.

41. T. W. Kao, "Principal stage of wake collapse in a stratified fluid: two-dimensional theory," Phys. Fluids, Vol. 19, 1976, p. 1071.

42. G. Dagan, "Free-surface gravity flow past a submerged cylinder," J. Fluid Mech., Vol. 49, 1971, p. 179.

43. C. Hunter, "On the calculation of wave patterns," J. Fluid Mech., Vol. 53, 1972, p. 637.

44. F. Ursell, "On Kelvin's shipwave pattern," J. Fluid Mech., Vol. 8, 1960, p. 418.

45. A. A. Hudimac, "Ship waves in a stratified ocean," J. Fluid Mech., Vol. 11, 1961, p. 229.

46. J. W. Miles, "Internal waves generated by a horizontally moving source," Geophys. Fluid Dyn., Vol. 2, 1971, p. 63.

47. P. M. Morse and H. Feshbach, Methods of Theoretical Physics, McGraw-Hill, New York, NY, 1953.

48. J. Clarke, "Josephson junction detectors," Science, Vol. 184, 1974, p. 1235.

49. J. Clarke, "Principles and limitations of SQUIDs," Bull. Am. Phys. Soc., Vol. 22, 1977, p. 86.

50. A. K. Sinha and P. K. Bhattacharya, "Vertical magnetic dipole buried inside a homogeneous earth," Radio Sci., Vol. 1, 1966, p. 379.

INITIAL DISTRIBUTION EXTERNAL TO THE APPLIED PHYSICS LABORATORY*

The work reported in TG 1315A was done under Navy Contract N00017 72-C-4401.
This work is related to Task X8, which is supported by NAVSEASYSCOM.

ORGANIZATION	LOCATION	ATTENTION	No. of Copies
DEPARTMENT OF DEFENSE			
DARPA	Washington,DC		1
DDC	Alexandria, VA 22314		12
Department of the Navy			
NAVSEASYSCOM	Washington, DC 20362		1
		SEA-09G3	2
NAVAIRSYSCOM	Washington, DC	AIR-50174	2
NAVPRO	Laurel, MD 20810		1
ONR	Arlington, VA 22217		1
Naval Undersea Center	San Diego, CA 92123		1
Naval Research Laboratory	Washington, DC 20375		1
		Dr. G.R. Hamilton	1
Naval Postgraduate School	Monterey, CA 93940		1
Naval Underwater Systems Center	Newport, RI 02840		1
Oceanographer of the Navy	Alexandria, VA 22332		1
Naval Oceanographic Office	Washington, DC 20373		1
Department of the Air Force			
Air Force OSR	Washington, DC 20332		1
OTHER GOVERNMENT AGENCIES			
NASA Scientific and Technical Info. Fac.	B/W International Airport		1
Goddard Space Flight Center	Beltsville, MD		1
National Science Foundation	Washington, DC 20550	Oceanography Div.	1
UNIVERSITIES			
Scripps Inst. of Oceanography	La Jolla, CA 92037		1
Woods Hole Oceanographic Inst.	Woods Hole, MA		1

Requests for copies of this report from DoD activities and contractors should be directed to DDC, Cameron Station, Alexandria, Virginia 22314 using DDC Form 1 and, if necessary, DDC Form 55

*Initial distribution of this document within the Applied Physics Laboratory has been made in accordance with a list on file in the APL Technical Publications Group

End
1-79